G. Hasan ATILIM UNIVERSITY 2022

EVALUATION OF MODIFIED AND EXTENDED PUSHOVER METHODS FOR RC BUILDINGS HAVING SETBACK IRREGULARITY

THE GRADUATE SCHOOL OF NATURAL AND APPLIED SCIENCES
OF
ATILIM UNIVERSITY

GHADEER HASAN

A MASTER OF SCIENCE THESIS
IN
THE DEPARTMENT OF CIVIL ENGINEERING

AUGUST 2022

EVALUATION OF MODIFIED AND EXTENDED PUSHOVER METHODS FOR RC BUILDINGS HAVING SETBACK IRREGULARITY

A THESIS SUBMITTED TO
THE GRADUATE SCHOOL OF NATURAL AND APPLIED SCIENCES
OF
ATILIM UNIVERSITY

BY

GHADEER HASAN

IN PARTIAL FULFILLMENT OF THE REQUIRMENT
FOR
THE DEGREE OF MASTER OF SCIENCE
IN
THE DEPARMENT OF CIVIL ENGINEERING

AUGUST 2022

Approval of the Graduate School of Natural and Applied Sciences, Atilim University.

Prof. Dr. Ender KESKİNKILIÇ
Director

I certify that this thesis satisfies all the requirements as a thesis for the degree of **Master of Science in Civil Engineering Department, Atılım University.**

Assoc. Prof. Dr. Yakup DARAMA
Head of Department

This is to certify that we have read the thesis "Evaluation of Modified and Extended Pushover Methods for RC Buildings Having Setback Irregularity" submitted by Ghadeer Hasan and that in our opinion it is fully adequate, in scope and quality, as a thesis for the degree of Master of Science.

Asst. Prof. Dr. Halit Cenan MERTOL
Supervisor

Examining Committee Members:

Assoc. Prof. Dr. Rıza Secer Orkun KESKİN
Civil Eng. Department, TED University

Asst. Prof. Dr. Halit Cenan MERTOL
Civil Eng. Department, Atılım University

Asst. Prof. Dr. Gökhan TUNÇ
Civil Eng. Department, Atılım University

Date: *17.08.2022*

I hereby declare that all information in this document has been obtained and presented in accordance with academic rules and ethical conduct. I also declare that, as required by these rules and conduct, I have fully cited and referenced all material and results that are not original to this work.

Name, Last Name : Ghadeer HASAN

Signature :

ABSTRACT

EVALUATION OF MODIFIED AND EXTENDED PUSHOVER METHODS FOR RC BUILDINGS HAVING SETBACK IRREGULARITY

Ghadeer Hasan
M. S., Department of Civil Engineering
Supervisor: Asst. Prof. Halit Cenan Mertol

August 2022, 94 pages

Irregular configurations of reinforced concrete buildings were frequently identified as one of the main causes of failures during previous earthquakes. The setback irregularity which occurs due to abrupt reduction of the lateral dimension of the building at specific levels of elevation may be catastrophic for buildings having various heights. Engineers are more likely to adopt simplified nonlinear static analytical procedures such as pushover analysis when evaluating the seismic performance of reinforced concrete buildings due to its ease in application. The use of conventional pushover analysis methods provides acceptable results low-rise buildings. However, these methods do not provide sufficient results for mid- and high-rise buildings whose behavior under seismic actions is not only governed by the fundamental mode shape. To overcome this problem, some advanced methods considering the effects of higher mode shapes were proposed by various researchers. However, the applicability of these methods to three dimensional high-rise buildings having setback irregularity was not addressed in the literature.

In this study, a total of 6 mid- and high-rise building models having setback irregularity at various locations were analyzed using nonlinear pushover analysis methods namely the Inverted Triangular Lateral Load Pattern (TLP) according to ASCE 7-22, First Modal Shape Lateral Load Pattern (FLP), Uniform Lateral Load Pattern (ULP), Modified Upper Bound Method (MUB), and Extended Upper Bound Method (EUB), to evaluate the applicability of these methods. The results obtained using these methods were compared to the Nonlinear Time History Analysis Method (NLTHA) which provided benchmark solutions to the problems. Three of the building models had 6 stories and the other three had 12 stories. The story heights of the models were all 4.5 m at the ground story and 3.2 m for the rest of the stories. All models had four bays in both plan view directions with a typical length of 6 m each. One model of each height level was a regular building and used for comparison purposes. Other two models of each height level had setback irregularity in various locations of the elevation in one direction. The results were assessed for seismic demand variables such as lateral displacements, interstory drift ratios, and plastic hinge rotations. The EUB method also provided more accurate results of interstory drift ratios of all irregular building models compared to those of the conventional pushover analysis procedures (TLP, FLP, and ULP). Conventional pushover methods were not sufficient to predict the plastic hinge rotations at the upper stories of the 6 and 12 story building models, whereas the EUB method provided reasonable estimates of these plastic hinge rotations for irregular buildings.

Keywords: Pushover Analysis, nonlinear Time History Analysis, Reinforced Concrete Buildings, Upper Bound.

ÖZ

DEĞİŞTİRİLMİŞ VE GENİŞLETİLMİŞ İTME YÖNTEMLERİNİN GERİ ÇEKME DÜZENSİZLİĞİ OLAN BETONARME BİNALAR İÇİN DEĞERLENDİRİLMESİ

Ghadeer Hasan
Yüksek Lisans, İnşaat Mühendisliği Bölümü
Tez Yöneticisi: Dr. Öğr. Üyesi Halit Cenan Mertol

Ağustos 2022, 94 sayfa

Betonarme binaların düzensiz konfigürasyonları, bu tip binalarda önceki depremler sırasında meydana gelen hasarların nedenlerinden biri olarak sıklıkla tanımlanmıştır. Belirli kot seviyelerinde binanın yanal boyutunun küçülmesi nedeniyle meydana gelen düzensizlik tipi (geri çekme), farklı yüksekliklere sahip binalar için felaket olabilir. Mühendislerin, uygulama kolaylığı nedeniyle, betonarme binaların sismik performansını değerlendirirken itme analizi gibi basitleştirilmiş doğrusal olmayan statik analiz prosedürleri benimsemeleri çok yaygındır. Geleneksel itme analiz yöntemlerinin kullanılması, az katlı binalar için kabul edilebilir sonuçlar sağlanaktadır. Ancak bu yöntem, sismik hareketler altındaki davranışı yalnızca temel mod şekli tarafından belirlenmeyen orta ve yüksek katlı binalar için yeterli sonuçları sağlamamaktadır. Bu sorunun üstesinden gelmek için, daha yüksek mod şekillerinin etkilerini dikkate alan bazı gelişmiş yöntemler çeşitli araştırmacılar tarafından önerilmiştir. Ancak bu yöntemlerin geri çekme düzensizliği olan üç boyutlu yüksek binalara uygulanabilirliği literatürde ele alınmamıştır.

Bu çalışmada, çeşitli konumlarda geri çekme düzensizliğine sahip toplam 6 orta ve yüksek katlı bina modeli, ASCE 7-22’ye göre Ters Üçgen Yanal Yük Dağılımı (TLP),

Birinci Mod Şekli Yanal Yük Dağılımı (FLP), Düzgün Yayılı Yanal Yük Modeli (ULP), Değiştirilmiş Üst Sınır Yöntemi (MUB) ve Genişletilmiş Üst Sınır Yöntemi (EUB) gibi doğrusal olmayan itme analiz yöntemleri kullanılarak analiz edilmiş ve bu yöntemlerin uygulanabilirliğini değerlendirilmiştir. Bu yöntemlerden elde edilen sonuçlar, daha kesin çözümler sunan Doğrusal Olmayan Zaman Alanı Analizi Yöntemi (NLTHA) ile karşılaştırılmıştır. Bina modellerinden üçü 6 katlı, diğer üçü 12 katlıdır. Modellerin kat yükseklikleri zemin katta 4.5 m, diğer katlarda ise 3.2 m olarak belirlenmiştir. Tüm modeller, her iki plan görünümü yönünde, her birinin tipik uzunluğu 6 m olan dört açıklığa sahiptir. Her yükseklik seviyesinden bir model planda simertik bir bina olarak tasarlanmış ve karşılaştırma amacıyla kullanılmıştır. Her yükseklik seviyesindeki diğer iki model de, bir yönde yüksekliğin çeşitli yerlerinde geri çekme düzensizliği bulunmaktadır. Sonuçlar, yanal yer değiştirmeler, katlar arası ötelenme oranları ve plastik mafsal dönüşleri gibi sismik talep değişkenleri için değerlendirilmiştir. EUB yöntemi, geleneksel itme analiz prosedürlerine (TLP, FLP ve ULP) kıyasla tüm düzensiz bina modellerinin katlar arası ötelenme oranları için daha doğru sonuçlarını sağlamıştır. 6 ve 12 katlı bina modellerinin üst katlarındaki plastik mafsal dönüşlerini tahmin etmek için geleneksel itme yöntemleri yeterli değildir, oysa EUB yöntemi düzensiz binalar için bu plastik mafsal dönüşleri için makul sonuçlar sağlamıştır.

Anahtar Kelimeler: İtme Analizi, Doğrusal Olmayan Zaman Alanı Analizi, Betonarme Binalar, Üst Sınır.

DEDICATION

To all readers

ACKNOWLEDGEMENTS

I would like to express my special thanks to my supervisor, Assist. Prof. Dr. Halit Cenan Mertol, who guided me throughout this research process and gave this opportunity to work with himself. Also, I learnt lots of knowledge, especially related to structural engineering and computer programming from him. I am glad working with him.

I would like to thank to the researchers who worked on this topic. I used their ideas, theses, articles, and studies to develop the study in this thesis.

I would like to thank to Atılım University who granted me a scholarship to perform this study. Also, I would like to thank to all the Academic Personnel of Civil Engineering Department at Atılım University for their efforts in this study.

Finally, I would like to convey my special thanks to my parents and my friends. They gave me this opportunity with their support.

TABLE OF CONTENTS

LIST OF FIGURES

LIST OF TABLES

CHAPTER 1

1. INTRODUCTION

1.1 Background

Natural disasters such as earthquakes are among the most destructive hazards to the buildings. Seismicity is commonly defined as the frequency of the projected ground acceleration resulting from seismic forces. Due to these seismic actions, the hazard level can be defined for various regions of the United States of America as shown in Figure 1.1. The structural designer's primary goal is to keep earthquakes from causing destruction, prevent loss of life and minimize the loss of property. The designers also assess the necessities of seismic hazards using advanced scientific perception and analytical modeling. Seismic loads are very unpredictable and must be modelled in a very accurate manner so that the actual performance of a structure can be predicted. Buildings constructed before the development of earthquake-resistant design approaches, such as non-seismic resistant reinforced concrete (RC) structures, lack the strength and deformation capacity necessary to survive the earthquakes. When there are structural flaws in design and construction, the effects of seismic forces are more pronounced, resulting in greater damage during an earthquake. Structures especially having columns with inadequate transverse reinforcement, are most likely to get damaged due to the lack of deformation capacity, which will ultimately lead to the total collapse of the building. Severe earthquakes may cause buildings to collapse since those structures will deform inelastically as the result of the ground motion. Post-elastic behavior needs to be considered in design of RC buildings during the evaluation process of the seismic performance of the building.

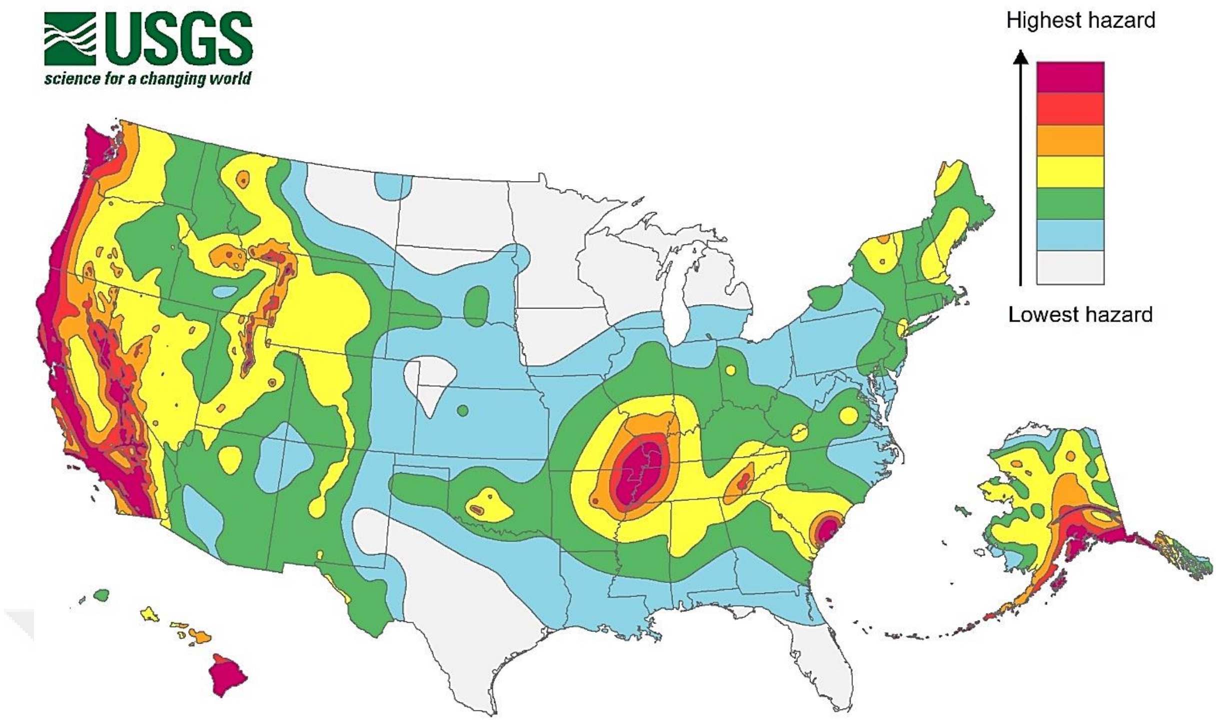

Figure 1.1 Seismic Hazard Map of USA [1]

Architectural requirements and designs rarely result in regular-shaped buildings. In general, buildings can be categorized as regular and irregular buildings due to their shapes and layouts of structural and nonstructural members. The irregularity can be due to the non-homogeneous and unsymmetrical distribution of plan, elevation, mass, and stiffness of the building. Therefore, types of irregular buildings can be summarized as buildings having:

1. Irregularity in plan,
2. Irregularity in elevation,
3. Irregularity in stiffness (uneven distribution of structural members),
4. Mass variation in plan (due to openings in slabs).

Examples of these types of irregularities are shown in Figure 1.2. An example of an irregular building constructed in Austin, Texas, USA is shown in Figure 1.3. Irregular buildings may lead to the complex distribution of forces and deformations. Such type of uneven distribution in mass, stiffness, and geometry may result in serious reduction of strength and stiffness of structural members, also unexpected stress concentrations.

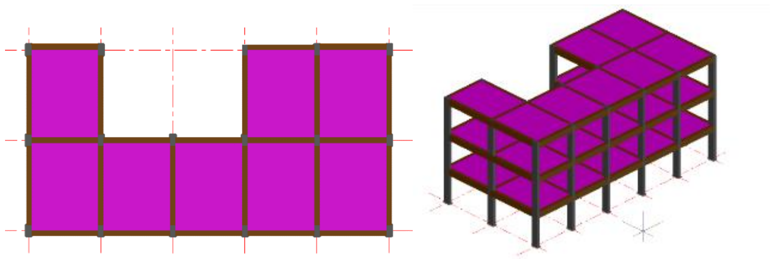

a) Irregularity in Plan

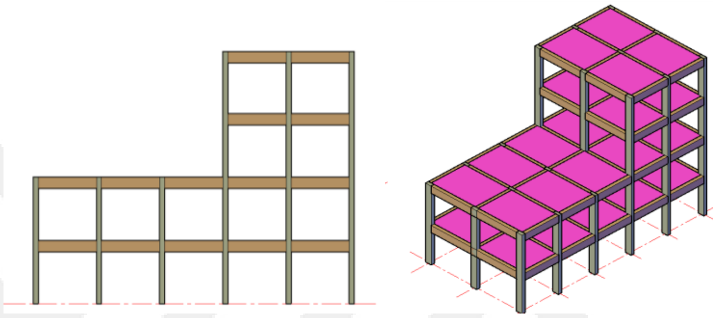

b) Irregularity in Elevation

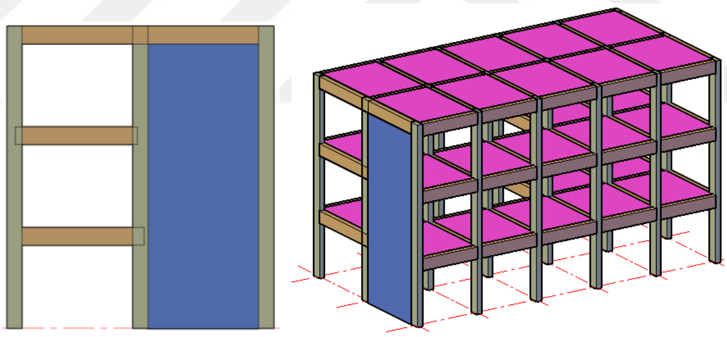

c) Irregularity in Stiffness

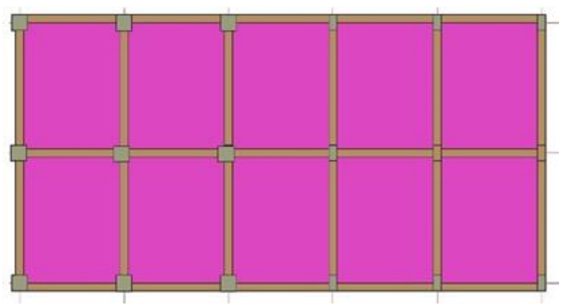

d) Mass variation in plan

Figure 1.2 Types of Irregular Buildings

Figure 1.3 Example of Irregular Building (One American Center, A Commercial Office Skyscraper, Austin, Texas, USA)

Earthquake damages are likely to occur in multi-story RC irregular buildings depending on the mass, stiffness, and strength of those buildings. Fully symmetrical buildings can never be constructed, since mass, stiffness, and strength variations are inevitable. The discontinuity of mass, stiffness, and strength at neighboring stories may play an important role in the performance of the building.

It is important to know how these irregular buildings behave during earthquakes. Buildings are typically designed for earthquake performance using elastic analysis. The elastic analysis techniques produce limited evaluation of the behavior, since these types of buildings will perform in a nonlinear manner during earthquakes. Necessary comprehensive investigation including the inelastic performance shall be conducted on those irregularly shaped buildings to properly design and evaluate their response against seismic activity. Furthermore, the maximum displacement of irregular buildings shall be determined to accurately predict seismic performance during the inelastic behavior.

1.2 Problem Definition

It is necessary to identify the limitations and efficiency of the pushover analysis methods to accurately predict the seismic demands of buildings with irregularities at different levels. The use of conventional pushover analysis methods such as, First Modal Shape Lateral Load Pattern (FLP), Uniform Lateral Load Pattern (ULP) according to FEMA 356 [2], Inverted Triangular Lateral Load Pattern (TLP) according to ASCE 7-22 [3] to evaluate the seismic behavior of buildings provides acceptable results for three dimensional (3D) low-rise buildings whose behavior is dominated by the fundamental period (first mode shape) of the building. However, for mid- and high-rise buildings whose behavior under seismic actions is not only governed by the fundamental mode shape, the conventional methods do not provide sufficient results. To overcome this problem, upper-bound methods (UB) such as the Modified Upper Bound Method (MUB) (3D Regular) and Extended Upper Bound Method (EUB) (3D Irregular) methods considering the effects of higher mode shapes were proposed by various researchers. Previously, the EUB method was applied to 3D irregular high-rise buildings having unsymmetrical plans. However, the applicability of the EUB method for 3D high-rise buildings having setback irregularity was not addressed in the literature.

1.3 Aim of Study

In this study, a total of 6 mid- and high-rise building models having setback irregularity at various locations were analyzed using nonlinear pushover analysis methods namely FLP, ULP, TLP, MUB, and EUB, to evaluate the applicability of these methods when the higher mode and torsional effects are more pronounced. The results obtained using these methods were compared to the NLTHA method which provided benchmark solutions to the problems. Three of the building models had 6 stories and the other three had 12 stories. The story heights of the models were all 4.5 m at the ground story and 3.2 m for the rest of the stories. All models had four bays in both plan view directions with a typical length of 6 m each. One model of each height level was a regular building and used for comparison purposes. Other two models of each height level had setback irregularity in various locations of the elevation in one direction. The analyses were performed using SAP2000 Structural Analysis Software [4]. The results were assessed for seismic demand variables such as lateral displacements, interstory drift ratios, and plastic hinge rotations.

1.4 Organization of Thesis

Five chapters make up this thesis.
Chapter 1 discusses the problem in general and explains the aim and organization of the study.

Chapter 2 gives a detailed literature review related to seismic analysis methods such as linear static, nonlinear static (pushover analysis), linear dynamic, and nonlinear dynamic.

Chapter 3, the properties of the building models used in this study are explained in details. The steps of the applied nonlinear pushover analysis are also presented in this chapter.

Chapter 4 explains the results of the various applied pushover analysis methods and discusses the findings based on lateral displacements, interstory drift ratios, and plastic hinge rotations.

Chapter 5 draws conclusions out of this study and provides recommendations for future studies.

CHAPTER 2

2. LITERATURE REVIEW

2.1 General

Inelastic seismic evaluation of tall buildings requires complicated analysis techniques such as Nonlinear Time History Analysis (NLTHA). However, structural engineers usually prefer to use much simpler nonlinear static analysis procedures (pushover analyses) which produce comparable and acceptable results, similar to that of NLTHA. The conventional pushover analysis method uses the first mode response of the buildings under lateral uniform and triangular loads. However, this technique is only limited to low- and medium-rise buildings, cannot be directly used for high-rise buildings. Since the conventional method has some limitations in predicting the inelastic seismic behavior of high-rise buildings, some methods were investigated in the literature. In this chapter, a review of literature is presented to explain the necessary information to evaluate the problem.

2.2 Seismic Analysis Methods of Structures

Since the designer needs to evaluate the behavior of the designed structure under various loads, numerical model of the structure is used to predict the behavior of that structure for those loads. Numerous approaches may be used to analyze structures subjected to earthquake forces. Each of these approached have different complexity and accuracy levels. These methods, linear static, nonlinear static, linear dynamic, and nonlinear dynamic analysis are explained in the subsections below.

2.2.1 Linear Static Analysis

This method may also be named as “Equivalent Static Method”. In this method, the total base shear of the building resulting from the ground motion is calculated using the fundamentals period of the structure and the acceleration response spectrum of the construction location. The response spectrum of the construction location is obtained using seismic hazard maps produced from the previous ground motion data. This calculated base shear is later distributed along the height of the building model and the analysis is performed under these applied loads.

This method has some restrictions since the building is assumed to behave linearly during the earthquake. Therefore, it may not be confidently used for buildings located in high seismic zones. Behavior of tall buildings may not only depend on the fundamental period of the building. Higher modes of vibration may have much more dominant effect on this behavior. Therefore, the application of this method on tall buildings may not predict the actual behavior. Additionally, structures with discontinuities (mass, stiffness, etc.) shall be carefully evaluated when this method is used for those types of structures.

2.2.2 Nonlinear Static Analysis

This method may also be named as "Pushover Analysis". Pushover analysis is a nonlinear analysis method used to determine capacity of the structure under static horizontal loads which are increased monotonically from zero till the collapse of the structure. It produces some capacity curves (load deflection curves) resulting from the application of this increasing force as a function of the displacement of the control point of the structure. The sequence of cracks, yielding, plastic hinge formation, and local/global failures is also obtained when this method is used. The accuracy of the results of pushover analysis is greatly affected by the estimation of target displacement (where the structure fails) and the selection of lateral load patterns.

The pushover analysis method is well-known for its use of two-dimensional analysis, and it was useful for both regular and irregular buildings in terms of height only [5]. Because of its simplicity, pushover analysis is used as the primary method to evaluate the seismic performance of buildings based on major standards and regulations. Pushover analysis combined with the equivalent two-dimensional single degree of freedom (SDOF) representation of the actual structure is occasionally used for the greatest simplicity. However, since this involves approximations, the reliability and accuracy of this method must be verified.

Earlier researches used this approach on symmetric structures, and because of the symmetry, the structure was modeled in two dimensions and pushover analysis was applied on this two-dimensional model. Eccentricity was not taken into account in these models. Asymmetric three-dimensional structures need the use of three-dimensional analysis because to the existing eccentricities caused by the structure's mass distribution or stiffness of its resistive parts being asymmetrical. Even though 3D-Pushover analysis is a rapid and effective technique, it raises certain problems, such as the optimal loading pattern for analysis and which direction the loading pattern should be applied. When comparing pushover analysis to nonlinear dynamic analysis, there are several factors that may be taken into account to determine how accurate a technique is.

Researchers investigated various aspects of pushover analysis to identify the limitations and weaknesses of this method and proposed improved pushover procedures that take into account the effects of lateral load patterns, higher modes, failure mechanisms, and so on.

Krawinkler and Seneviratna [6] conducted one of the first studies in the literature, presenting a comprehensive investigation of the benefits, drawbacks, and applicability of pushover analysis examining various aspects of the procedure. The basic concepts and main assumptions of pushover analysis were identified such as target displacement estimation of multi degree of freedom (MDOF) structure through equivalent SDOF domain and the applied modification factors, importance of lateral load pattern on pushover predictions, conditions under which pushover predictions are adequate or not, and information obtained from pushover analysis. The precision of pushover predictions was tested on a low-rise building of four stories two-dimensional steel frame subjected to Northridge Earthquake in 1994. Nine ground motion records were taken into consideration. Pushover analysis results at the target displacement associated with the individual records were used to calculate the seismic demands. When the results of pushover and nonlinear dynamic analysis were compared, it was discovered that pushover analysis provides good predictions of seismic demands for low-rise structures with uniform distributions of inelastic behavior over the height. It was also suggested that this method should be used with caution and judgement due to its many limitations, as the method is approximate in nature and contains many unresolved issues that need to be investigated.

When just one basic mode determines the overall dynamic response, the pushover analysis method is the most appropriate for the structures in consideration. This is a drawback of the method since the analysis is only based on the effect of the first natural frequency and ignores the rest of the frequencies. The effect of higher modes for tall buildings may be very significant. A number of previous efforts were published in the literature to extend pushover analysis to account for higher mode effects (Paret et al. [7], Sasaki et al. [8], Moghadam and Tso [9], Chopra and Goel [10], and Chopra and Goel [11]).

It is more important to choose a reasonable lateral load pattern during pushover analysis than it is to determine the goal displacement. Recommendations for invariant lateral load patterns from FEMA's study include uniform, inverted triangular and elastic first-mode vibration distribution. High-rise asymmetric-plan constructions can't be accurately predicted by pushover analysis processes since they don't take into account the effects of higher modes and torsion. When applied to tall structures with irregular floor layouts, the load patterns discussed above might provide deceptive findings that are just not acceptable. Another aspect that influences the seismic response of the asymmetric-plan structure is a linked translational-torsional impact. The present pushover approach for asymmetric-plan buildings must be retrofitted and extended accordingly.

The conventional pushover analysis outlined in FEMA 356 (2000) [2] and ATC 40 (1996) [12] is limited to buildings with regular geometry. Because of its limitations for irregular structures with significant higher modes effects, conventional nonlinear static (pushover) analysis outlined in FEMA 356 (2000) [2] and ATC 40 (1996) [12] may not be able to accurately evaluate the seismic performance of irregular buildings.

There were a few studies available in the literature to investigate the effects of the irregular shape of the buildings. Most of them were two-dimensional [13, 14] and some of them were three-dimensional. However, they had simple plan views having maximum three spans in both directions [15]. No studies were performed to evaluate the effect of both the irregularity in plan and irregularity in elevation, at the same time.

The conventional pushover procedure is clearly flawed when higher-mode effects are significant. Several researchers [10, 16, 17, 18] have proposed enhanced pushover analysis procedures that focused on higher mode effects and followed elastic modal combination rules. For low and medium-rise structures, these procedures may provide more accurate estimations for story displacements and drift ratios, but they still had limitations when evaluating high-rise structures [19, 20]. First, estimations for roof displacement and story drift ratio were not precise and conservative. Second, they were unable to accurately predict the extent of plastic hinge rotation, which was an important criterion when assessing the structural safety of a building.

A pushover analysis procedure was proposed by T. S. Jan [21] where the effects of higher modes were considered. The basic features of the proposed procedure were the response spectrum-based higher mode displacement contribution ratios, a proposed expression for determining the lateral load pattern and the upper-bound (absolute sum) modal combination rule for determining the target roof displacement. In this study five different-height buildings were used to demonstrate the proposed procedure. Three other types of analysis were performed for comparison purposes.

Oğuz [13] evaluated the effects and the accuracy of invariant lateral load patterns used in the pushover analysis. The estimations of the structural behavior due to randomly selected individual ground motions producing elastic and various levels of nonlinear response was investigated. A small number of RC and steel moment resisting frames were used in this study, and only a few ground motion excitations were investigated. Various response parameters calculated using pushover procedure were compared to the results obtained from nonlinear dynamic analysis. Furthermore, the lateral load shape was restricted to uniformly distributed loads, which has a significant impact on the accuracy of displacement and base shear values.

Elsharida [14] evaluated the efficiency and capability of the Enhanced Pushover Analysis (EPA) procedures for estimating the seismic demands of twelve regular and irregular special RC moment-resisting frames with varying story counts (4, 8, 12, 16, 20, and 24). The structural responses provided by the EPA methods were compared to the results obtained from the NLTHA. Conventional pushover analyses based on the first mode and uniform lateral load pattern were also demonstrated for comparison purposes. Only vertical irregularities were considered in this study, which was limited to only two-dimensional frames.

Daei and Poursha [15] investigated the applicability and validity of enhanced pushover procedures in estimating the seismic demands of mid- and high-rise RC buildings. The applied earthquake loads were generated from a pulse-like near-fault ground motions with forward-directivity and fling-step effects, as well as non-pulse-like near-fault and far-fault ground motions, using nonlinear response history analysis (NL-RHA). Three plan-symmetric buildings were examined in their study, including the 9-, 12-, and 18-story RC frames designed in accordance with the provisions of ASCE 7-10 and ACI 318-14. The interstory drift ratios and story shears, which represent deformation and force demands, were the engineering demand parameters considered in their study. Furthermore, the seismic performance of the RC buildings was evaluated using the conventional and enhanced multi-modal pushover procedures in accordance with the ASCE 41-17 standard's systematic evaluation scheme.

Based on the researches to modify to the conventional pushover analysis procedures to consider higher mode effects three methods were developed. These methods include upper-bound, modified upper-bound, and extended upper-bound pushover analysis methods.

2.2.2.1 Upper-Bound Pushover Analysis (UB)

The UB method was proposed to consider the effect of higher modes in two-dimensional tall building. A new expression for determining the lateral load pattern and an upper-bound modal combination rule for determining roof displacement were defined in the UB method. It was shown that using modes higher than the second mode yielded negligible contribution ratios for predicting the structural seismic response of tall buildings [21].

The target roof displacement used in this method is determined using the average displacement values of NLTHA for various available ground motions. This target displacement is used in pushover analysis with different lateral load patterns such as uniform load pattern (ULP), inverted triangular load pattern (TLP), and elastic first mode pattern (FLP).

The UB method has been used in several researches [21, 23]. Models with variations in plan-view and elevation (setback) were investigated in these studies. The results of the building models were compared the results of NLTHA obtained using the ground motion data of eleven earthquakes.

2.2.2.2 Modified Upper-Bound Pushover Analysis (MUB)

The procedures described above are only applicable to planar frames and symmetric-plan three-dimensional building structures. Several efforts have been made to extend the pushover analysis method for unsymmetrical three-dimensional building having torsional effects. To calculate the lateral force distribution, the upper-bound of the contribution ratio ($\left(\frac{q_2}{q_1}\right)_{UB}$) of the second mode was used as follows [21]:

$$\left(\frac{q_2}{q_1}\right)_{UB} = \left|\frac{\Gamma_2 D_2}{\Gamma_1 D_1}\right| \qquad \text{Equation 2-1}$$

where q_1 and q_2 are the modal coordinates for the first two modes, Γ_1 and Γ_2 are the modal participation factors for the first two modes, and D_1 and D_2 are the spectral displacements computed from elastic analysis.

This method had the potential to evaluate the seismic demands at lower stories of tall building [22]. On the contrary, the pushover analysis with a triangular or uniform load distribution can accurately estimate the seismic demands at lower stories of tall buildings where the effect of higher modes is not significant. Combining the peak responses from the upper-bound (UB) and conventional pushover analyses can change the seismic demands. As a result, MUB method defines a method to combine the responses of the UB and pushover analyses. The upper-bound lateral force, $f_{s,UB}$, is used in upper-bound pushover analysis:

$$f_{s,UB} = \omega_1^2 m\phi_1 + \omega_2^2 m\phi_2 \left(\frac{q_2}{q_1}\right)_{UB} \qquad \text{Equation 2-2}$$

where ω_i and ϕ_i are the natural frequency and natural vibration mode shape of the structure for the i^{th} mode, and m is the mass of the story. The target roof displacement determined for UB can be used in this method.

When the structure enters the inelastic behavior under increasing lateral forces, the changes in modal properties are not taken into account in this method. The seismic demands of the building are calculated using the envelope of the peak seismic responses computed from the MUB pushover (r_2) and conventional pushover (r_C) analyses. Various pushover analyses can be used and the results can be enveloped [24].

$$\mathrm{r_t} = \max.(\mathrm{r_C}, \mathrm{r_2}) \qquad \text{Equation 2-3}$$

where $r_{\mathrm{C}} = r_{TLP}$ for mid-rise buildings, $r_{\mathrm{C}} = r_{ULP}$ for high-rise buildings, r_{TLP} and r_{ULP} are the peak seismic responses obtained from conventional pushover analysis using TLP and ULP, respectively.

Note that conventional pushover analysis controls the seismic demands at lower stories of tall buildings, whereas upper-bound pushover analysis controls the seismic demands at upper stories where the effect of higher modes is significant.

2.2.2.3 Extended Upper-Bound Pushover Analysis (EUB)

Poursha and Samarin [22] investigated the limitations of UB method. The main objective of this study was to extend the application of UB method to unsymmetrical-plan tall buildings considering torsional effects. The extension was performed using the upper-bound lateral forces with different patterns for various unsymmetrical-plan tall buildings as shown in Figure 2.1. The upper-bound lateral forces were calculated using the upper-bound contribution ratio of higher modes. Their findings revealed that the extended method could predict the inelastic seismic demands of unsymmetrical-plan tall buildings with reasonable accuracy.

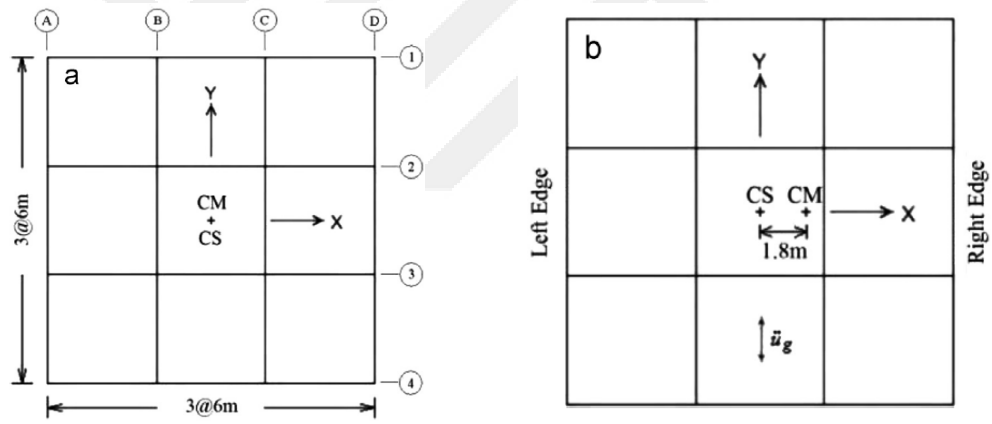

(a) symmetrical buildings (b) one-way unsymmetrical-plan buildings

Figure 2.1 The analyzed tall buildings' plans [22]

The UB method [21] uses only the first two modes of the seismic response of the building. Therefore, the effects of other higher modes are ignored. The EUB enhances this drawback considering the effect of other higher modes. In this study, only the first four modes were used in the EUB due to three dimensional irregularities.

The primary steps of EUB are listed below:

1. The elastic characteristics of a structure such as natural frequencies $\{\omega_n\}$ and mode shapes $\{\Phi_n\}$ for the selected building is determined.
2. The mode shape $\{\phi_n\}$ is normalized to have a roof degree of freedom of $\phi_{nr} = 1$ for all the modes.
3. The upper-bound of the contribution ratio of the nth mode ($(\mathrm{q}_n/\mathrm{q}_1)_{\mathrm{UB}}$) using the elastic response spectrum of the chosen earthquake is determined using the expression below:

$$\sum_n^4 \left(\frac{\mathrm{q}_n}{\mathrm{q}_1}\right)_{\mathrm{UB}} = \sum_n^4 \left|\frac{\Gamma_n \mathrm{D}_n}{\Gamma_1 \mathrm{D}_1}\right| \qquad \text{Equation 2.4}$$

where q_n (n=1, 2, 3, and 4) is the modal coordinate of the n^{th} mode, Γ_n are the modal participation factors of the n^{th} mode, and D_n are the spectral displacements obtained from the elastic displacement response spectrum.

4. The spectral displacements obtained from the elastic displacement response spectrum is calculated using the expressions below:

$$\mathrm{q}_n = \Gamma_n \mathrm{D}_n \qquad \text{Equation 2-5}$$

$$\mathrm{f}_n = \frac{1}{\Gamma_n} \rightarrow \mathrm{f}_n = \frac{\omega_n}{2\pi} \rightarrow \omega_n = \frac{2\pi}{T} \qquad \text{Equation 2-6}$$

$$\mathrm{S}_d(\mathrm{D}_n) = \mathrm{S}_a \frac{T^2}{4\pi^2} g \qquad \text{Equation 2-7}$$

where, S_d is the spectral displacement, S_a is the spectral acceleration, T is the time period, and g is the gravitational acceleration.

5. The applied load pattern (distribution of the lateral loads over the height of the building) for the EUB method is obtained using the expression below:

$$\{f_s\}_{UB} = \sum_{n=1}^4 F_{\mathrm{n}} = F_1 + F_2 + F_3 + F_4 \qquad \text{Equation 2-8}$$

$$F_1 = \{f_{S,UB}\} = \omega_1{}^2[m]\{\phi_1\} \qquad \text{Equation 2-9}$$

$$F_2 = \{f_{S,UB}\} = \omega_1{}^2[m]\{\phi_1\} + \omega_2{}^2[m]\{\phi_2\}\left(\frac{q_2}{q_1}\right)_{UB} \qquad \text{Equation 2-10}$$

$$F_3 = \{f_{S,UB}\} = \omega_1{}^2[m]\{\phi_1\} + \omega_2{}^2[m]\{\phi_2\}\left(\frac{q_2}{q_1}\right)_{UB} + \omega_3{}^2[m]\{\phi_3\}\left(\frac{q_3}{q_1}\right)_{UB} \quad \text{Equation 2-11}$$

$$F_4 = \{f_{S,UB}\} = \omega_1{}^2[m]\{\phi_1\} + \omega_2{}^2[m]\{\phi_2\}\left(\frac{q_2}{q_1}\right)_{UB} + \omega_3{}^2[m]\{\phi_3\}\left(\frac{q_3}{q_1}\right)_{UB} + \omega_4{}^2[m]\{\phi_4\}\left(\frac{q_4}{q_1}\right)_{UB} \quad \text{Equation 2-12}$$

where ω_i and ϕ_i are the natural frequency and natural vibration mode shape of the structure for the i^{th} mode.

6. The obtained load pattern is applied along the height of the building model using an FE Software (such as SAP2000).
7. After applying gravity loads on the model, the UB and conventional pushover are performed using the monotonically increased lateral load profile $\{f_s\}_{UB}$ till the target displacement is reached or the building collapses. The following sub-steps are followed until the control node at the roof displaces till the target displacement obtained in the previous step.
   7.1. Perform a conventional pushover analysis using the TLP for the medium-rise irregular buildings and the ULP for the high-rise buildings until the target displacement is reached. For torsionally-flexible systems, the conventional pushover analysis is performed by using F_1, Equation 2-9.
   7.2. Perform the EUB using the upper-bound lateral forces (f_{si}) derived from Equation 2-9 to Equation 2-12 until the target displacement at the roof level is reached.
8. Determine the greatest seismic demand values for both of the conventional and UB, separately. The maximum values obtained from these analyses are denoted as r_{fsi} and r_C.
9. Period ratios are calculated as the ratio of the translational period to the torsional period ($\text{Period Ratios} = \frac{\text{Translational Period}}{\text{Torsional Period}}$). Buildings can be categorized into three, torsionally-stiff buildings (TS) which have period ratios greater than unity, torsionally-flexible buildings (TF) have period ratios less than unity [25]. For

torsionally-similarly-stiff buildings (TSS), the period ratio is very close to unity. Based on this information, determine the envelope values (r) using the following expressions:

$$r_{UB} = \text{Max}\{r_C, r_{fs2}\} \text{for TS and TF systems } T > 2.2 \qquad \text{Equation 2-13}$$

$$r_{UB} = \text{Max}\{r_C, r_{fs1} r_{fs2}, r_{fs3},\} \text{for TSS systems } T < 2 \qquad \text{Equation 2-14}$$

where $r_C = r_{TLP}$ for the TS and TSS medium-rise systems, r_C=r_{ULP} for the TS and TSS high-rise systems, r_C=r_{fs1} for the TF systems, r_{fs1} is the peak seismic response obtained by the upper-bound pushover analysis with the lateral force, f_{s1}.

The studies of the effects of torsional stiffness and the nature of its rigidity, whether it is TF, TSS, or TS, are limited in the literature. However, it is critical to study the 3D irregular structures. The upper-bound contribution ratios of the first four modes dominate the displacement response in the case of TSS systems. All models in this study were TSS systems therefore, the results of two more modes were included in addition to the first two modes in the EUB Method [22].

2.2.3 Linear Dynamic Analysis

One of the linear dynamic analysis methods is the “Response Spectrum Method”. In this method, multiple modes shapes were considered. For all the mode shapes, a response is obtained using the design spectrum based on the modal mass frequency and mass. Then these responses are combined using various combination methods including absolute sum, square root of sum of squares, and complete quadratic combination methods.

This method also has some limitations. The buildings having plan and elevation irregularities cannot be modelled using this method.

Takeda et al. [26] proposed a model to analyze the response of RC structures subjected to strong earthquake motions by presenting a realistic conceptual model that recognizes the structure's constantly varying stiffness and energy-absorbing characteristics. The model's applicability to RC was experimentally tested using specimens subjected to dynamic base motions.

The following conclusions was the most important points drawn from Takeda et al. [26] study:

1. Throughout the simulated earthquake, the stiffness and energy-absorbing capacity of the RC test specimens changed significantly and, at times, very quickly.
2. Based on a static force-displacement relationship that accounts for changes in stiffness for loading and unloading as a function of prior loading history, an RC system dynamic response may be accurately predicted.
3. At all degrees of excitation, the dynamic response computed on the basis of the proposed force displacement relationship matched the observed response.
4. It wasn't essential to invoke additional energy absorption sources using the suggested force-displacement hysteresis loops to forecast the dynamic response.

The Capacity Spectrum Method [27, 28], used most often to estimate the seismic performance of buildings. The Method is recommended by ATC-40 [12] as a structural displacement design and evaluation tool. Freeman created the method, which has undergone several modifications since then. ATC-40 [12] describes in detail the most recent three versions (Procedures A, B, and C) of the Capacity Spectrum Method. The method requires the creation of a structural capacity curve and its comparison with the estimated demand response spectrum shown in Figure 2.2, both of which are represented by the ADRS (Acceleration-Displacement Response Spectrum).

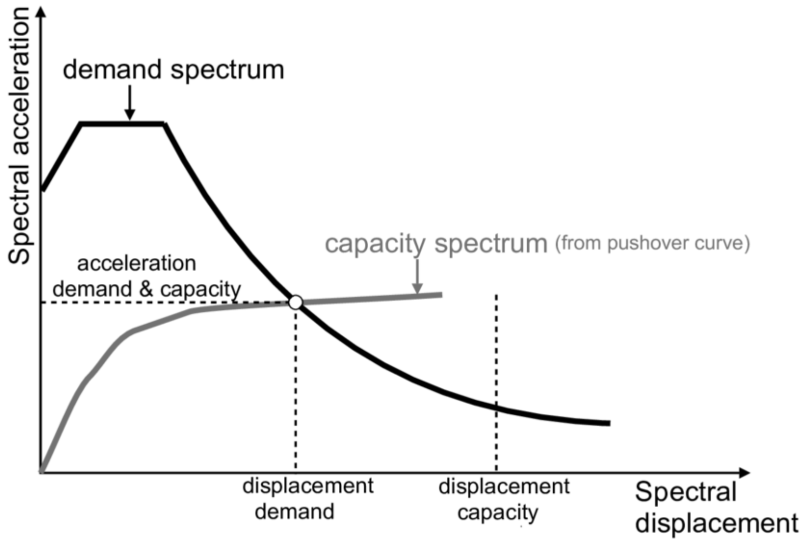

Figure 2.2 Capacity Spectrum Method [27]

2.2.4 Nonlinear Dynamic Analysis

This method may also be named as NLTHA. Time history analysis is used to evaluate the seismic responses of structures. NLTHA was extensively used for modelling the real behavior of buildings under seismic activity since the 1960s. Additionally, the NLTHA is adopted by many researchers in previous investigations due to its accuracy and capability in capturing the inelastic responses of any structure with any type of irregularities. However, this kind of analysis is not very feasible due to extensive time and effort needed to construct the model, input preparation, computing time, computer expenses, and result interpretation. Nonlinear analytical methodologies and structural models for the estimation of inelastic seismic demands were simplified by researchers as a consequence of these findings. It is very common to reduce the complexity of a model of MDOF structure into an SDOF system to analyze the system in a faster manner.

Rosenblueth and Herrera [29] proposed a method to predict the maximum deformation of an inelastic SDOF system as the maximum deformation of a linear elastic SDOF system with a lower lateral stiffness (higher period of vibration, T_{eq}) and a higher damping coefficient (ζ_{eq}) than the inelastic system. A sequence of equivalent linear systems with successively updated values of T_{eq} and ζ_{eq} were used to predict the deformation of the inelastic system. The authors represented period shift using secant stiffness at maximum deformation, and equivalent damping ratio is calculated by equating the energy dissipated per cycle in nonlinear and equivalent linear SDOF systems subjected to harmonic loading.

The seismic demands calculated using NLTHA are impacted by variables such as modeling parameters and ground motion characteristics (frequency content, intensity, magnitude, and duration). Instead of evaluating the target displacement, NLTHA is used to investigate the design displacements after the structure has been subjected to a series of seismic ground motion data. Because of this, it is very crucial to select the right set of ground motion data. This may be achieved performing additional calculations. A nonlinear static approach or pushover analysis has been performed to evaluate the seismic demands and identify the plastic hinge mechanisms in the building. Using NLTHA, it is possible to identify the zones that have suffered major deformations and obtain specific details to achieve the desired performance.

Mahaney [30] proposed the Acceleration Displacement Response Spectrum (ADRS) which was a plot of displayed the spectral accelerations versus the spectral displacements and radial lines denoting the period, T. The demand response spectrum, also known as the inelastic response spectrum, was generated by first obtaining the elastic response spectrum and then applying spectral reduction factors to that spectrum. These factors were dependent on the amount of effective damping. A performance point was determined for the purpose of assessing the overall performance of the structure. This point was defined as the intersection of the capacity spectrum and the demand spectrum. This point served as the basis for the determination (after being adjusted to account for nonlinear effects). The spectral reduction factors were dependent on the type of structural behavior (hysteretic qualities) and the duration of ground motion. The prediction of these reduction factors involving approximations was a primary flaw for this method.

CHAPTER 3

3. MODEL DESCRIPTION AND APPLIED LOADS

3.1 General

During earthquake motions, the behavior of a three-dimensional RC building is determined by the distribution of mass, stiffness, and strength in both the horizontal and vertical direction of the building. Damage of buildings due to earthquakes motion typically begins at the locations of plastic hinges at the elements of lateral load resisting system.

Irregular plan and elevation configurations are frequently identified as one of the primary causes of failures during earthquakes. There are numerous examples of buildings failing during earthquakes due to such vertical and horizontal discontinuities. The sudden reduction of the dimensions of plan area and height of the building at specific levels of elevation causes a common type of geometrical irregularity in building structures. This type of structure is known as an irregular (setback) building.

Many studies have been conducted to better understand the behavior of regular and irregular structures and to find ways to improve their performance.

One of the analyses and design methods used is to represent the entire three-dimensional buildings by two-dimensional frames in series for framed buildings. With reservations about the results for the various load conditions and the irregularities in the building height, width. When studying irregular buildings that are susceptible to earthquakes, how much can the analysis of three-dimensional structures be depended upon? This is the primary goal of this investigation.

Building modeling involves the modeling and assembly of its various load-carrying elements. The mass distribution, strength, stiffness, and deformability must all be accurately represented by the model. The modeling of material properties and structural elements used in this study is discussed further below.

3.2 Model Definition

The RC moment-resisting frame building model used in this study had a square-shaped plan view. All models had four bays in both plan view directions with a typical length of 6 m each as shown in Figure 3.1.

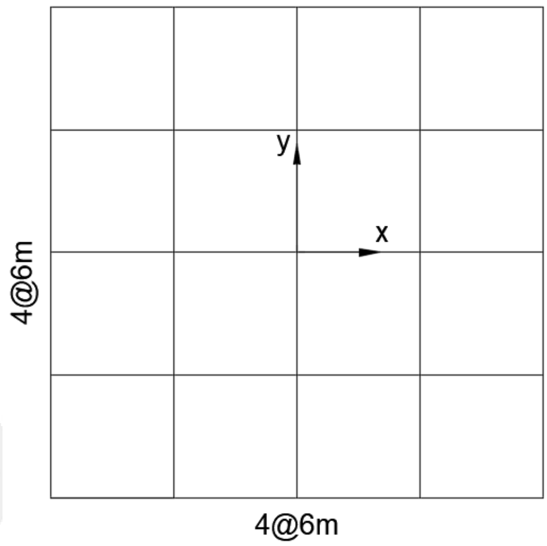

Figure 3.1 Typical Plan of Building Models for All Cases

A total of six models were used in the analyses. Three of the building models had 6 stories and the other three had 12 stories. The story heights of the models were all 4.5 m at the ground story and 3.2 m for the rest of the stories. One model of each height level was a regular building. Other two models of each height level had setback irregularity in elevation in one direction. The building models used in this study are shown in Figure 3.2. The beams and columns were idealized as line elements which passed from the centerline of each member. Rigid story diaphragms were defined at each story level.

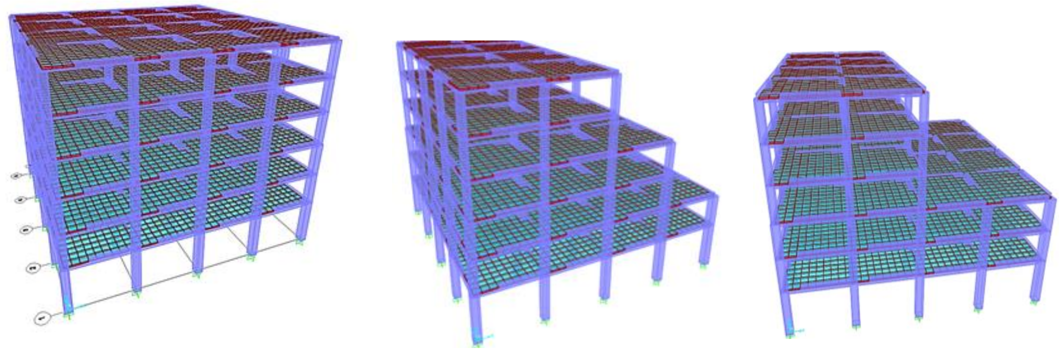

a) M1-6S-R c) M3-6S-IR d) M5-6S-IR

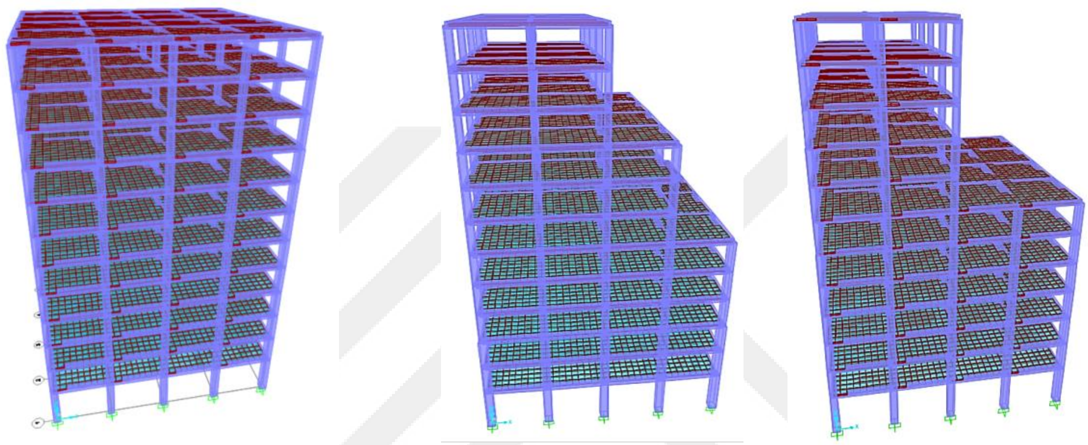

b) M2-12S-R d) M4-12S-IR e) M6-12S-IR

Figure 3.2 Regular and Setback Building Models used in This Study

The setback irregularity was modelled only in one direction (x-direction) Perpendicular to the direction of earthquake. The setback irregularity can be defined using two parameters (area and height setback ratio). The height setback ratio (H_R) is defined as the ratio of the height of the setback to the base height ($H_R = \frac{(Setback\ height)}{(Base\ height)}$) and the area setback ratio (B_R) is defined as the ratio of area of the setback to the base area ($B_R = \frac{(Setback\ area)}{(Base\ area\ )}$) [31]. Two different setback irregularities (one and two levels) were used in the modelling.

In model M3-6S-IR (two-levels setback irregularity) in the plan area of the building at the roof story and one story below (Story 5 and 6) was reduced to half (50% reduction) of the base area by changing the slab length only in the x-direction. For the lower two stories (Story 3 and 4) the plan area was reduced to 75% of the base area by changing the slab length again only in the x-direction. No reduction of the plan area was applied for the rest of the stories (Story 1 and 2). The height setback ratio of the two-levels setback irregularity in this model (H_{R1} and H_{R2}) were both equal to 1, for both area setback ratios (B_{R1} and B_{R2}) of 0.75 and 0.5, respectively.

In model M4-12S-IR (two-levels setback irregularity) the plan area of the building at the roof story and two stories below (Story, 10, 11, and 12) was reduced to half (50% change) of the base area by changing the slab length only in the x-direction. For the lower three stories (Story 7, 8, and 9) the plan area was reduced to 75% of the base area by changing the slab length again only in the x-direction. No reduction of the plan area was applied for the rest of the stories (Story 1, 2, 3, 4, 5, and 6). The height setback ratio of the two-levels setback irregularity in this model (H_{R1} and H_{R2}) were both equal to 0.5, for both area setback ratios (B_{R1} and B_{R2}) of 0.75 and 0.5, respectively.

In model M5-6S-IR (one-level setback irregularity) the plan area of the building at the roof story and two stories below (Story 4, 5, and 6) was reduced to half (50% change) of the base area by changing the slab length only in the x-direction. No reduction of the plan area was applied for the lower three stories (Story 1, 2, and 3). The height setback ratio of the one-level setback irregularity in this model (H_{R1}) was equal to 0.5, for the area setback ratio (B_{R1}) of 0.5.

Finally, in model M6-12S-IR (one-level setback irregularity) the plan area of the building at the roof story and four stories below (Story 9, 10, 11, and 12) was reduced to half (50% change) of the base area by changing the slab length only in the x-direction. No reduction of the plan area was applied for the lower seven stories (Story 1, 2, 3, 4, 5, 6 and 7). The height setback ratio of the one-level setback irregularity in this model (H_{R1}) was equal to 0.71 for the area setback ratio (BR1) of 0.5.

Based on ASCE 7-22 [3], the ratio of the story length (L_K) to the reduced story length above (L_{K+1}) in one direction shall be more than 1.3 for a building to be classified as setback as shown in Figure 3.3. In this study, all the models having setback irregularity satisfied this condition.

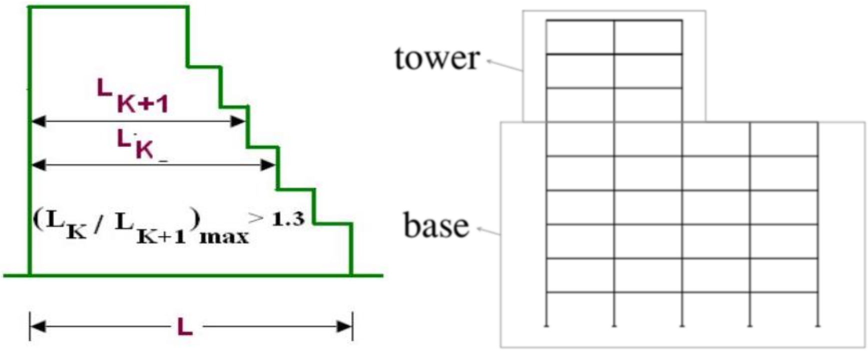

Figure 3.3 Criteria for Setback Irregularity According to ASCE 7-22 [3]

3.2.1 Material Properties

The material properties for concrete and reinforcing steel used in modelling are shown in Table 3.1

Table 3.1 Material Properties of Concrete and Reinforcement

Material	Designation	Characteristic Strength (MPa)	Modulus of Elasticity, E (GPa)	Unit Weight (kgf/m^3)
Concrete	C30/37	$f_{ck} = 30$	25.7	2500
Steel Reinforcement	S420	$f_{yk} = 420$	200	7850

3.2.2 Dead and Live Loads

The RC building models were moment resistance frames consisting of slabs, beams, and columns. The building models were designed for dead, live, and earthquake loads using the Soil Site Class C according to ASCE 7-22 [3]. All RC members were designed according to the provisions of ACI 318-19 [32]. The superimposed dead loads on slabs in addition to the self-weight of the structure was considered as 3.5 kN/m^2 (based on ASCE 7-22 [3]). The live load used in the analysis was equal to 2.4 kN/m^2 (for offices based on ASCE 7-22 [3]) for all the stories. Additionally, the dead loads of the internal and external walls were calculated as 6.5 and 10.4 kN/m, respectively. All these loadings are shown in Table 3.2.

Table 3.2 Dead and Live Loads used in Analysis

Superimposed DL on Slabs	3.5 kN/m^2
Live Loads (office)	2.4 kN/m^2
DL of Internal Walls	6.5 kN/m
DL of External Walls	10.4 kN/m

A preliminary design was performed to design the structural members of all the models (as shown in Appendix A). These members were designed to resist the gravity dead and live load safely. The slabs were designed as 150 mm thick. The dimensions and detailing of the designed structural members (beams and columns) for all the models are shown in Table 3.3 to Table 3.8. All the columns of the models at the same story level had the same dimensions. The dimensions of the beams and columns were changed at every three stories for economic purposes. The uncracked section properties (moment of inertia) for beams and columns were used in the analysis.

Table 3.3 Details of Beams for Regular Buildings (M1-6S-R and M2-12S-R)

Beam Designation	**b (mm)**	**h (mm)**	**Shape**	**# of Stories**		**Top Reinforcement**	**Bottom Reinforcement**
				6	**12**		
EB1 (External Beams)	350	550	L-Shaped	4-6	10-12	6ϕ25	6ϕ25
IB1 (Internal Beams)	450	550	T-Shaped	1-3	7-9	6ϕ20	6ϕ20
EB2 (External Beams)	400	650	L-Shaped	-	4-6	8ϕ25	8ϕ25
IB2 (Internal Beams)	450	600	T-Shaped	-	1-3	4ϕ25	4ϕ25

Table 3.4 Details of Columns for Regular Buildings (M1-6S-R and M2-12S-R)

Column Designation	**b (mm)**	**h (mm)**	**Shape**	**# of Stories**		**Top Reinforcement**	**Bottom Reinforcement**
				6	**12**		
C1	550	550	Square	4-6	10-12	5ϕ16	5ϕ16
C2	600	600	Square	1-3	7-9	6ϕ20	6ϕ20
C3	700	700	Square	-	4-6	6ϕ25	6ϕ25
C4	850	850	Square	-	1-3	6ϕ25	6ϕ25

Table 3.5 Details of Beams for Irregular Two-Level Setback Buildings (M3-6S-IR and M4-12S-IR)

Beam Designation	**b (mm)**	**h (mm)**	**Shape**	**# of Stories**		**Top Reinforcement**	**Bottom Reinforcement**
				6	**12**		
EB1 (External Beams)	350	550	L-B	4-6	10-12	4ϕ20	4ϕ16
IB1 (Internal Beams)	450	550	T-B	1-3	7-9	6ϕ20	5ϕ20
EB2 (External Beams)	400	650	L-B	-	4-6	4ϕ30	4ϕ25
IB2 (Internal Beams)	450	600	T-B	-	1-3	4ϕ25	4ϕ25

Table 3.6 Details of Columns for Irregular Two-Level Setback Buildings (M3-6S-IR and M4-12S-IR)

Column Designation	b (mm)	h (mm)	Shape	# of Stories		Top Reinforcement	Bottom Reinforcement
				6	12		
C1	550	550	Square	4-6	10-12	4ϕ25	4ϕ25
C2	600	600	Square	1-3	7-9	6ϕ20	5ϕ16
C3	700	700	Square	-	4-6	4ϕ25	4ϕ25
C4	850	850	Square	-	1-3	4ϕ25	4ϕ25

Table 3.7 Details of Beams for Irregular One-Level Setback Buildings (M5-6S-IR and M6-12S-IR)

Beam Designation	b (mm)	h (mm)	Shape	# of Stories		Top Reinforcement	Bottom Reinforcement
				6	12		
EB1 (External Beams)	350	450	L-B	4-6	10-12	6ϕ25	6ϕ25
IB1 (Internal Beams)	450	650	T-B	1-3	7-9	6ϕ25	6ϕ25
EB2 (External Beams)	350	450	L-B	-	4-6	6ϕ25	6ϕ25
IB2 (Internal Beams)	350	650	T-B	-	1-3	6ϕ25	6ϕ25

Table 3.8 Details of Columns for Irregular One-Level Setback Buildings (M5-6S-IR and M6-12S-IR)

Column Designation	b (mm)	h (mm)	Shape	# of Stories		Top Reinforcement	Bottom Reinforcement
				6	12		
C1	550	550	Square	4-6	10-12	6ϕ25	6ϕ25
C2	620	620	Square	1-3	7-9	6ϕ25	6ϕ25
C3	700	700	Square	-	4-6	6ϕ25	6ϕ25
C4	850	850	Square	-	1-3	7ϕ25	7ϕ25

3.2.3 Earthquake Loading

Two different methods were used to calculate the earthquake forces on the models. These methods are defined in the following subsections.

3.2.3.1 Elastic Acceleration Response Spectrum

The elastic acceleration response spectrum was produced using the ASCE 7-22 [3]. The spectral response acceleration parameter at short periods (S_s) and spectral response acceleration parameter at a period of 1 s (S_1) were determined for the selected location (a high-seismic region in Los Angeles, CA, USA) and are shown in Table 3.9.

Table 3.9 Site Parameters

S_s	S_1
1.974	0.703

The corresponding adjusted values (S_{MS}, S_{M1}) considering the selected Site Class C were calculated using the following expressions:

$$S_{MS} = F_a S_s \qquad \text{Equation 3-1}$$

$$S_{M1} = F_V S_1 \qquad \text{Equation 3-2}$$

where site coefficients F_a and F_v were determined using Table 3.10 and Table 3.11.

Table 3.10 Site Coefficient, F_a According to ASCE 7-22 [3]

Site Class	S_s≤0.25	S_s=0.5	S_s=0.75	S_s=1.0	S_s=1.25	S_s≥1.25
A	0.8	0.8	0.8	0.8	0.8	0.8
B	0.9	0.9	0.9	0.9	0.9	0.9
C	1.3	1.3	1.2	1.2	1.2	1.2
D	1.6	1.4	1.2	1.1	1.0	1.0
E	2.4	1.7	1.3	Site-specific geotechnical investigation is required.		
F	Site-specific geotechnical investigation is required.					

Table 3.11 Site Coefficient, F_v According to ASCE 7-22 [3]

Site Class	S_1≤0.1	S_1=0.2	S_1=0.3	S_1=0.4	S_1=0.5	S_1≥0.5
A	0.8	0.8	0.8	0.8	0.8	0.8
B	0.8	0.8	0.8	0.8	0.8	0.8
C	1.5	1.5	1.5	1.5	1.5	1.4
D	2.4	2.2	2.0	1.9	1.8	1.7
E	4.2	Site-specific geotechnical investigation is required.				
F	Site-specific geotechnical investigation is required.					

Design earthquake spectral response acceleration parameter at short period, S_{DS}, and at 1 s period, S_{D1}, were calculated using the following expressions (ASCE 7-22 [3]):

$$S_{DS} = \frac{2}{3} S_{MS} \qquad \text{Equation 3-3}$$

$$S_{D1} = \frac{2}{3} S_{M1} \qquad \text{Equation 3-4}$$

All the parameters used to produce the elastic acceleration response spectrum are shown in Table 3.12.

Table 3.12 Parameters used to Produce Elastic Acceleration Response Spectrum

F_a	F_V	S_{MS}	S_{M1}	S_{DS}	S_{D1}
1.2	1.4	2.3688	0.9842	1.5792	0.6561

The response spectrum diagram defined in ASCE 7-22 [3] is shown in Figure 3.4. The expressions used to produce the elastic acceleration response spectrum are shown after this figure:

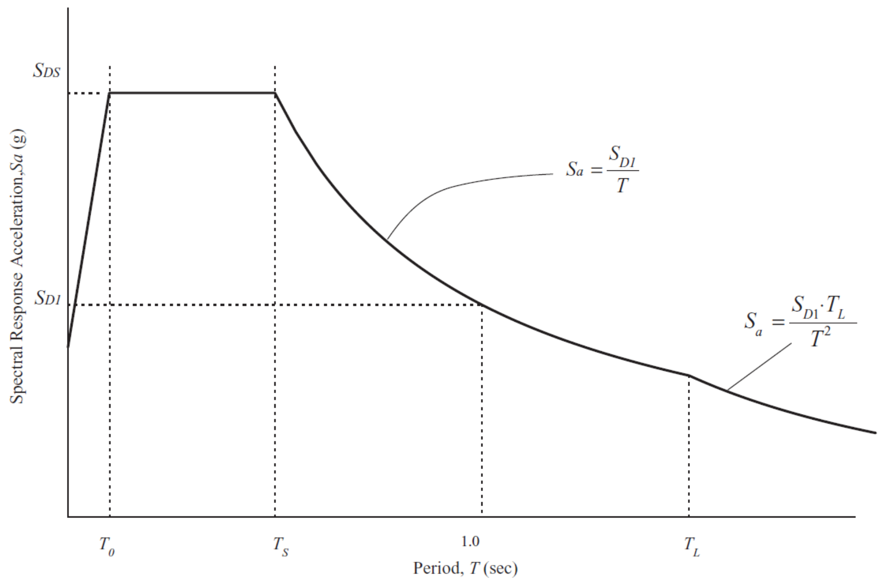

Figure 3.4 Response Spectrum According to ASCE 7-22 [3]

$T_0 = 0.2\frac{S_{D1}}{S_{DS}}$ Equation 3-5

$T_S = \frac{S_{D1}}{S_{DS}}$ Equation 3-6

$T_L = 8\ s$ Equation 3-7

$S_a = S_{DS}\left(0.4 + 0.6\frac{T}{T_0}\right)$ when $T \le T_0$ Equation 3-8

$S_a = S_{DS}$ when $T_0 \le T \le T_S$ Equation 3-9

$S_a = \frac{S_{D1}}{T}$ when $T_S \le T \le T_L$ Equation 3-10

$S_a = \frac{S_{D1} \times T_L}{T^2}$ when $T_L \le T$ Equation 3-11

Using the above expressions, the elastic acceleration response spectrum used in this study was produced as shown in Figure 3.5. The seismic design factors used in the analysis are shown in Table 3.13.

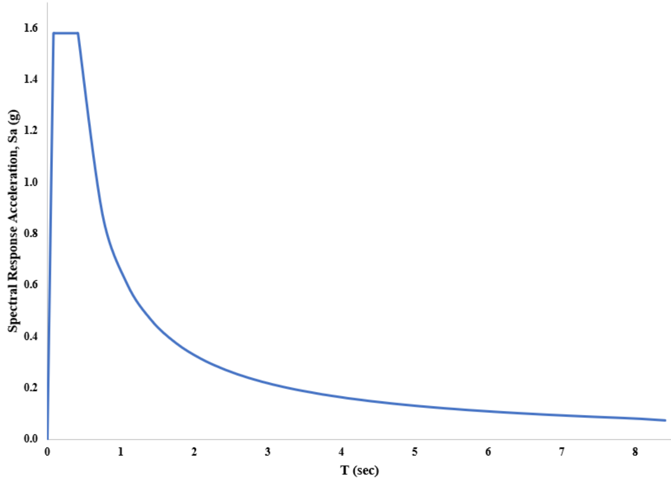

Figure 3.5 Elastic Acceleration Response Spectrum

Table 3.13 Seismic Design Factors According to ASCE 7-22 [3]

Response Modification Factor (R)	8
Over strength Factor (Ω)	3
Importance Factor (I)	1
Displacement Amplification Factor (C_d)	5.5

Based on ATC-40 [12], the elastic acceleration response spectrum calculated above can be converted to a two-value diagram which are the coefficients C_A and C_V as shown in Figure 3.6. Based on the data (Table 3.14 and Table 3.15) used in this study, the values of the coefficients, C_A and C_V, were determined as 0.4 and 0.56, respectively. These values applied to the building models are shown in Figure 3.7.

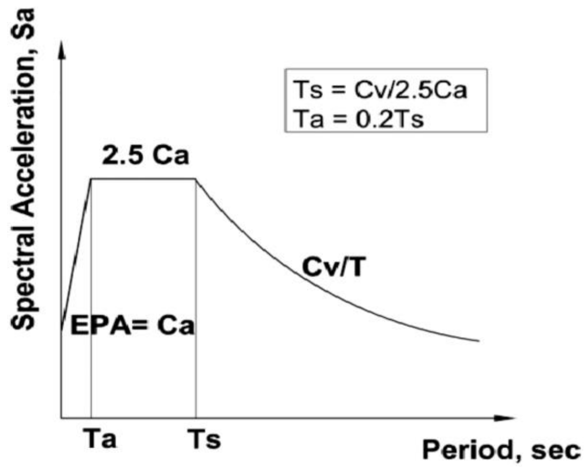

Figure 3.6 Elastic Acceleration Response Spectrum Defined in ATC-40 [12]

Table 3.14 Seismic coefficient C_A According to ATC-40 [12]

Soil Profile Type	Shaking Intensity					
	=0.075	=0.15	=0.2	=0.3	=0.4	>0.4
S_B	0.08	0.15	0.20	0.30	0.40	1.0
S_C	0.09	0.18	0.24	0.33	**0.40**	1.0
S_D	0.12	0.22	0.28	0.35	0.44	1.1
S_E	0.19	0.30	0.34	0.36	0.36	0.9
S_F	Site-specific geotechnical investigation required to determined C_A					

Table 3.15 Seismic coefficient C_V According to ATC-40 [12]

Soil Profile Type	Shaking Intensity					
	=0.075	=0.15	=0.2	=0.3	=0.4	>0.4
S_B	0.08	0.15	0.20	0.30	0.40	1.0
S_C	0.13	0.25	0.32	0.45	**0.56**	1.4
S_D	0.18	0.32	0.40	0.54	0.64	1.6
S_E	0.26	0.5	0.64	0.84	0.96	2.4
S_F	Site-specific geotechnical investigation required to determined C_A					

Figure 3.7 Seismic Coefficients Defined in SAP2000 [3] according to ATC-40 [12]

3.2.3.2 Ground Motion Records

NLTHA was performed to produce a collection of trustworthy reference that could be used to assess the precision of other analysis methods. Ground motion characteristics such as duration, frequency, site conditions, magnitude, etc. have significant effects on the nonlinear behavior of structures. On the contrary, the linear behavior is much less sensitive to ground motion characteristics. Therefore, an adequate number of strong ground motion records shall be used to predict the nonlinear behavior of the structures. The adequacy is a relative phenomenon however, minimum of eleven ground motion records was recommended for the NLTHA of the RC structural models by most of the design codes such as ASCE7-22 [4].

In this study, a group of eleven ground motion records were obtained from Berkeley's Pacific Earthquake Engineering Research (PEER) Center's [33] strong ground motion database as shown in Figure 3.8. These ground motions were chosen from earthquakes with moment magnitudes ranging from 6.61 to 7.36. Near-field earthquakes are the earthquakes occurring in fields close to the fault. Recordings with less than 10 km distance to the fault line may have near-field effects that may produce inconsistent results in the analysis. Therefore, the selected ground motion records were located between 11.46 and 45.48 km from a rupturing fault as shown in Table 3.16. All the ground motions were recorded on very dense soil and soft rock profile which simulated the effect of Site Class C. All the records were scaled up to a peak ground acceleration of 1×g to ensure that the building frames would deform inelastically when exposed to these ground motions. The direct integration method was used for the analysis type. A damping ratio of 5% was used for the first and second modes of structural vibration to define the Rayleigh damping. All analyses included the P-Delta effects. According to the requirements of ASCE 7-22 [3], the final responses of the NLTHA for each building were determined as the average value of the peak structural response obtained from nonlinear dynamic analyses of each earthquake ground motion record.

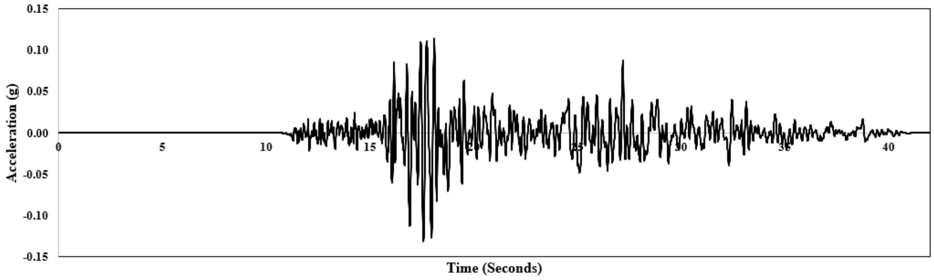

1. Record: Duzce, Turkey (1999, Lamont 1061)

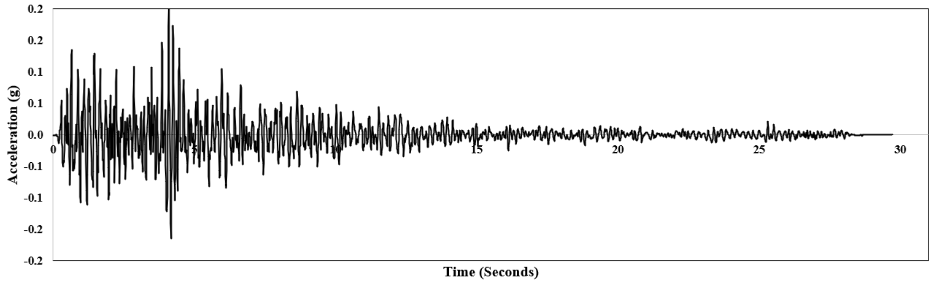

2. Record: San Fernando (1971, Santa Anita Dam)

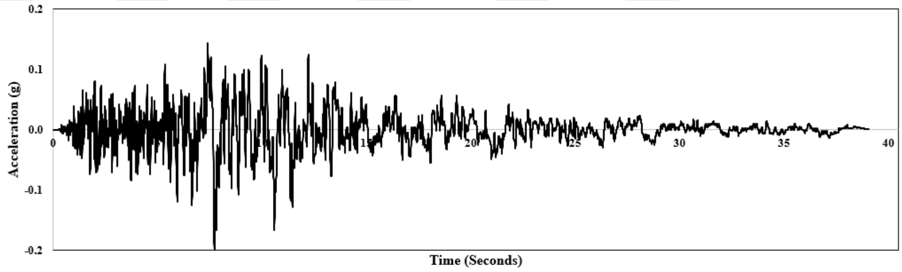

3. Record: Loma Prieta (1989, APEEL7 - Pulgas)

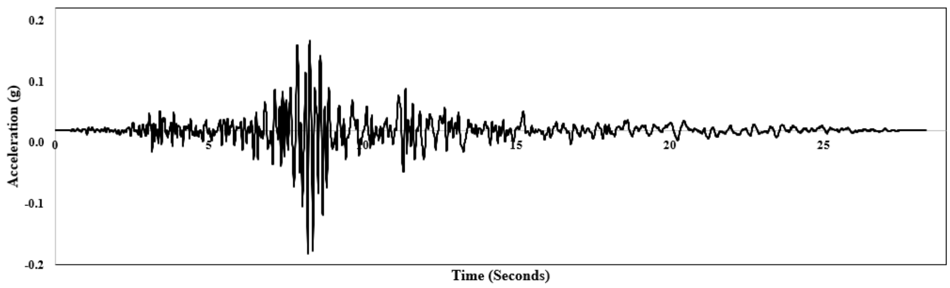

4. Record: Imperial-Valley (1979, Superstition Mtn. Camera)

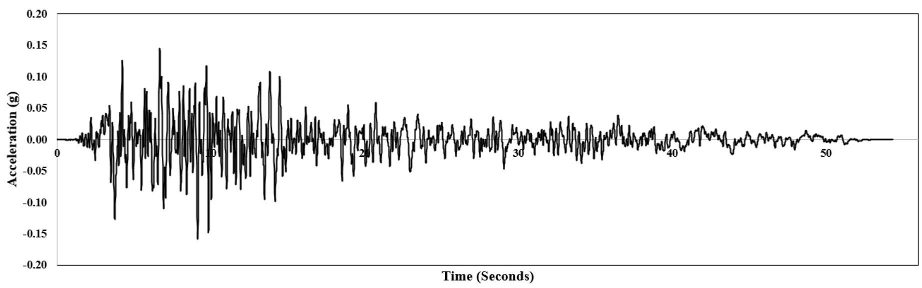

5. Kern County (1952, Taft Lincoln School)

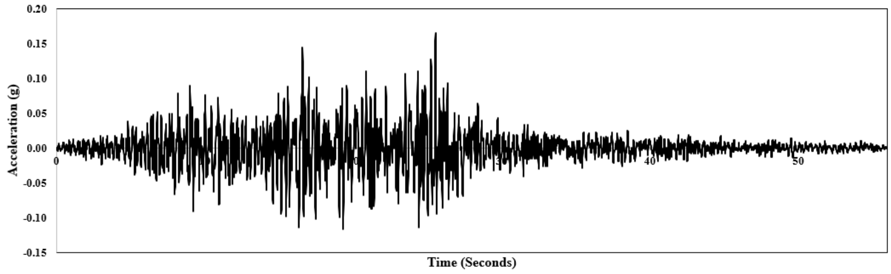

6. Landers (1992, Big Bear Lake)

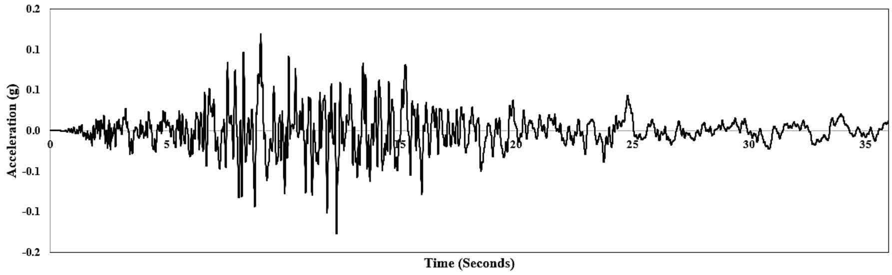

7.Loma Prieta (1989, Fremont - M. San Jose)

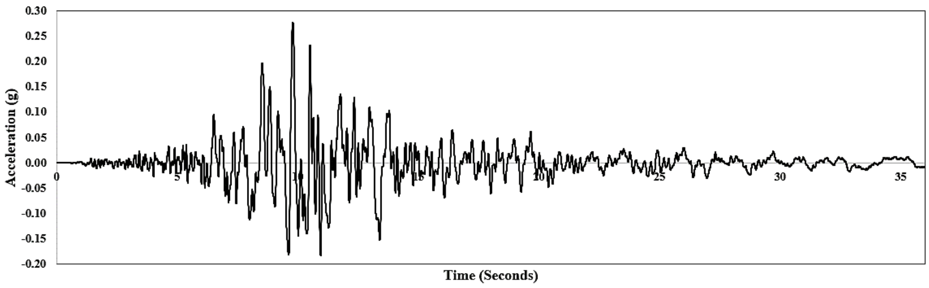

8. Loma Prieta (1989 Palo Alto - SLAC Lab)

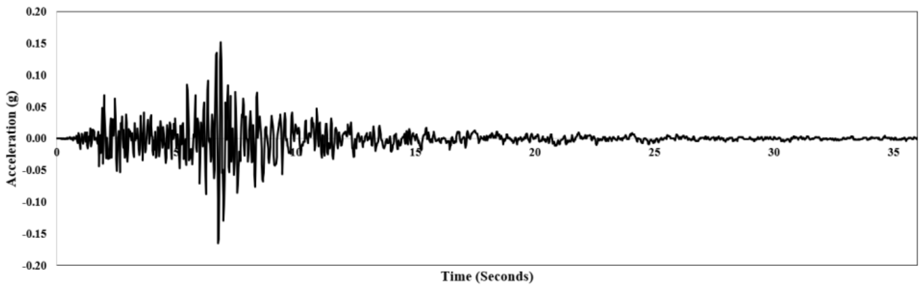

9. Northridge-01 (1994, Lake Hughes)

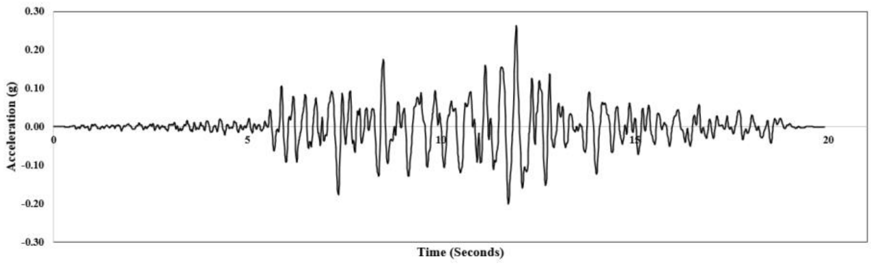

10. Northridge-01 (1994, Pasadena - N. Sierra Madre)

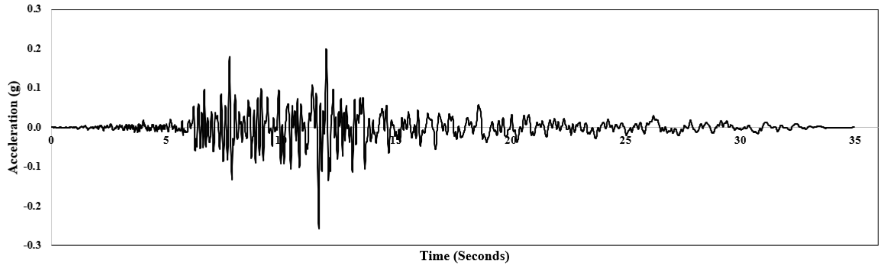

11. Northridge-01 (1994, San Gabriel – E. Grand Ave.)

Figure 3.8 Acceleration-Time Histories of Ground Motion Records

Table 3.16 Earthquakes Records Used in This Study (All Recorded on Soil Type C)

Earthquake Name	Station	Magnitude	R_{rup} (km)	PGA(g)
Duzce Turkey	Lamont 1061 - 1999	7.14	11.46	0.131
Kern County	Taft Lincoln School - 1952	7.36	38.89	0.159
San Fernando	Santa Anita Dam - 1971	6.61	30.7	0.22
Imperial Valley-6	Superstition Mtn. Camera - 1979	6.53	24.61	0.23
Landers	Big Bear Lake - 1992	7.28	45.48	0.165
Loma Prieta	APEEL7 – Pulgas - 1989	6.93	41.86	0.16
Loma Prieta	Fremont - M. San Jose - 1989	6.93	39.51	0.13
Loma Prieta	Palo Alto - SLAC Lab -1989	6.93	30.86	0.28
Northridge	Lake Hughes #9 - 1994	6.69	25.36	0.806
Northridge	Pasadena - N. Sierra Madre - 1994	6.69	36.12	0.26
Northridge	San Gabriel – E. Grand Ave. - 1994	6.69	39.31	0.26

The pseudo-acceleration response spectrum of each ground motion record was scaled to match the 5% damped spectrum at the fundamental period of structure (ASCE 7-22 [3]). The mean elastic pseudo-acceleration spectra (for 5% damped behavior) of the scaled ground motion records is shown in Figure 3.9.

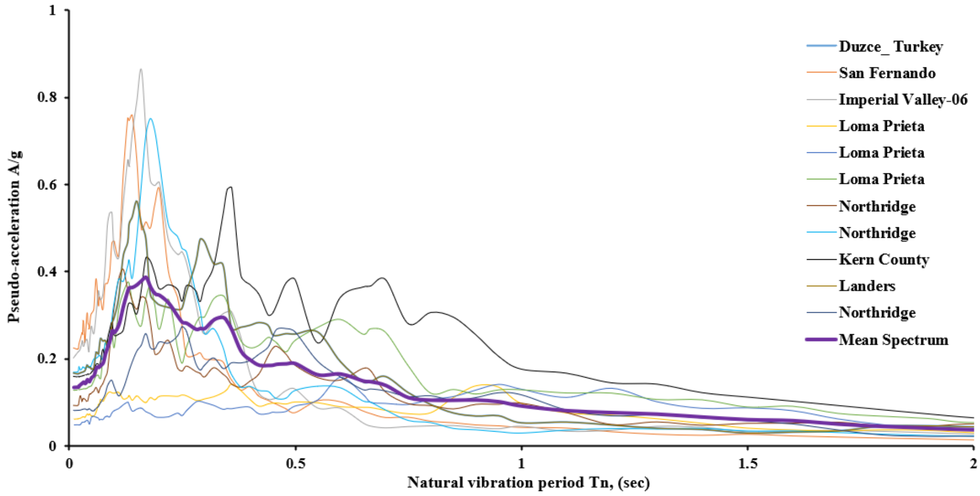

Figure 3.9 Pseudo-Acceleration Spectra of Ground Motion Records Used

3.3 Application of Pushover Analysis

The models were produced in accordance with the linear analysis approach. Typically, a gravity load pushover is force controlled and lateral pushover is displacement controlled. In this study, more than one pushover load cases were defined and performed for each of the model. The user defined pushover displacement magnitude was obtained from NLTHA for each model. The load pattern was taken as acceleration in y-direction. Finally, the static nonlinear pushover analysis was performed.

The seismic masses of the models were defined as the full dead load (including the superimposed dead load) and 25% of the live load (specified by ASCE 7-22 [3]) as shown in Figure 3.10. The load patterns consisted of dead, live, and superimposed dead loads. The earthquake loads were applied using the elastic acceleration response spectrum obtained using ASCE 7-22 [3]. This earthquake loading was applied in x- and y-directions. However, in this study only the results in y-direction were evaluated, since that direction was the direction of the application of setback. The defined load patterns and seismic load pattern specified by ASCE 7-22 [3] are shown in Figure 3.11 and Figure 3.12.

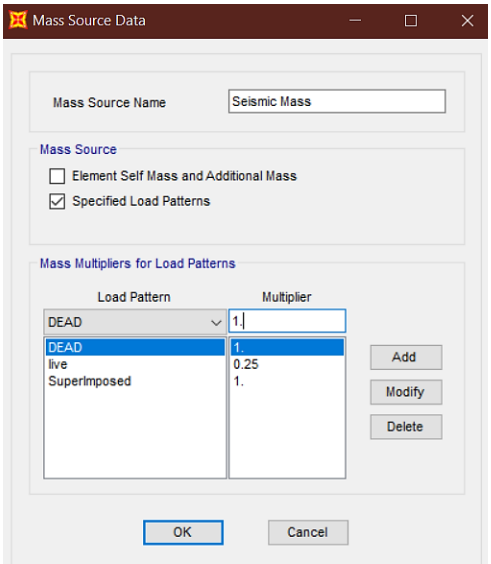

Figure 3.10 Definition of Seismic Mass

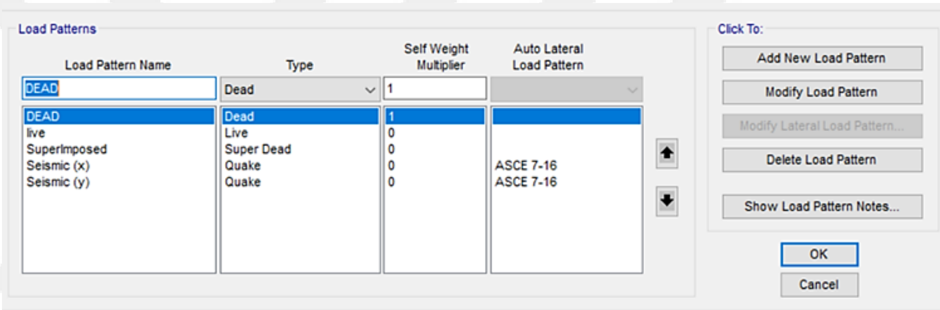

Figure 3.11 Definition of Load Patterns

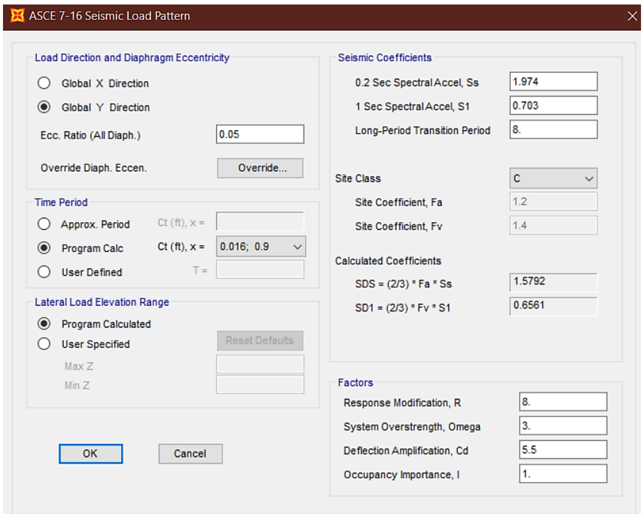

Figure 3.12 Deifinition of Seismic Load Pattern According to ASCE 7-22 [3]

The load cases were defined as shown in Figure 3.13. The pushover analysis started from the load case "Gravity" which included the effect of dead, superimposed dead, and live loads as shown in Figure 3.14.

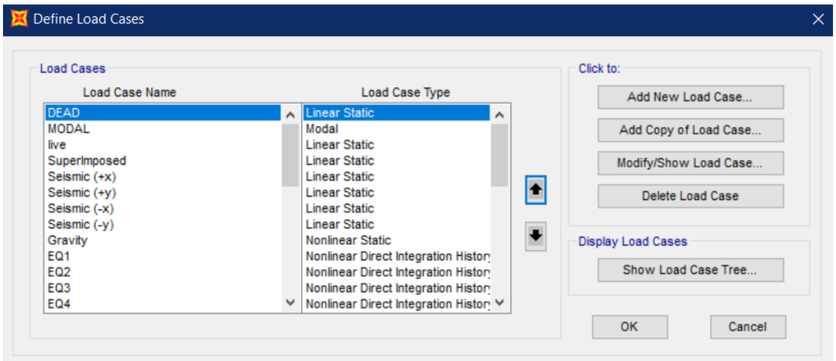

Figure 3.13 Definition of Load Cases

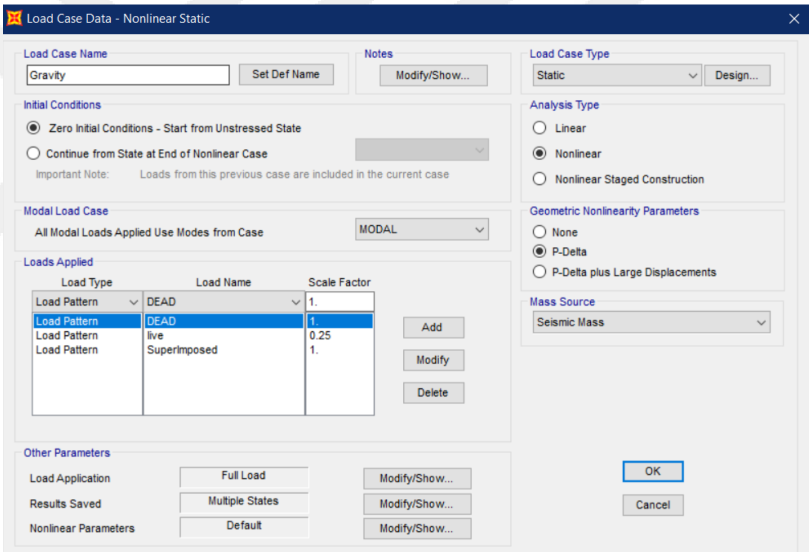

Figure 3.14 Definition of Load Case Data for Nonlinear Static Analysis

The conventional pushover analysis was performed for all the models using three different lateral load patterns (TLP, ULP, and FLP (first mode was used in calculation of the lateral loads)). The results of these analyses were used to obtain the seismic behavior of the models at the lower stories. Later the regular and irregular buildings were analyzed using the MUB and EUB, respectively, to include the effect of higher modes in the analysis. In MUB, the first and second mode (as a summation of modes) were used to determine the lateral load pattern. In EUB, the analysis is performed four times. The EUB is performed for first mode only, summation of first two modes, summation of first three modes, and summation of first four modes as shown in Figure 3.15.

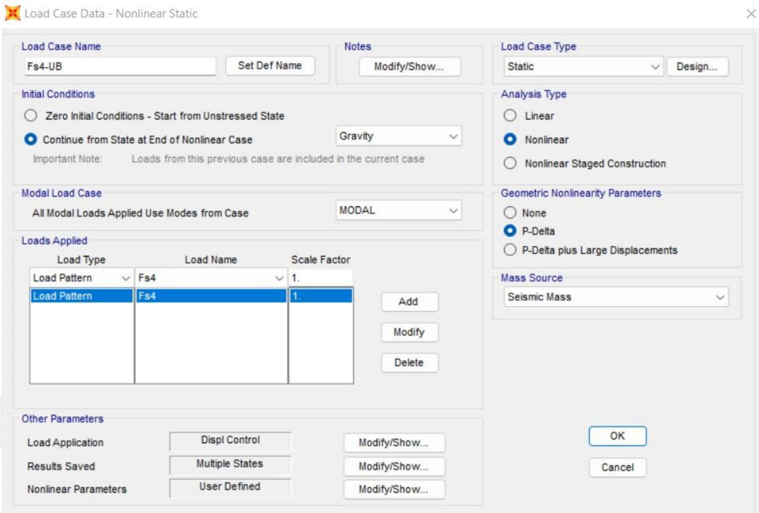

Figure 3.15 Definition of Load Case Data for EUB (summation of first four modes)

The pushover analysis was performed in a displacement-controlled manner at a joint at the roof story of each model. The target displacements used in these analyses were obtained from the maximum average displacement values of the NLTHA for the roof story. Note that only the results in y-direction was evaluated, since that direction was the direction of the application of setback. During the analysis, multiple states were selected to be saved. This enabled to review the results of the analysis also at intermediate steps. An example of the defined values for pushover analysis are shown in Figure 3.16.

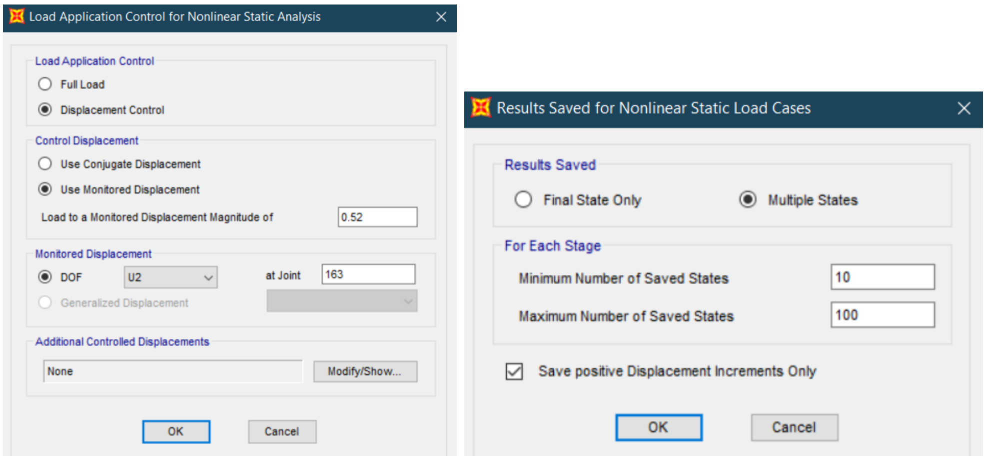

a) Load Application b) Results Saved

Figure 3.16 Nonlinear Static Analysis for Different Pushover Load Cases Control

3.3.1 Plastic Hinges

Plastic hinge is a state of an inelastic behavior of structural members at their ends. When a structural member is under bending, after a specific rotation value at the ends, the rotation of the structural member starts increasing without carrying any more bending. The member cannot return to its initial position even the flexural load is removed. To simulate this behavior in the models, hinges shall be assigned at the ends of the structural members. In this study (Figure 3.17), M3 hinges were assigned to the ends of the beams and P-M2-M3 hinges were assigned to the ends of the columns since the columns also carry axial loading According to ASCE 41-13 [34]. The assigned hinge properties for beams and columns are shown in Figure 3.18 to Figure 3.21.

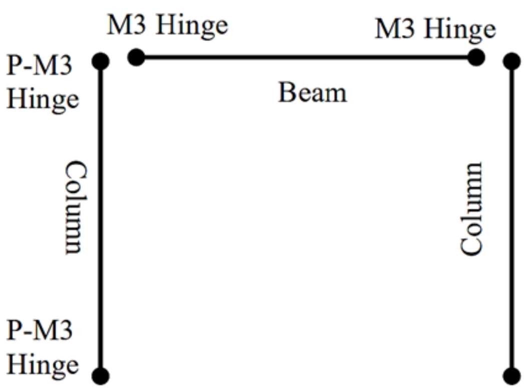

Figure 3.17 Definition of Plastic Hinge Assignment for Beams and Columns

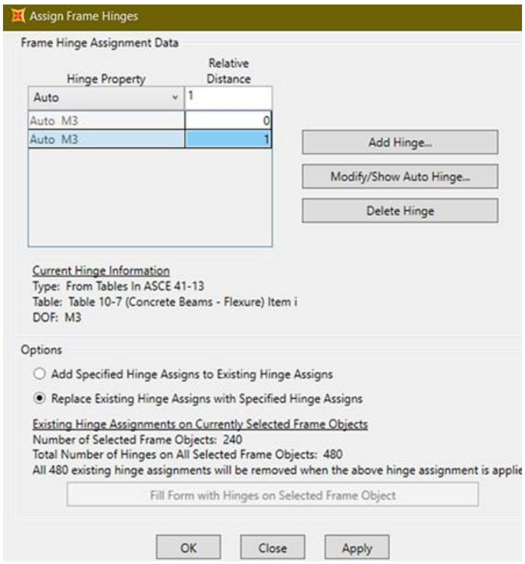

Figure 3.18 Definition of Frame Hinge Assignment for Beams

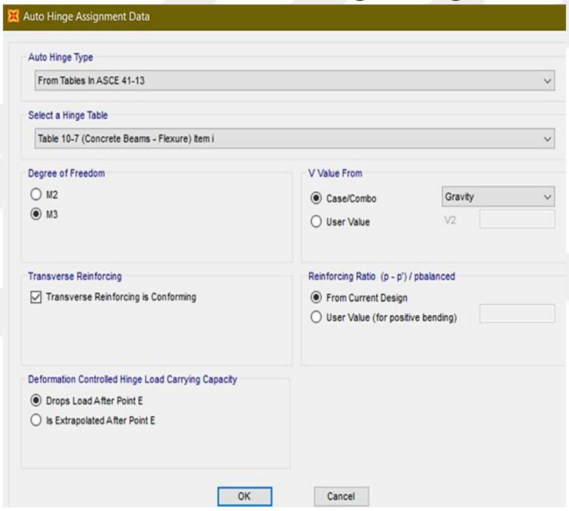

Figure 3.19 Definition of Auto Hinge Assignment for Beams

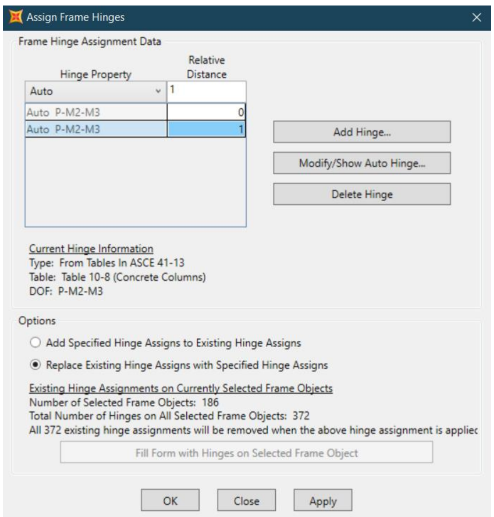

Figure 3.20 Definition of Frame Hinge Assignment for Columns

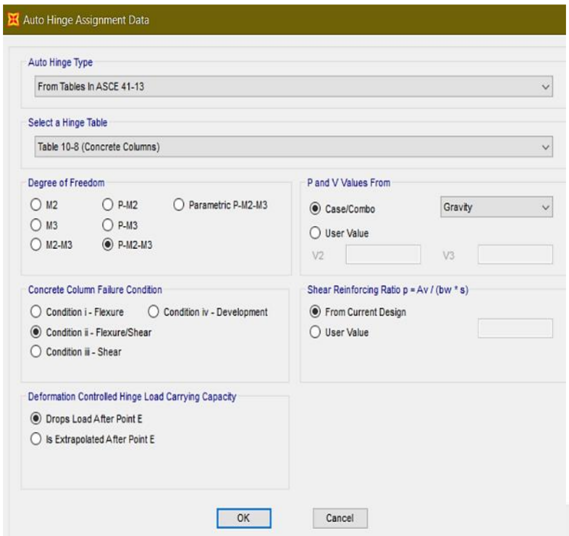

Figure 3.21 Definition of Auto Hinge Assignment for Columns

In pushover analysis, the formation of hinges at intermediate deflection values can be tracked for each deflection increase. The power of this method lies under this property which enables the designer to observe the structural behavior of successive loss of strength owing to seismic action and thereby the loss of the structure stiffness.

CHAPTER 4

4. RESULTS AND DISCUSSIONS RELATED TO SEISMIC DEMAND USING ENHANCED PUSHOVER ANALYSIS

4.1 General

SAP2000 Software [3] was used to perform the NLTHA and pushover analysis of building models. This software can perform pushover analyses on two- and three-dimensional models, either a displacement-controlled or a force-controlled manner. Pushover analyses were performed on mid-(6 story), and high-rise (12 story) RC frames using various lateral load patterns to investigate the effects of lateral load pattern on the global behavior of structure. The capacity curve and demand predictions of pushover analysis were also obtained. The accuracy of various lateral load patterns to estimate the seismic behavior of models subjected to eleven ground motion records was determined. The calculated response parameters obtained from pushover analysis such as story displacements, interstory drift ratios, story shears, and plastic hinge locations were compared to the results obtained from the NLTHA. The NLTHA results were the control values which yields the actual behavior of the model buildings.

The fundamental time period of the structure is an important parameter which represents the dynamic response of the structure under seismic action. However, the seismic design codes specify the same expression of the fundamental time period for both regular and irregular building structures. Free vibration analyses of the frames were performed using SAP2000 [3] to determine elastic periods and mode shapes. The dynamic properties of the first four modes in y-direction of the model buildings used in this study are summarized in Table 4.1. The summation of modal mass participation ratios of the first four modes in y-direction is also shown in this table. The first four modes in y-direction were normalized to have unit modal amplitude value at roof story level as shown in Figure 4.1. The results indicated that the period of the building models decreased with the increase in the vertical setback irregularity. For regular building models, since the model is symmetric, the first and second modes were identical. For regular building models, no torsional mode shape was obtained in y-direction. For irregular building models, the torsional mode shape appeared to be an effective mode that might have a noticeable effect on the behavior of the model.

Table 4.1 Natural Periods of The First Four Translational Modes of Vibration

Model	Natural Time Periods (sec)				Modal Participating Factors (Γ_n)				Summation of Modal Participating Mass Ratio of First Four Modes in Y-Direction (%)
	T_1	T_2	T_3	T_4	Γ_1	Γ_2	Γ_3	Γ_4	
M1-6S-R	1.66	1.66	0.51	0.26	1.31	1.31	-0.47	0.24	95
M2-12S-R	2.36	2.36	0.85	0.47	1.36	1.36	-0.55	0.32	90
M3-6S-IR	1.44	1.04	0.50	0.28	1.43	1.54	-0.68	0.35	96
M4-12S-IR	2.24	1.60	0.86	0.49	1.49	1.57	-0.81	0.51	91
M5-6S-IR	1.43	1.04	0.55	0.48	1.43	1.56	-0.50	-0.70	93
M6-12S-IR	2.45	1.80	0.96	0.48	1.46	1.63	-0.54	0.45	87

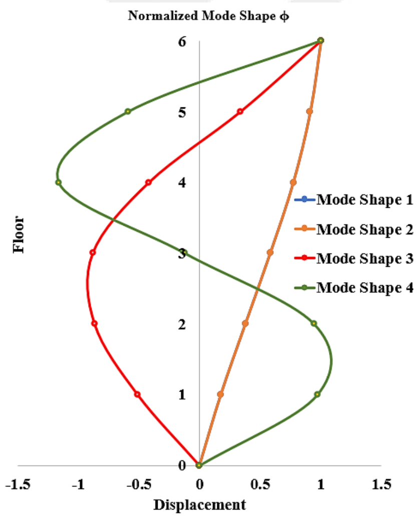

a) M1-6S-R

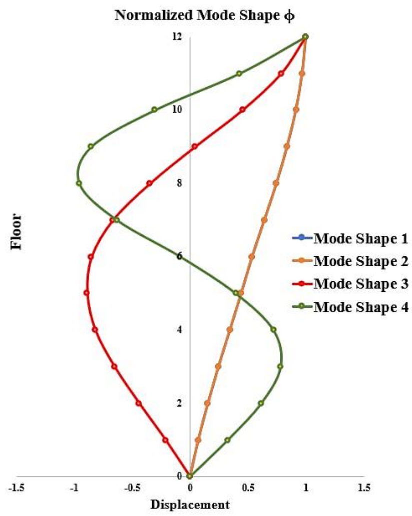

b) M2-12S-R

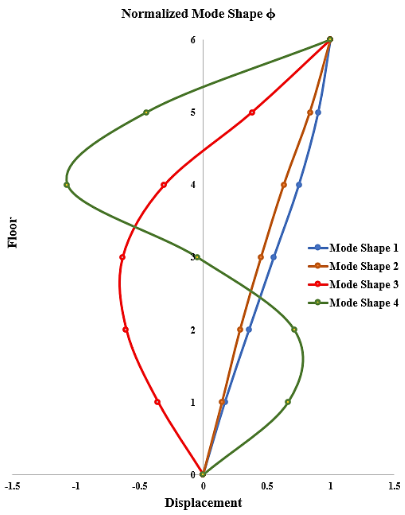

c) M3-6S-IR

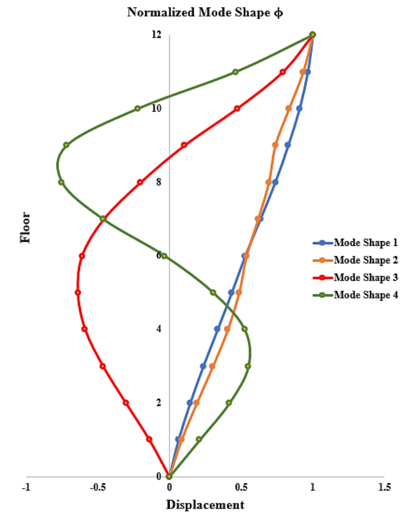

d) M4-12S-IR

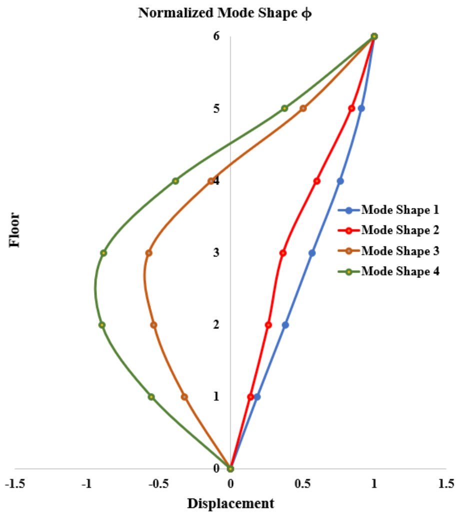

e) M5-6S-IR

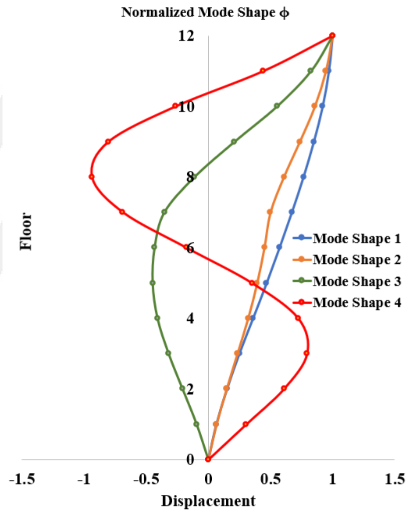

f) M6-12S-IR

Figure 4.1 Normalized First Four Mode Shapes of Building Models Used in This Study

The seismic demands (story displacement and plastic hinge rotations) were obtained for a selected frame in the model only in y-direction. For regular structures, any frame may be selected to obtain these seismic demands. However, in irregular buildings, a continuous frame that is not interrupted by irregular geometry was selected.

4.2 Results of NLTHA

The NLTHA was performed to determine the target displacement values for the pushover analysis. The average value of the roof displacements was calculated using the NLTHA for each ground motion was used as the target displacement value at the top floor for all the models. The values of the target displacements for each model are shown in Table 4.2.

Table 4.2 Target Displacement Values for Regular and Irregular Building Models

Model	Target Displacement (m)
M1-6S-R	0.33
M2-12S-R	0.45
M3-6S-IR	0.29
M4-12S-IR	0.48
M5-6S-IR	0.21
M6-12S-IR	0.51

4.3 Lateral Load Patterns for Pushover Analysis

Three different lateral load patterns, namely ULP, FLP, and TLP, were used to apply the lateral loading on the models due to earthquake. These lateral loads are explained in the following subsections.

4.3.1 Uniform Lateral Load Pattern (ULP)

The ULP can be defined as the application of the lateral forces at any story proportional to the mass of that story as a portion of base shear (FEMA 356 [2]). The expression of the calculation of story forces is shown in the equation below.

$$F_i = \frac{\mathrm{m_i}}{\sum m_i}\mathrm{V_b} \qquad \text{Equation 4-1}$$

where F_i is the lateral force at i^{th} story, m_i is the mass of i^{th} story, and V_b is the total design lateral force or shear at the base of the model obtained from analysis.

Typical calculations of the story forces for the ULP for Model M1-6S-R are shown in Table 4.3. The story forces for other models are shown in Table 4.4.

Table 4.3 Typical Calculation of Lateral Story Force Calculations According to ULP (M1-6S-R)

Story	Mass, m_i (kg)	$\frac{m_i}{\sum m_i}$	F_i (kN)

0	0	0	0
1	8418601	0.1735	698
2	8246964	0.1700	684
3	8126957	0.1675	674
4	8006963	0.1651	664
5	8006954	0.1651	664
6	7704463	0.1588	639
$\sum m_i$=	48510902	$\sum V_b$=	4023

Table 4.4 Lateral Story Force Calculations of Other Models According to ULP

Story	**F_i (kN)**				
	M2-12S-R	**M3-6S-IR**	**M4-12S-IR**	**M5-6S-IR**	**M6-12S-IR**
0	0	0	0	0	0
1	684	222	664	815	653
2	663	455	644	801	632
3	647	531	628	781	616
4	631	698	612	429	600
5	631	587	612	437	600
6	622	627	598	422	593
7	593		445		592
8	593		445		318
9	589		437		315
10	585		306		312
11	585		306		312
12	564		293		299
$\sum V_b$=	7385	3119	5987	3685	5841

4.3.2 First Modal Shape Lateral Load Pattern (FLP)

In FLP, the lateral forces are calculated in proportion to the elastic modal shape amplitudes and mass for each floor (FEMA 356 [2]). The expression of the calculation of story forces, F_i, is shown in the equation below.

$$F_i = \frac{m_i \, \phi_i}{\sum m_i \, \phi_i} V_b \qquad \text{Equation 4-2}$$

where ϕ_i is the amplitude of the elastic mode shape at i^{th} story.

Typical calculations of the story forces for the FLP for Model M1-6S-R are shown in Table 4.5. The story forces for other models are shown in Table 4.6.

Table 4.5 Typical Calculation of Lateral Story Force Calculations for FLP (M1-6S-R)

Story	$m_i\phi_i$	$m_i\phi_i/\Sigma m_i\phi_i$	Lateral Forces (kN)
0	0	0	0
1	1473311	0.048292	194
2	3111484	0.101987	410
3	4729980	0.155038	624
4	6183355	0.202677	815
5	7305894	0.239471	963
6	7704463	0.252535	1016
$\sum m_i\phi_i$=	30508487	$\sum V_b$=	4023

Table 4.6 Lateral Story Force Calculations of Other Models According to FLP

Story	F_i (kN)				
	M2-12S-R	**M3-6S-IR**	**M4-12S-IR**	**M5-6S-IR**	**M6-12S-IR**
0	0	0	0	0	0
1	87	709	87	273	83
2	183	687	192	549	189
3	285	521	305	800	307
4	389	506	424	588	431
5	500	354	547	715	562
6	598	354	650	759	678
7	682		580		794
8	793		676		487
9	884		745		534
10	959		571		573
11	1015		607		604
12	1011		603		597
$\sum V_b$=	7385	3119	5987	3685	5841

4.3.3 Triangular Lateral Load Pattern (TLP)

This lateral load pattern is defined in ASCE 7-22 [3]. In TLP, the total base shears are distributed to the story levels in proportion to the multiplication of the mass and height of that story as shown in Figure 4.2. The lateral seismic force, F_x, induced at any level shall be determined from the following expression:

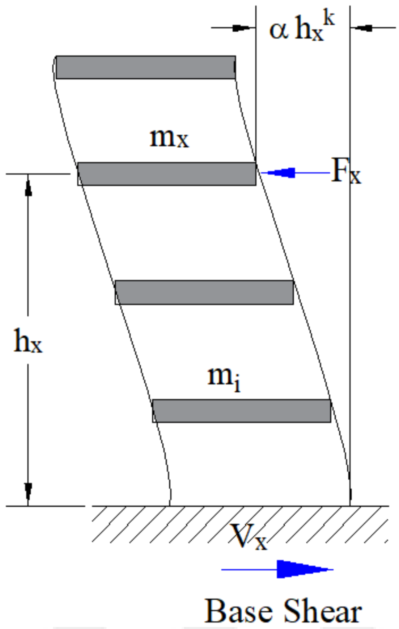

Figure 4.2 Lateral Load Distribution in TLP (ASCE 7-22 [3])

$$C_{vx} = \frac{F_x}{V_b} = \frac{m_x h_x^k}{\sum_n^{i=1} m_i h_i^k} \quad \text{Equation 4-3}$$

$$F_x = C_{vx} V_b \quad \text{Equation 4-4}$$

where C_{vx} is the vertical distribution factor of the story x, V_b is the total design base shear of the structure, m_i and m_x are the portion of the total effective seismic masses of the structure assigned to level i and x, F_x is the inertial force at level x, h_i and h_x are the heights from the base to level i and x, and k is the exponent related to the structure period as follows:

$k = 1$ for $T_1 \leq 0.5$ s Equation 4-5

$k = 2$ for $T_1 \geq 2.5$ s Equation 4-6

For structures that have a period between 0.5 and 2.5 s, k may be taken as 2 or determined by linear interpolation between 1 and 2. The variation of this exponent k for various fundamental period values is shown in Figure 4.3.

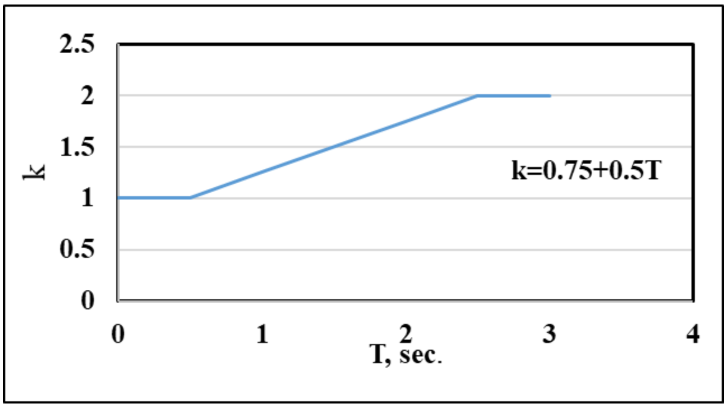

Figure 4.3 Variation of Exponent k for Various Fundamental Period Values

Typical calculations of the story forces for the TLP for Model M1-6S-R are shown in Table 4.7. The story forces for other models are shown in Table 4.8.

Table 4.7 Typical Calculation of Lateral Story Force Calculations for TLP (M1-6S-R)

Story	m_x **(tons)**	**k**	h_i **(m)**	h_i^k	$m_i h_i^k$	C_{vi}	**F_i (kN)**
1	8419	1.582	4.5	11	90849	0.0322	130
2	8247	1.582	7.7	25	208118	0.0737	297
3	8127	1.582	10.9	44	355348	0.1259	507
4	8007	1.582	14.1	66	526015	0.1864	750
5	8007	1.582	17.3	91	726910	0.2576	1036
6	7704	1.582	20.5	119	914802	0.3242	1304
				$\sum m_i h_i^k$=	2822042	$\sum V_b$=	4023

Table 4.8 Lateral Story Force Calculations of Other Models According to TLP

Story	**F_i (kN)**				
	M2-12S-R	**M3-6S-IR**	**M4-12S-IR**	**M5-6S-IR**	**M6-12S-IR**
0	0	0	0	0	0
1	24	175.6	28	204	28
2	67	375.2	80	440	80
3	132	474.3	156	713	155
4	215	671.8	255	572	253
5	323	635.4	384	785	381
6	447	786.8	526	972	529
7	570		523		705
8	734		674		489
9	913		830		606
10	1109		710		733
11	1333		853		881
12	1520		967		1000
$\sum V_b$=	7385.299	3119.059	5987.278	3684.95	5840.572

Figure 4.4 to Figure 4.9 depict the lateral load distributions for regular and irregular buildings, respectively. The influence of mass distribution effects for irregular building has a noticeable effect on shear force distribution in these figures.

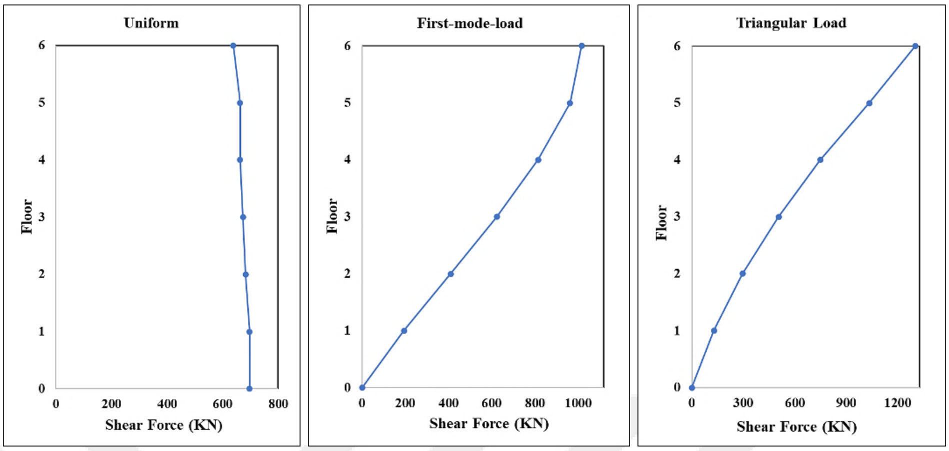

a) ULP b) FLP c) TLP

Figure 4.4 Lateral Load Patterns for Building Model M1-6S-R

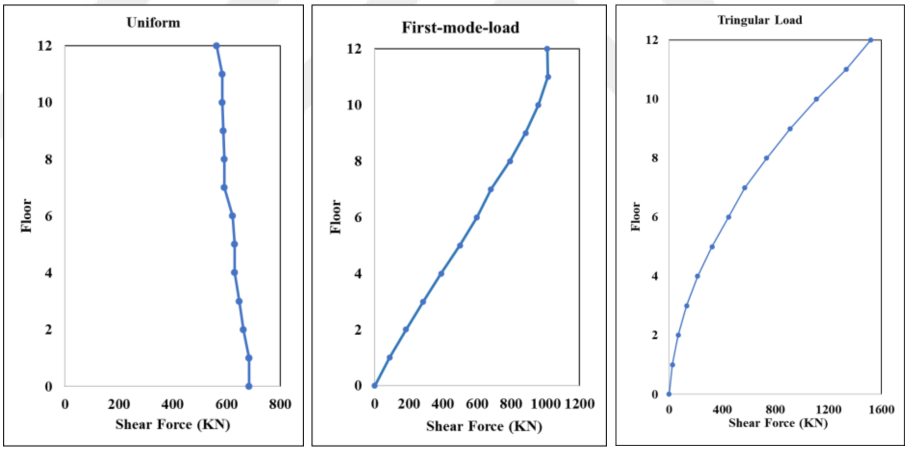

a) ULP b) FLP c) TLP

Figure 4.5 Lateral Load Patterns for Building Model M2-12S-R

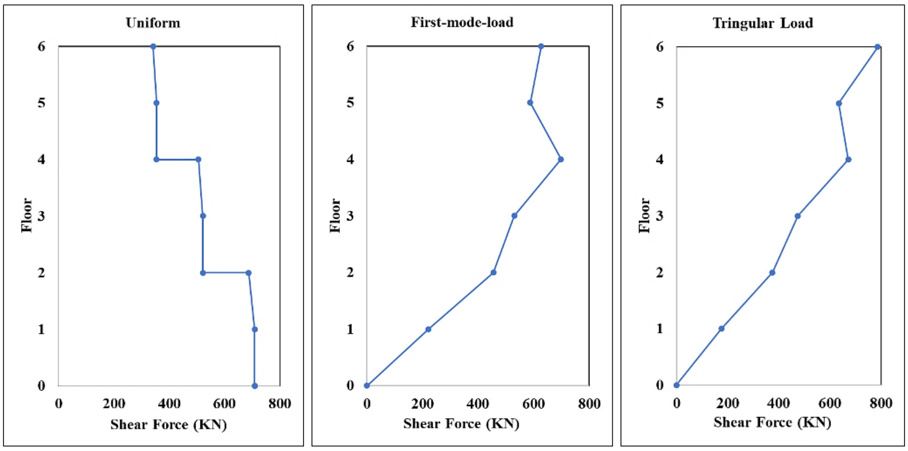

a) ULP b) FLP c) TLP

Figure 4.6 Lateral Load Patterns for Building Model M3-6S-IR

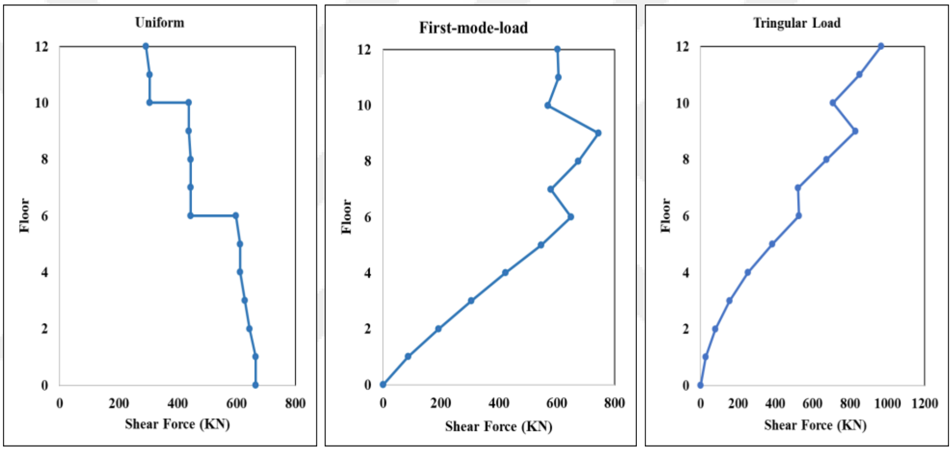

a) ULP b) FLP c) TLP

Figure 4.7 Lateral Load Patterns for Building Model M4-12S-IR

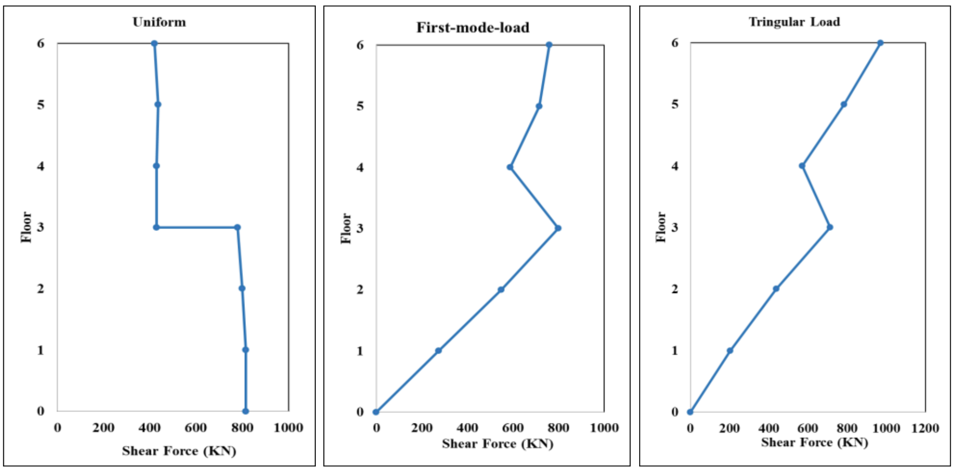

a) ULP b) FLP c) TLP

Figure 4.8 Lateral Load Patterns for Irregular Building M5-6S-IR

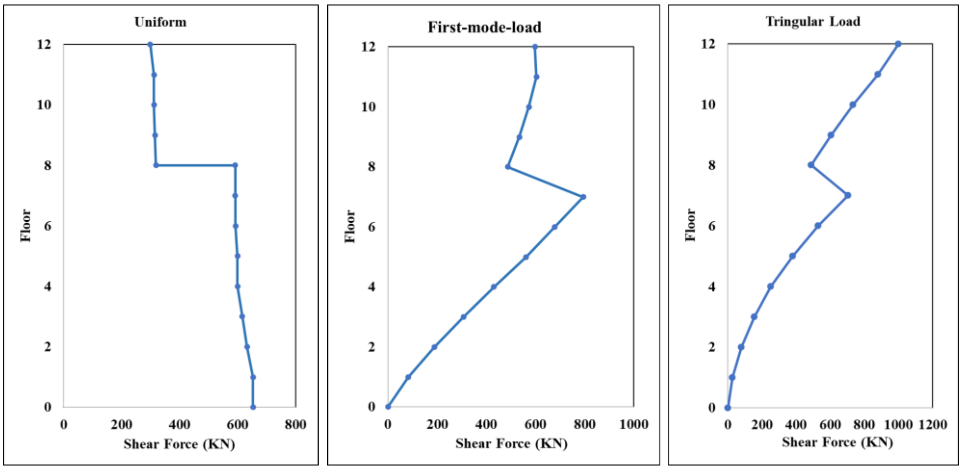

a) ULP b) FLP c) TLP

Figure 4.9 Lateral Load Patterns for Irregular Building M6-12S-IR

4.4 Displacements and Interstory Drift Ratios

The evaluation of the story displacements and corresponding interstory drift ratios (ratio of displacement difference between two consecutive stories to the story height as shown in the equation below) during an earthquake is one of the most important measuring tools. By comparing the evaluated interstory drift ratios to the limits of the codes and standards, the designer can determine whether the behavior of the building frame is acceptable or not. According to ASCE 7-22 [3] for buildings in the Risk II Category, the maximum story drift ratio is limited to 0.020.

$$Storey\ Drift\ Ratio = \frac{D_{x+1} - D_x}{h_x} \qquad \text{Equation 4-7}$$

where D_{x+1} is the displacement of top of the calculated story, D_x is the displacement of bottom of the calculated story, and h_x is the height of the calculated story.

The story displacements and drift ratios obtained from all the analysis (TLP, FLP, ULP, MUB, EUB, and NLTHA) of all the models are presented in this section.

It is worth noting that the response of the EUB procedure is obtained using combination ratio of responses derived from the four first modes of vibration and for all the structural models. Conventional pushover analysis controls the seismic demands of lower stories, whereas upper-bound pushover analysis controls the seismic demands of upper stories, where higher modes have a greater influence. According to these analyses, the maximum values of displacements and interstory drift ratios presented here are for the internal frame of the building models in the Y-direction. Story displacement values and interstory drift ratios of the building models studied in this research are shown in Table 4.9 to Table 4.20.

Table 4.9 Story Displacements for Model M1-6S-R

Story	Height (m)	TLP (m)	FLP (m)	ULP (m)	NLTHA (m)	MUB (m)
6	20.5	0.331	0.3249	0.3306	0.2986	0.3310
5	17.3	0.317	0.3068	0.3175	0.2853	0.3078
4	14.1	0.277	0.2751	0.2852	0.2625	0.2687
3	10.9	0.197	0.2147	0.2223	0.2217	0.2089
2	7.7	0.138	0.1535	0.1592	0.1720	0.1459
1	4.5	0.078	0.0884	0.0919	0.1092	0.0740
0	0	0	0	0	0	0

Table 4.10 Interstory Drift Ratios for Model M1-6S-R

Story	Height (m)	TLP (%)	FLP (%)	Uniform (%)	NLTHA (%)	MUB (%)
6	20.5	0.45	0.41	0.42	0.46	0.41
5	17.3	1.16	1.01	0.71	1.22	1.01
4	14.1	2.26	1.96	1.28	1.87	1.96
3	10.9	1.83	1.97	1.55	1.97	1.97
2	7.7	1.88	2.10	1.96	2.25	2.10
1	4.5	1.73	2.04	2.43	1.64	2.04
0	0	0	0	0	0	0

Table 4.11 Story Displacements for Model M2-12S-RR

Story	Height (m)	TLP (m)	FLP (m)	Uniform (m)	NLTHA (m)	MUB (m)
12	39.7	0.4523	0.4540	0.4495	0.4521	0.4509
11	36.5	0.4418	0.4463	0.4440	0.4389	0.4440
10	33.3	0.4242	0.4332	0.4346	0.4155	0.4296
9	30.1	0.3982	0.4134	0.4206	0.3838	0.4091
8	26.9	0.3654	0.3875	0.4026	0.3474	0.3825
7	23.7	0.3255	0.3541	0.3793	0.3127	0.3486
6	20.5	0.2809	0.3138	0.3496	0.2713	0.3082
5	17.3	0.2360	0.2702	0.3146	0.2383	0.2648
4	14.1	0.1890	0.2219	0.2711	0.1956	0.2172
3	10.9	0.1414	0.1700	0.2175	0.1488	0.1661
2	7.7	0.0960	0.1180	0.1577	0.1009	0.1151
1	4.5	0.0524	0.0662	0.0930	0.0539	0.0645

0	0	0	0	0	0	0

Table 4.12 Interstory Drift Ratios for Model M2-12S-RR

Story	Height (m)	TLP (%)	FLP (%)	Uniform (%)	NLTHA (%)	MUB (%)
12	39.7	0.33	0.24	0.17	0.41	0.22
11	36.5	0.55	0.41	0.29	0.73	0.45
10	33.3	0.81	0.62	0.44	0.99	0.64
9	30.1	1.03	0.81	0.56	1.14	0.83
8	26.9	1.25	1.04	0.73	1.09	1.06
7	23.7	1.39	1.26	0.93	1.29	1.26
6	20.5	1.41	1.36	1.09	1.03	1.35
5	17.3	1.47	1.51	1.36	1.33	1.49
4	14.1	1.49	1.62	1.67	1.46	1.60
3	10.9	1.42	1.63	1.87	1.50	1.59
2	7.7	1.36	1.62	2.02	1.47	1.58
1	4.5	1.16	1.47	2.07	1.20	1.43
0	0	0	0	0	0	0

Table 4.13 Story Displacements for Model M3-6S-IR

Story	Height (m)	TLP (m)	FLP (m)	Uniform (m)	NLTHA (m)	EUB (m)
6	20.5	0.2886	0.2900	0.2504	0.2901	0.2907
5	17.3	0.2685	0.2697	0.2388	0.2734	0.2810
4	14.1	0.1893	0.2280	0.2196	0.2264	0.2314
3	10.9	0.1435	0.1792	0.1907	0.1795	0.1817
2	7.7	0.1034	0.1318	0.1557	0.1363	0.1337
1	4.5	0.0611	0.0800	0.1096	0.0877	0.0812
0	0	0	0	0	0	0

Table 4.14 Interstory Drift Ratios for Model M3-6S-IR

Story	Height (m)	TLP (%)	FLP (%)	Uniform (%)	NLTHA (%)	EUB (%)
6	20.5	0.63	0.63	0.36	0.52	0.30
5	17.3	2.47	1.30	0.60	1.47	1.55
4	14.1	1.43	1.52	0.90	1.47	1.56
3	10.9	1.25	1.48	1.10	1.35	1.50
2	7.7	1.32	1.62	1.44	1.52	1.64
1	4.5	1.36	1.78	2.44	1.95	1.80
0	0	0	0	0	0	0

Table 4.15 Story Displacements for Model M4-12S-IR

Story	Height (m)	TLP (m)	FLP (m)	Uniform (m)	NLTHA (m)	EUB (m)
12	39.7	0.5074	0.5090	0.5056	0.5058	0.5060
11	36.5	0.4539	0.4960	0.5000	0.4845	0.4899
10	33.3	0.4197	0.4724	0.4831	0.4478	0.4548
9	30.1	0.3773	0.4389	0.4581	0.4009	0.4089
8	26.9	0.3310	0.3989	0.4276	0.3529	0.3603
7	23.7	0.2830	0.3527	0.3910	0.3122	0.3151
6	20.5	0.2380	0.3018	0.3485	0.2743	0.2715
5	17.3	0.1931	0.2482	0.3007	0.2345	0.2254
4	14.1	0.1470	0.1914	0.2453	0.1885	0.1746

3	10.9	0.1015	0.1338	0.1825	0.1384	0.1230
2	7.7	0.0611	0.0815	0.1195	0.0899	0.0741
1	4.5	0.0263	0.0358	0.0592	0.0442	0.0332
0	0	0	0	0	0	0

Table 4.16 Interstory Drift Ratios for Model M4-12S-IR

Story	Height (m)	TLP (%)	FLP (%)	Uniform (%)	NLTHA (%)	EUB (%)
12	39.7	1.670	0.438	0.175	0.666	0.503
11	36.5	1.069	0.738	0.528	1.147	1.097
10	33.3	1.325	1.047	0.781	1.466	1.434
9	30.1	1.447	1.250	0.953	1.500	1.519
8	26.9	1.500	1.444	1.144	1.272	1.413
7	23.7	1.406	1.591	1.328	1.184	1.363
6	20.5	1.403	1.675	1.494	1.244	1.441
5	17.3	1.441	1.775	1.731	1.438	1.588
4	14.1	1.422	1.800	1.963	1.566	1.613
3	10.9	1.263	1.634	1.969	1.516	1.528
2	7.7	1.088	1.428	1.884	1.428	1.278
1	4.5	0.822	0.796	1.316	0.982	0.738
0	0	0	0	0	0	0

Table 4.17 Story Displacements for Model M5-6S-IR

Story	Height (m)	TLP (m)	FLP (m)	Uniform (m)	NLTHA (m)	EUB (m)
6	20.5	0.2085	0.2039	0.2018	0.2148	0.2108
5	17.3	0.1929	0.1894	0.1860	0.2007	0.1947
4	14.1	0.1627	0.1625	0.1555	0.1709	0.1625
3	10.9	0.0879	0.1071	0.0881	0.1307	0.1179
2	7.7	0.0596	0.0758	0.0598	0.0964	0.0800
1	4.5	0.0308	0.0422	0.0309	0.0550	0.0402
0	0	0	0	0	0	0

Table 4.18 Interstory Drift Ratios for Model M1-6S-R

Story	Height (m)	TLP (%)	FLP (%)	Uniform (%)	NLTHA (%)	EUB (%)
6	20.5	0.49	0.45	0.50	0.44	0.50
5	17.3	0.94	0.84	0.95	0.93	1.01
4	14.1	2.34	1.73	2.11	1.26	1.39
3	10.9	0.88	0.98	0.89	1.07	1.19
2	7.7	0.90	1.05	0.90	1.29	1.24
1	4.5	0.68	0.94	0.69	1.22	0.89
0	0	0	0	0	0	0

Table 4.19 Story Displacements for Model M6-12S-IR

Story	Height (m)	TLP (m)	FLP (m)	Uniform (m)	NLTHA (m)	EUB (m)
12	39.7	0.5074	0.5090	0.5056	0.5058	0.5060
11	36.5	0.4539	0.4960	0.5000	0.4845	0.4899
10	33.3	0.4197	0.4724	0.4831	0.4478	0.4548
9	30.1	0.3773	0.4389	0.4581	0.4009	0.4089
8	26.9	0.3310	0.3989	0.4276	0.3529	0.3603
7	23.7	0.2830	0.3527	0.3910	0.3122	0.3151

6	20.5	0.2380	0.3018	0.3485	0.2743	0.2715
5	17.3	0.1931	0.2482	0.3007	0.2345	0.2254
4	14.1	0.1470	0.1914	0.2453	0.1885	0.1746
3	10.9	0.1015	0.1338	0.1825	0.1384	0.1230
2	7.7	0.0611	0.0815	0.1195	0.0899	0.0741
1	4.5	0.0263	0.0358	0.0592	0.0442	0.0332
0	0	0	0	0	0	0

Table 4.20 Interstory Drift Ratios for Model M6-12S-IR

Story	Height (m)	TLP (%)	FLP (%)	Uniform (%)	NLTHA (%)	EUB (%)
12	39.7	0.687	0.538	0.475	0.666	0.667
11	36.5	1.069	0.738	0.528	1.147	1.097
10	33.3	1.325	1.047	0.781	1.466	1.434
9	30.1	1.447	1.250	0.953	1.500	1.519
8	26.9	1.500	1.444	1.144	1.272	1.413
7	23.7	1.406	1.591	1.328	1.184	1.363
6	20.5	1.403	1.675	1.494	1.244	1.441
5	17.3	1.441	1.775	1.731	1.438	1.588
4	14.1	1.422	1.800	1.963	1.566	1.613
3	10.9	1.263	1.634	1.969	1.516	1.528
2	7.7	1.088	1.428	1.884	1.428	1.278
1	4.5	0.822	0.796	1.316	0.982	0.738
0	0	0	0	0	0	0

The envelopes of story displacements and interstory drift ratios envelopes are shown in Figure 4.10 to Figure 4.15. The calculated errors of the results of TLP, FLP, ULP, MUB, and EUB methods compared to the NLTHA method are shown Table 4.21. In this table the smallest error values (best estimates) are shown in bold fonts. These figures indicated that the EUB method provided better predictions for irregular buildings. Based on these results, the predictions of interstory drift ratios of regular 6 story building model obtained using the TLP method provided more accurate results than other methods when compared to the NLTHA method. The results of the TLP method were in better agreement with the results of the NLTHA method compared to those of the FLP, ULP, and MUB methods. Especially at lower stories, the errors of the TLP and MUB methods compared to the NLTHA method for Model M1-6S-R were equal to approximately 1.8 and 6.3%, respectively. The results obtained from the ULP method had an error of approximately 17% for the same model. The reason for this behavior was that the behavior of regular building models were similar to the behavior of the models subjected to triangular lateral loads with equal masses of eccentricity for each story (no torsional effects). The errors of the TLP and MUB methods for Model M2-12S-R were equal to approximately 13.25 and 19.91%, respectively. The greatest error of the story drift ratios was obtained for the ULP method as approximately 36.96% for the same model.

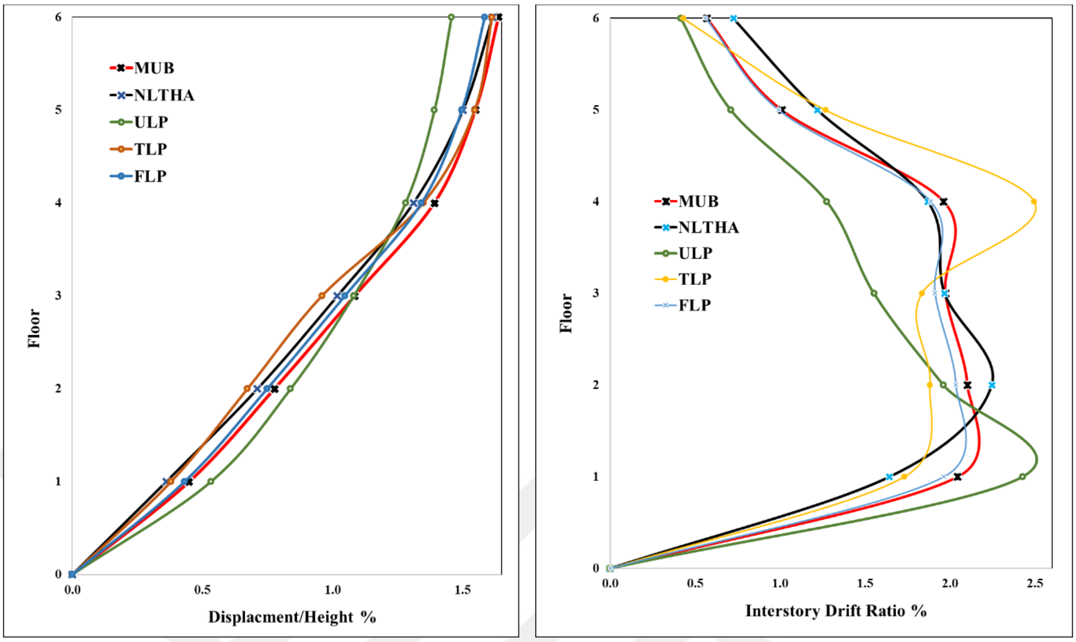

Figure 4.10 Maximum Story Displacements/Height and Interstory Drift Ratios Obtained Using FLP, TLP, ULP, MUB, and NLTHA (M1-6S-R)

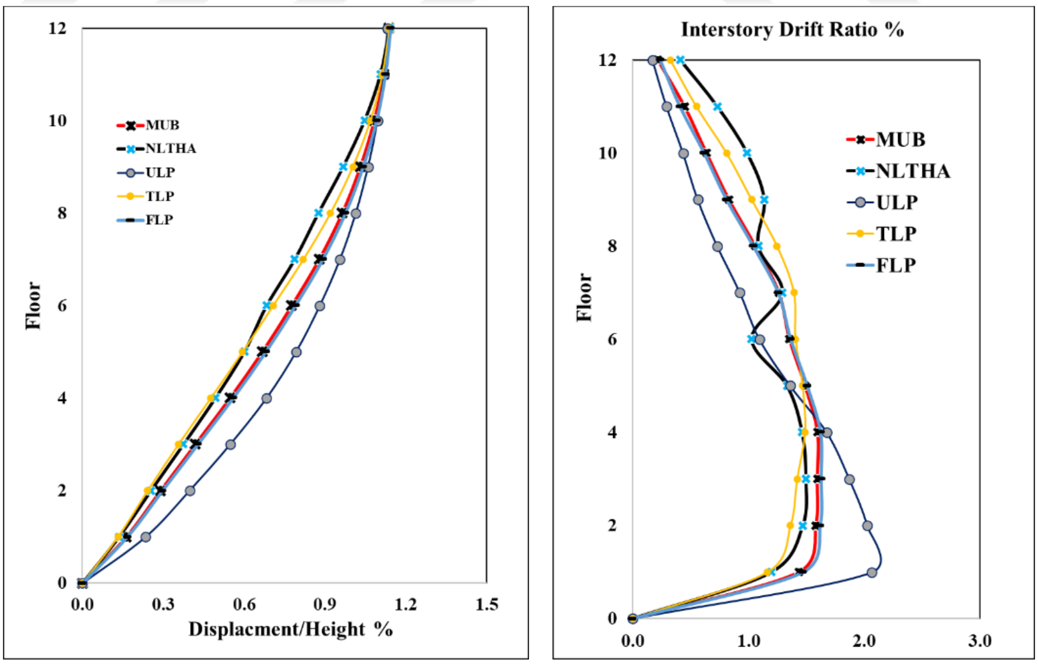

Figure 4.11 Maximum Story Displacements/Height and Interstory Drift Ratios Obtained Using FLP, TLP, ULP, MUB, and NLTHA (M2-12S-R)

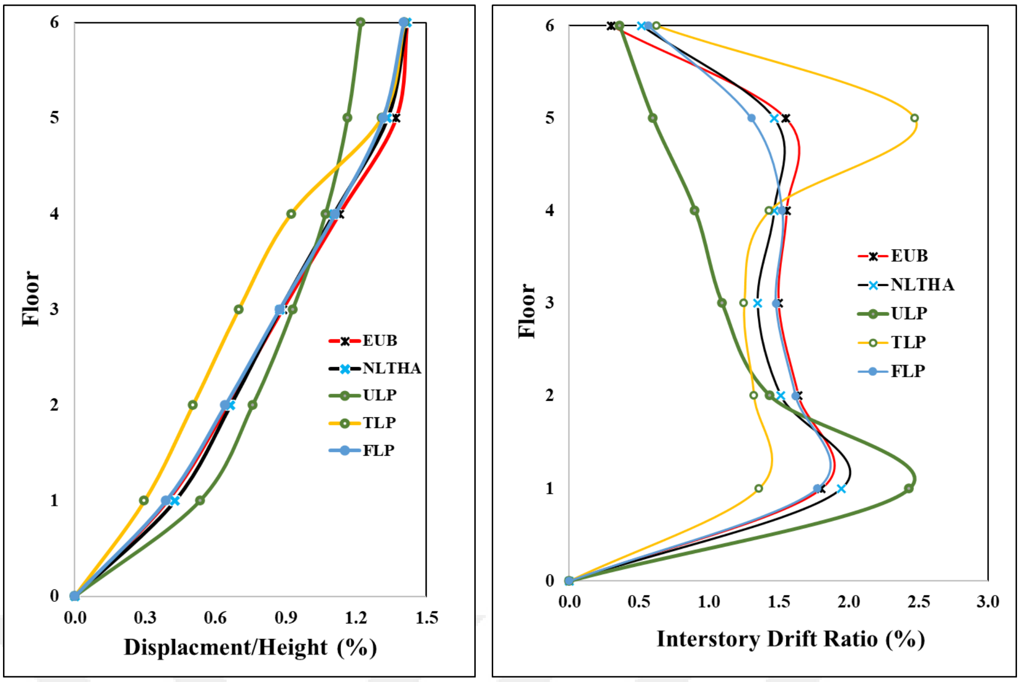

Figure 4.12 Maximum Story Displacements/Height and Interstory Drift Ratios Obtained Using FLP, TLP, ULP, EUB, and NLTHA (M3-6S-IR)

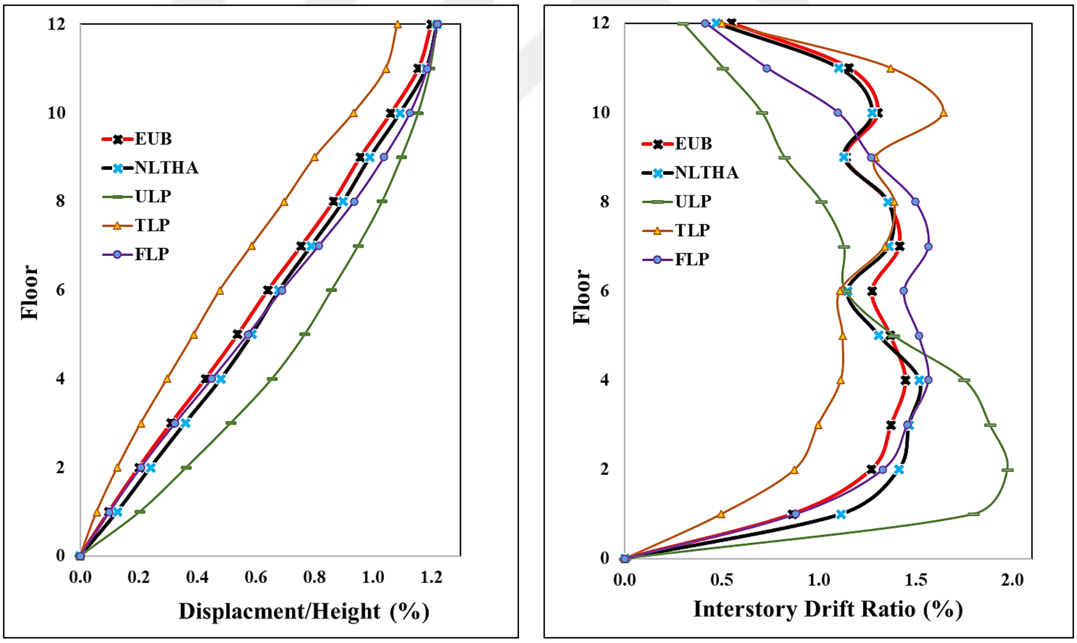

Figure 4.13 Maximum Story Displacements/Height and Interstory Drift Ratios Obtained Using FLP, TLP, ULP, EUB, and NLTHA (M4-12S-IR)

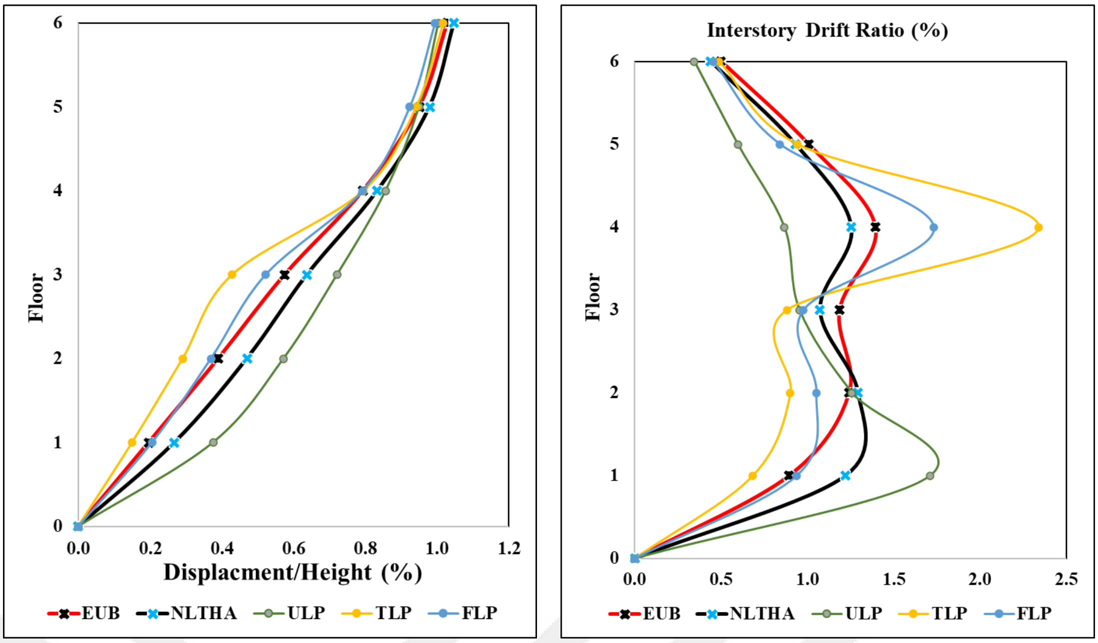

Figure 4.14 Maximum Story Displacements/Height and Interstory Drift Ratios Obtained Using FLP, TLP, ULP, EUB, and NLTHA (M5-6S-IR)

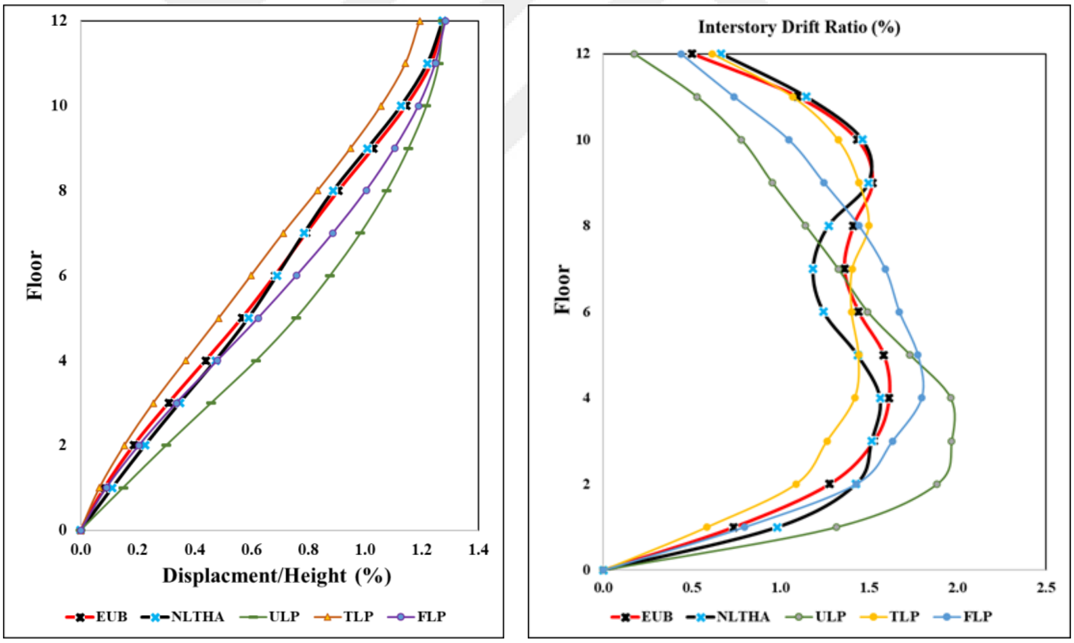

Figure 4.15 Maximum Story Displacements/Height and Interstory Drift Ratios Obtained Using FLP, TLP, ULP, EUB, and NLTHA (M6-12S-IR)

Table 4.21 Calculated Errors of Interstory Drift Ratios of TLP, FLP, ULP, MUB, and EUB Methods Compared to NLTHA Method

Models	Various Pushover Analysis Procedures			
	TLP (%)	**FLP (%)**	**ULP (%)**	**MUB (%)**
M1-6S-R	**1.80**	6.32	17.06	6.23
M2-12S-R	**13.25**	21.41	36.96	19.91
	TLP (%)	**FLP (%)**	**ULP (%)**	**EUB (%)**
M3-6S-IR	6.03	3.70	21.18	**3.09**
M4-12S-IR	20.62	14.00	29.68	**7.33**
M5-6S-IR	31.96	30.26	29.30	**12.77**
M6-12S-IR	25.87	22.29	32.87	**10.34**

These errors are similar to the mean absolute error of [5] results. As seen from the figures, the EUB method controlled the seismic demands at upper stories, whereas this method considerably underestimates the responses at the lower stories. The resulting lateral force distribution had larger values at upper stories than those of lower ones. For all the irregular building models, the results obtained using the EUB method were closer to those obtained using the NLTHA method. The EUB method also provided more accurate results of interstory drift ratios compared to those of the conventional pushover analysis procedures (TLP, FLP, and ULP). Furthermore, the responses for the upper stories of all models having setback irregularity were overestimated when this procedure (EUB) was used. The errors for the EUB method were calculated as 3.09, 7.33, 12.77, and 10.34% for M3-6S-IR, M4-12S-IR, M5-6S-IR, and M6-12S-IR, respectively.

The EUB and FLP methods generally resulted in more accurate results and provided better predictions of the response along with the height of the building models studied in this research when compared to those of the NLTHA method. On the other hand, the predictions at the lower stories for 12-story building model were better when the EUB and MUB methods were used. The reason for this behavior was due to the use of the uniform load distribution along the height of the building model which controlled the response at the lower stories. However, these methods (EUB and MUB) overestimated the results of this building model at the upper six stories when the results of story drift ratios were combined.

Calculated errors of the story drift ratios of the TLP, FLP, ULP, MUB, and EUB methods compared to the NLTHA method for 6 and 12 story building models are visualized in bar charts as shown in Figure 4.16 and Figure 4.17, respectively.

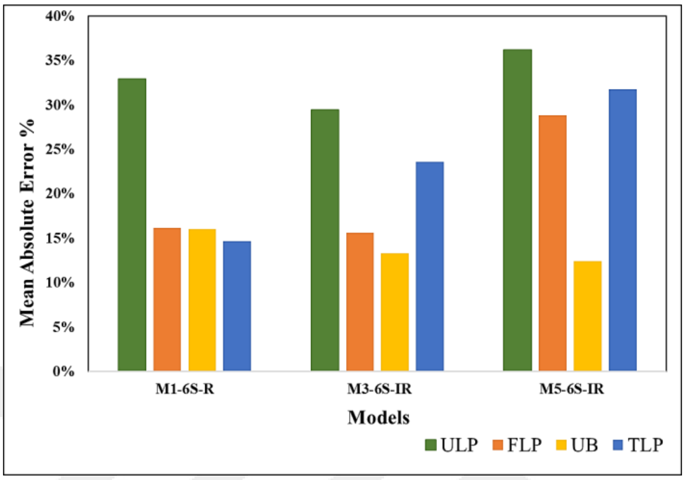

Figure 4.16 Calculated Errors of Story Drift Ratios of TLP, FLP, ULP, MUB, and EUB Methods Compared to NLTHA Method for 6 Story Building Models

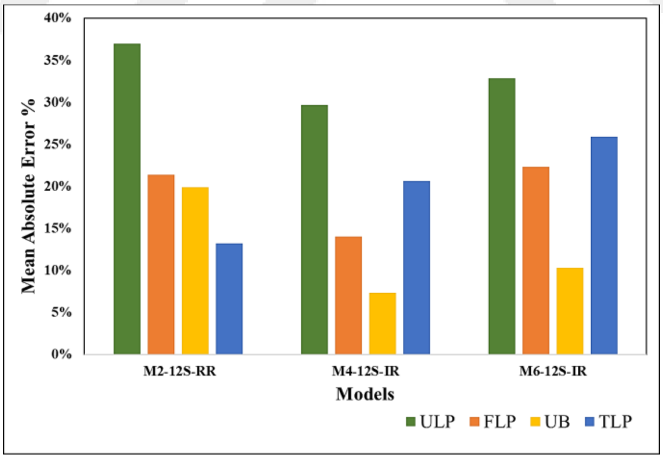

Figure 4.17 Calculated Errors of Story Drift Ratios of TLP, FLP, ULP, MUB, and EUB Methods Compared to NLTHA Method for 12 Story Building Models

4.5 Plastic Hinge Rotations

The height-wise variation of plastic hinge rotations for 6 and 12 story building models are shown in Figure 4.18 and Figure 4.19, respectively. The calculated errors of the results of TLP, FLP, ULP, MUB, and EUB methods compared to the NLTHA method are shown Table 4.22. In this table the smallest error values (best estimates) are shown in bold fonts. The EUB and MUB methods provided more accurate results of plastic hinge rotations compared to those of the conventional pushover analysis procedures (TLP, FLP, and ULP). These procedures (TLP, FLP, and ULP) overestimated the predictions at mid-story levels of high-rise regular building models. These methods underestimated the plastic hinge rotations of the 6 story building models at the lower stories, whereas a better correlation was achieved between the predictions of these methods and those obtained using the NLTHA. Predictions of the plastic hinge rotations of the EUB and MUB methods were better at upper stories. The responses for the upper stories of all models having setback irregularity were overestimated when this procedure (EUB) was used. The errors of the plastic hinge rotations for the EUB method were calculated approximately as 37.88, 41.54, 33.78, and 32.87% for M3-6S-IR, M4-12S-IR, M5-6S-IR, and M6-12S-IR, respectively.

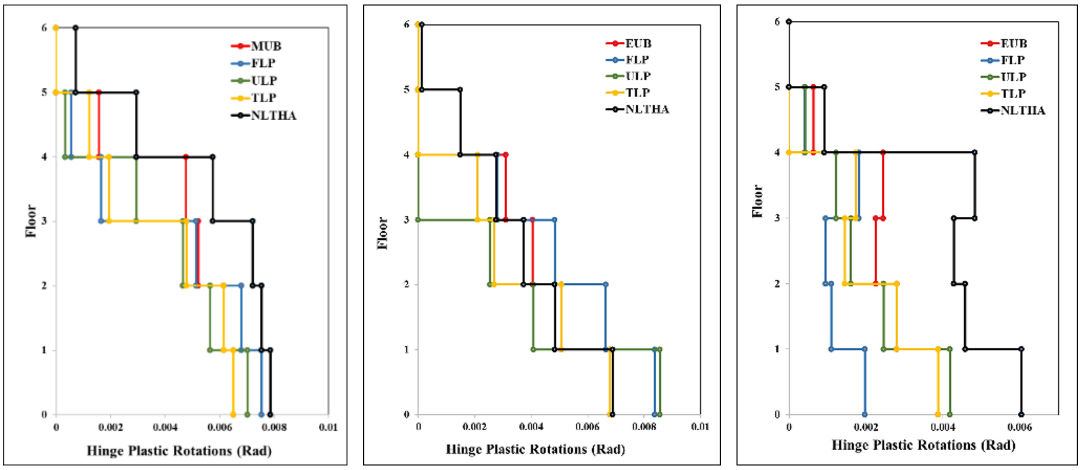

a) M1-6S-R b) M3-6S-IR c) M5-6S-IR

Figure 4.18 Maximum Plastic Hinge Rotations Obtained Using FLP, TLP, ULP, EUB, MUB, and NLTHA (6 Story Building Models)

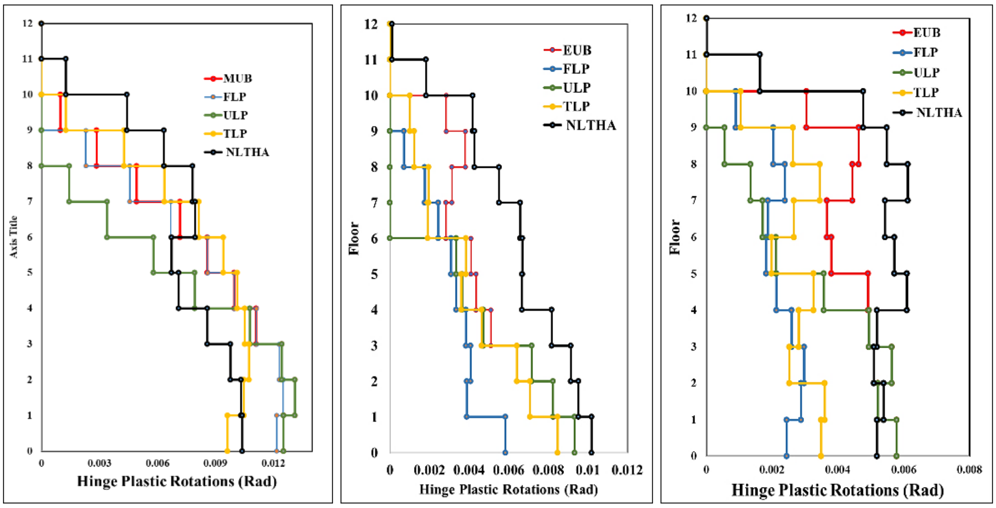

a) M2-12S-R b) M4-12S-IR c) M6-12S-IR

Figure 4.19 Maximum Plastic Hinge Rotations Obtained Using FLP, TLP, ULP, EUB, MUB, and NLTHA (12 Story Building Models)

Table 4.22 Calculated Errors of Plastic Hinge Rotations of TLP, FLP, ULP, MUB, and EUB Methods Compared to NLTHA Method

Models	**Various Pushover Analysis Procedures**			
	TLP (%)	**FLP (%)**	**ULP (%)**	**MUB (%)**
M1-6S-R	49.04	46.19	51.42	**37.79**
M2-12S-R	**29.04**	40.16	47.01	37.55
	TLP (%)	**FLP (%)**	**ULP (%)**	**EUB (%)**
M3-6S-IR	39.07	48.39	62.02	**37.88**
M4-12S-IR	57.29	69.10	68.83	**41.54**
M5-6S-IR	63.15	56.52	44.75	**33.78**
M6-12S-IR	58.23	66.19	55.88	**32.87**

Based on these results, the predictions of plastic hinge rotations of regular 12 story building model (M2-12S-R) obtained using the TLP method provided more accurate results compared to the NLTHA method. The results of the TLP method were in better agreement with the results of the NLTHA method compared to those of the FLP, ULP, and MUB methods. The error of plastic hinge rotations of the TLP method compared to the NLTHA method for Model M2-12S-R were equal to approximately 29.04%. The results obtained from the ULP method had an error of approximately 47.01% for the same model.

Conventional pushover methods (TLP, FLP, and ULP) were not sufficient to predict the plastic hinge rotations at the upper stories of the 6 and 12 story building models, whereas the MUB method provided reasonable estimates of these plastic hinge rotations.

Calculated errors of the plastic hinge rotations of the TLP, FLP, ULP, MUB, and EUB methods compared to the NLTHA method for 6 and 12 story building models are visualized in bar charts as shown in Figure 4.20 and Figure 4.21, respectively.

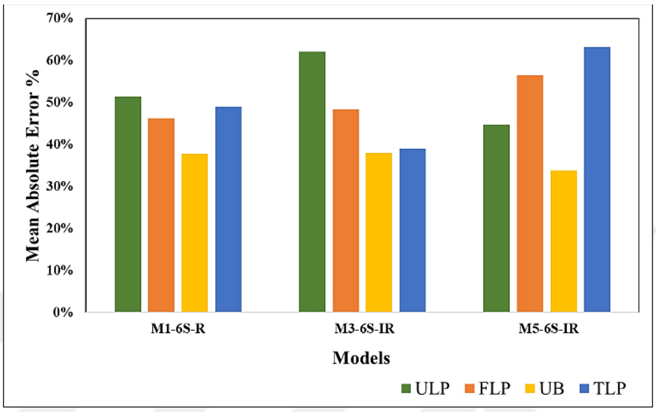

Figure 4.20 Calculated Errors of Plastic Hinge Rotations of TLP, FLP, ULP, MUB, and EUB Methods Compared to NLTHA Method for 6 Story Building Models

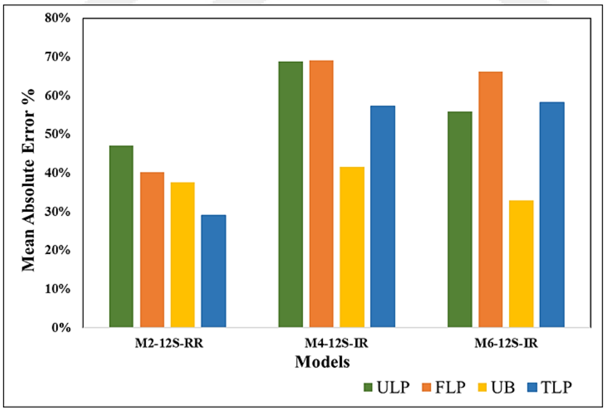

Figure 4.21 Calculated Errors of Plastic Hinge Rotations of TLP, FLP, ULP, MUB, and EUB Methods Compared to NLTHA Method for 12 Story Building Models

CHAPTER 5

5. SUMMARY, CONCLUSIONS, AND RECOMMENDATIONS

5.1 Conclusions

It is necessary to identify the limitations and efficiency of the pushover analysis methods to accurately predict the seismic demands of buildings with irregularities at different levels. The use of conventional pushover analysis methods such as TLP, FLP, and ULP to evaluate the seismic behavior of buildings provides acceptable results for 3D low-rise buildings whose behavior is dominated by the fundamental period (first mode shape) of the building. However, for mid- and high-rise buildings whose behavior under seismic actions is not only governed by the fundamental mode shape, the conventional methods do not provide sufficient results. To overcome this problem, upper-bound methods such as the MUB (3D Regular) and EUB (3D Irregular) methods considering the effects of higher mode shapes were proposed by various researchers. Previously, the EUB method was applied to 3D irregular high-rise buildings having unsymmetrical plans. However, the applicability of the EUB method for 3D high-rise buildings having setback irregularity was not addressed in the literature.

In this study, a total of 6 mid- and high-rise building models having setback irregularity at various locations were analyzed using nonlinear pushover analysis methods namely TLP, FLP, ULP, MUB, and EUB, to evaluate the applicability of these methods when the higher mode and torsional effects are more pronounced. The results obtained using these methods were compared to the NLTHA method which provided benchmark solutions to the problems. Three of the building models had 6 stories and the other three had 12 stories. The story heights of the models were all 4.5 m at the ground story and 3.2 m for the rest of the stories. All models had four bays in both plan view directions with a typical length of 6 m each. One model of each height level was a regular building and used for comparison purposes. Other two models of each height level had setback irregularity in various locations of the elevation in one direction. The analyses were performed using SAP2000 Structural Analysis Software [3]. The results were assessed for seismic demand variables such as lateral displacements, interstory drift ratios, and plastic hinge rotations.

The primary findings from this study can be summarized as follows:

- The predictions of interstory drift ratios of regular 6 story building model obtained using the TLP method provided more accurate results than other methods when compared to the NLTHA method. The results of the TLP method were in better agreement with the results of the NLTHA method compared to those of the FLP, ULP, and MUB methods. Especially at lower stories, the errors of the TLP and MUB methods compared to the NLTHA method for Model M1-6S-R were equal to approximately 1.8 and 6.3%, respectively. The results obtained from the ULP method had an error of approximately 17% for the same model. The reason for this behavior was that the behaviors of regular building models were similar to the behavior of the models subjected to triangular lateral loads with equal masses of eccentricity for each story (no torsional effects).
- The EUB method controlled the seismic demands at upper stories, whereas this method considerably underestimates the responses at the lower stories. The resulting lateral force distribution had larger values at upper stories than those of lower ones. For all the irregular building models, the results obtained using the EUB method were closer to those obtained using the NLTHA method. The EUB method also provided more accurate results of interstory drift ratios compared to those of the conventional pushover analysis procedures (TLP, FLP, and ULP). Furthermore, the responses for the upper stories of all models having setback irregularity were overestimated when this procedure (EUB) was used.
- The EUB and FLP methods generally resulted in more accurate results and provided better predictions of the response along with the height of the building models studied in this research when compared to those of the NLTHA method. On the other hand, the predictions at the lower stories for 12-story building model were better when the EUB and MUB methods were used. The

reason for this behavior was due to the use of the uniform load distribution along the height of the building model which controlled the response at the lower stories. However, these methods (EUB and MUB) overestimated the results of this building model at the upper six stories when the results of story drift ratios were combined.

- The EUB and MUB methods provided more accurate results of plastic hinge rotations compared to those of the conventional pushover analysis procedures (TLP, FLP, and ULP). These procedures (TLP, FLP, and ULP) overestimated the predictions at mid-story levels of high-rise regular building models. These methods underestimated the plastic hinge rotations of the 6 story building models at the lower stories, whereas a better correlation was achieved between the predictions of these methods and those obtained using the NLTHA. Predictions of the plastic hinge rotations of the EUB and MUB methods were better at upper stories. The responses for the upper stories of all models having setback irregularity were overestimated when this procedure (EUB) was used.
- The predictions of plastic hinge rotations of regular 12 story building model (M2-12S-R) obtained using the TLP method provided more accurate results compared to the NLTHA method. The results of the TLP method were in better agreement with the results of the NLTHA method compared to those of the FLP, ULP, and MUB methods.
- Conventional pushover methods (TLP, FLP, and ULP) were not sufficient to predict the plastic hinge rotations at the upper stories of the 6 and 12 story building models, whereas the MUB method provided reasonable estimates of these plastic hinge rotations.

5.2 Recommendations for Future Research Work

The following recommendations were made for future studies:

- Multi-story RC buildings with setbacks in only one direction were studied in this research. 3D building models with setback irregularities in both orthogonal directions (x- and y- directions in plan-view) may have future research potential.

- To improve the accuracy of seismic demand predictions and the accuracy of maximum displacement demand predictions for various pushover methods, more building models having fundamental periods more than 3 s may be included in the future studies.
- This study covered only framed buildings without shear walls. New studies may be performed on high-rise shear walled RC buildings having setback irregularity.

REFERENCES

[1] Earthquake Hazards, "Long-Term National Seismic Hazard Map." Internet: www.usgs.gov/media/images/2018-long-term-national-seismic-hazard-map, 2018 [Accessed: Apr. 24, 2022].

[2] FEMA, "American Society of Civil Engineers, FEMA 356 Prestandard and Commentary for the Seismic Rehabilitation of Building," *Rehabilitation*, no. Nov. 2000.

[3] ASCE 7-22, "Minimum Design Loads and Associated Criteria for Buildings and Other Structures." 2022.

[4] SAP2000 V20, "Structural and Earthquake engineering software Design." Internet: https://wiki.csiamerica.com/display/sap2000, Jan. 2021, [Accessed: Apr. 24, 2022].

[5] A. Y. Rahmani, M. Badaoui, N. Bourahla, R. Bento, "Extension of The Improved Upper-Bound Pushover Analysis for Seismic Assessment of Steel Moment Resisting Frames with Setbacks." *Bulletin of Earthquake Engineering* , Dec. 2021.

[6] H. Krawinkler and G.D.P.K. Seneviratna, "Pros and Cons of a Pushover Analysis of Seismic Performance Evaluation." *Engineering Structures*, vol. 20, no. 4-6, pp. 452- 464,1998.

[7] T.F. Paret, K.K. Sasaki, D.H. Elibeck, and S.A. Freeman, "Approximate inelastic procedures to identify failure mechanism from higher mode effects." *in Proc. of the Eleventh World Conference on Earthquake Engineering*, 1996, pp. 966.

[8] K. K. Sasaki, S. A. Freeman, and T. F. Paret, "Multimode pushover procedure (MMP)-A method to identify the effects of higher modes in a pushover analysis." *In proc. of the 6th US national conference on earthquake engineering*, 1998, pp. 12.

[9] A. S. Moghadam and W. K. Tso, “A pushover procedure for tall buildings.” *Twelfth European Conference on Earthquake Engineering*, no. 395, 2002.

[10] A. K. Chopra and R. K. Goel, “A modal pushover analysis procedure for estimating seismic demands for buildings.” *Earthquake Engineering and Structural Dynamics*, vol. 31, no. 3, pp. 561–582, 2002.

[11] A. K. Chopra and R. K. Goel, “A modal pushover analysis procedure to estimate seismic demands for unsymmetric-plan buildings.” *Earthquake Engineering and Structural Dynamics*, vol. 33, no. 8, pp. 903–927, 2004.

[12] ATC-40, “Seismic Evaluation and Retrofit of Concrete Buildings.” Redwood City, California Nov.1996.

[13] S. Oğuz, “Evaluation of Pushover Analysis Procedures for Frame Structures.” M.S. Thesis, Middle East Technical University, Ankara, 2005.

[14] M. Elsharida, “Evaluation of Enhanced Pushover Analysis Procedures for Regular and Irregular Reinforced Concrete Buildings.” M.Sc. Thesis, Atilim University, Ankara, Turkey 2021.

[15] A. Daei, and M. Poursha, “On the Accuracy of Enhanced Pushover Procedures for Seismic Performance Evaluation of Code-Conforming RC Moment-Resisting Frame Buildings Subjected to Pulse-Like and Non-Pulse-Like Excitations.” *Structures*, vol. 32, pp. 929-945, 2021.

[16] S.W. Han, Y.K. Wen, “Method of reliability-based seismic design. I: equivalent non-linear system.” *Journal of Structural Engineering*, vol. 123, no. 3, pp. 256–65, 1997.

[17] B. Gupta, “Enhanced pushover procedure and inelastic demand estimation for performance-based seismic evaluation of buildings.” Ph.D. dissertation, University of Central Florida, Orlando, 1999.

[18] B. Gupta, S.K. Kunnath "Adaptive spectra-based pushover procedure for seismic evaluation of structures." *Earthquake Spectra*, vol. 16, no. 2, pp. 367–91,2000.

[19] T.S. Jan, M.W. Liu, Y.C. Kao, "Pushover analysis and seismic demands of structures to near-fault earthquakes." *Engineering Structures*, vol. 31, no. 2, pp. 2002.

[20] M.W. Liu, Y.C. Kao, T.S. Jan, "A new pushover analysis procedure for high-rise buildings." *The 25th Conference on Theoretical and Applied Mechanics*, 2002, p. D008.

[21] T. S. Jan, M.W. Liu, and Y.C. Kao, "An upper-bound pushover analysis procedure for estimating the seismic demands of high-rise buildings." *Engineering Structures*, vol. 26, no. 1, pp. 117–128, 2004.

[22] M. Poursha and E.T. Samarin, "The modified and extended upper-bound (UB) pushover method for the multi-mode pushover analysis of unsymmetric-plan tall buildings." *Soil Dynamics and Earthquake Engineering*, vol. 71, pp. 114–127, 2015.

[23] M. Poursha, F. Khoshnoudian, and A. S. Moghadam, "A consecutive modal pushover procedure for estimating the seismic demands of tall buildings," *Engineering Structures*, vol. 31, no. 2, pp. 591–599, 2009.

[24] P. Fajfar "A nonlinear analysis method for performance based seismic design." *Earthquake Spectra*, vol. 16, no. 3, pp. 573–592, 2000.

[25] P. Fajfar, D. Marusic, I. Perus, "Torsional effects in the pushover-based seismic analysis of buildings." *Journal of Earthquake Engineering*, vol. 9, no. 6, pp. 831–54, 2005.

[26] T. Takeda, M.A. Sözen and N.N. Nielson, "Reinforced Concrete Response to Simulated Earthquakes." *Journal of Structural Division*, vol. 96, no. 3, 2557-2573, 1970.

[27] S.A. Freeman, “Development and Use of Capacity Spectrum Method.” *Proceedings of the Sixth U.S. National Conference on Earthquake Engineering*, 1998, pp. 269.

[28] P. Fajfar, “Capacity spectrum method based on inelastic demand spectra.” *Earthquake engineering and structural dynamics*, vol. 28, no. 9, 979-994, 1999.

[29] E. Rosenblueth, M. ASCE and I. Herrera, “On a Kind of Hysteretic Damping.” *Journal of the Engineering Mechanics Division*, ASCE. vol. 90, no. 4, pp. 37-48, 1964.

[30] Mahaney J.A., Paret T.F., Kehoe B.E. and Freeman S.A., “The Capacity Spectrum Method for Evaluating Structural Response During the Loma Prieta Earthquake.” *Earthquake Conf., Central U.S. Earthquake Consortium*, Memphis, Tenn, vol.2, pp. 501-510, 1993.

[31] S. Mashhadi, A. Asadi, F. Homaei, and H. Tajammolian, “Seismic response of mid-rise steel MRFs: the role of geometrical irregularity, frequency components of near-fault records, and soil-structure interaction.” *Bulletin of Earthquake Engineering*, vol. 19, no. 9, pp. 3571–3595, 2021.

[32] ACI 318-19, ACI 318-19 - Building Code Requirements for Structural Concrete. 2019.

[33] Pacific Earthquake Engineering Research Center, “PEER Ground Motion Database - PEER Center.” Internet: https://ngawest2.berkeley.edu/, [Accessed: Apr. 24, 2022].

[34] ASCE/SEI 41-13, “Seismic Evaluation and Retrofit of Existing Buildings.” 2022.

APPENDICIES

A. DESIGN OF BEAMS AND COLUMNS ACCORDING TO ACI 318-19M

Material	Designation	Stress limit state (MPa)	Modulus of Elasticity E (GPa)	Mass density r (kg/m^3)
Concrete	C30/37	30	25.7	2500
Steel	Rebars	420	200	7850

- Grade fc´= 4000 psi
- Steel (Rebars) ASTM A615 Grade 60
- Loads on slabs

    1. Dead
        - ‡ Self-weight = 0.15 *24 =3.6 kN/m^2
        - ‡ Superimposed = 3.5 kN/m^2
    2. Live load
        - ‡ offices =2.4 kN/m^2

$$W_u = 1.2(3.6 + 3.5) + 1.6 * 2.4 = 12.36\ \frac{\text{kN}}{\text{m}}$$

Load transfer on beams

The ACI code prescribes minimum values of h, height of beam, for which deflection calculations are not required.

Minimum values of h to avoid deflection calculations				
Type of beam construction	simply supported	one end continuous	both ends continuous	cantilever
beams or joists	ℓ/16	ℓ/18.5	ℓ/21	ℓ/8
one way slabs	ℓ/20	ℓ/24	ℓ/28	ℓ/10

Figure A. 1 Depth of Beam for Preliminary Design

For simply supported Beam

$$h_{min} = \frac{Span}{16} = \frac{6}{16} = 0.375\ m$$

For practical purpose use h = 450 mm

- **External beams (AB)**

$$Wu\ = \frac{w_u * S}{3} + W_{self} = \frac{12.36 * 6}{3} + 0.3 * 0.4 * 24 * 1.2 = 28.176\ KN.m$$

- **Moment (M^-) from slab**

$$= 0.05 * W_u\, l^2 = 0.05 \ * \ 12.36 \ * \ 6^2 = 22.25 \ \frac{kN.m}{m}$$

- **Design for bending moment using coefficient method**

$$M^- = \frac{w_u\, l^2}{10} = \frac{w_u\, l^2}{10} = \frac{28.18 * 6^2}{10} = 101.448\, kN.m$$

$$M^+ = \frac{w_u\, l^2}{14} = \frac{28.18 * 6^2}{14} = 72.46\, kN.m$$

- **Negative bending moment**

$$d = h - d' = 450 - 40 - 10 - \frac{16}{2}$$

$$A_{S\,\mathrm{top}} = \frac{M_u\, 10^6}{\mathrm{\phi\ fy} * 0.9 * \mathrm{d}} = \frac{101.45 * 10^6}{0.9 * 420 * 0.9 * 392} = 760.7\, mm$$

$$4\, \phi\, 25 = 6 * 201 = 1206\, mm$$

$$\mathrm{a} = \frac{A_S f y}{0.85\ \mathrm{fc}' * \mathrm{b}} = \frac{1206 * 420}{0.85 * 30 * 350} = 56\, mm$$

$$A_S = \frac{M_u * 10^6}{\mathrm{\phi\ fy}\ (\mathrm{d} - \frac{\mathrm{a}}{2})} = \frac{101.45 * 10^6}{0.9 * 420 * \left(392 - \frac{56}{2}\right)} = 737.3\, m^2$$

$$4\, \phi\, 25 = 4 * 314 = 1256\, mm$$

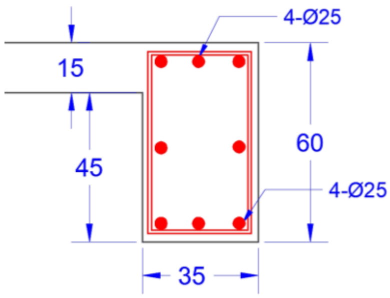

External beam

- **Internal Beam**

$$W_u = 2 * \frac{W_u * S}{3} + W_{beam} = 2 * 24.72 + 3.46 = 52.9\ \frac{\mathrm{KN}}{\mathrm{m}}$$

$$M_u^- = \frac{w_u\, l^2}{10} = \frac{52.9 * 36}{10} = 190.44\, KN.m$$

$$A_S = \frac{M_u * 10^6}{\mathrm{\phi\ fy} * 0.9 * \mathrm{d}} = \frac{190.44 * 10^6}{0.9 * 420 * 392} = 1285.2\, m^2$$

$$A_S = \frac{\text{As fy}}{0.5\ \text{fc}' * \text{b}} = \frac{1285.2 * 420}{0.85 * 30 * 350} = 60.5\ mm$$

$$A_S = \frac{M_u * 10^6}{\phi\ \text{fy}\ (\text{d} - \frac{\text{a}}{2})} = \frac{101.44 * 10^6}{0.9 * 420 * \left(392 - \frac{60.5}{2}\right)} = 741.8\ m^2$$

$$M^+ = \frac{w_u\ l^2}{14} = \frac{52.9 * 6^2}{14} = 136.02\ kN.m$$

$$A_S = \frac{M_u\ * 10^6}{0.81 * \text{fy} * \text{d}} = \frac{136.02 * 10^6}{0.81 * 420 * 392} = 1020\ m^2$$

$$\text{A} = \frac{A_S fy}{0.85\ \text{fc}' * \text{b}} = \frac{1020 * 420}{0.85 * 30 * 350} = 48\ mm$$

$$6\ \phi\ 20 = 6 * 314 = 1884\ mm$$

$$A_S = \frac{M_u * 10^6}{\phi\ \text{fy}\ (\text{d} - \frac{\text{a}}{2})} = \frac{178.6 * 10^6}{0.9 * 420 * \left(342 - \frac{16.85}{2}\right)} = 1416\ mm^2$$

$$6\ \phi\ 20 = 6 * 201 = 1884\ mm$$

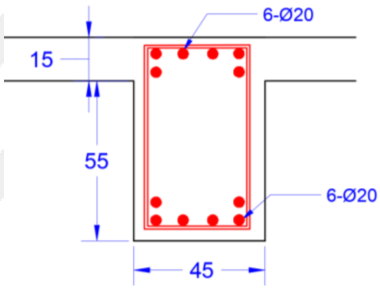

Internal Beam

- **Load on column**

- Either from computer output
- Or from load partitioning

Using tributary area method

- **Internal column**

$$\text{Pu} = 6^2 * 12.36 + 3.46 * (6 + 6)\ \ = 635.52\ \ \text{kN}/story$$

For six stories

$$\text{Pu} = 6 * 635.52 = 3813.12\ \text{KN}$$

$$\frac{\text{M}_\text{u}}{\text{P}_\text{u}} \simeq \text{e}_\text{min} = 0.05 \rightarrow Assume\ \ \frac{e}{h} = 0.1$$

Using interaction diagram of column, use h=b=650mm

$$K_n = \frac{P_u}{\phi * fc' * b * h} = \frac{3.813}{0.65 * 30 * 0.5^2} = 0.782$$

Use $\rho_{min} = 0.01$

ρ is the ratio of tensile longitudinal reinforcement (for beams & columns)

$$A_S = 0.01 * 650^2 = 2500\ m^2 \rightarrow 6\ \phi\ 20 = 6 * 201$$

$$= 1885\ mm\ for\ top\ \&\ bottom\ reinforcement$$

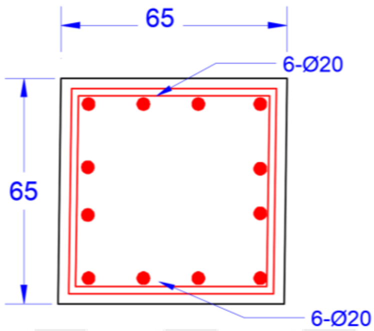

Lower Stories Columns

For the upper stories use h=b=550mm

$$Pu = 3 * 635.52 = 1905\ KN$$

$$K_n = \frac{P_u}{\phi * fc' * b * h} = \frac{1.905}{0.65 * 30 * 0.4^2} = 0.61$$

Use $\rho_{min} = 0.01$

$$A_S = 0.01 * 400^2 = 1600\ m^2$$

$$6\ \phi\ 16 = 6 * 201 = 1206\ mm, \qquad 4\ \phi\ 20 = 4 * 314 = 1256\ mm$$

- **External column**

$$P_u = 6 * 3 * 12.36 * 3.46\left(\frac{6}{2} + 6\right) = 328\ KN$$

$Upper\ stories\ \ P_u = 3 * 328 = 984\ kN$

$$Mu = \frac{W_u\ l^2}{16} = \frac{69.46 * 6^2}{16} = 156\ \ kN.\mathrm{m}$$

$$e = \frac{M_u}{P_u} = \frac{156}{984} = 0.158 \rightarrow \frac{e}{h} = 0.158/0.4 = 0.396$$

$$K_n = \frac{P_u}{\phi * fc' * b * h} = \frac{0.984}{0.65 * 30 * 0.4^2} = 0.315$$

Use $\rho_{min} = 0.01 \rightarrow A_S = 0.01 * 550^2 = 1600\ \mathrm{m}^2$

$5\ \phi\ 16 = 5 * 201 = 1005$ mm for top & bottom reinforcement

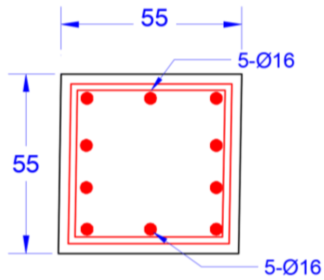

Upper Stories Columns

A.1 Analysis of Rectangular Reinforced Concrete Beam

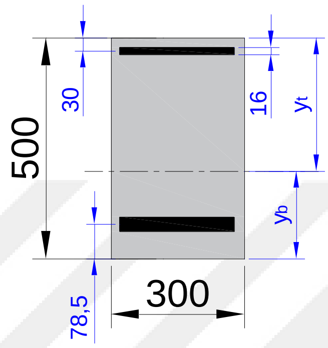

Equivalent Transformed Non-Cracked Concrete Section

$$A_g = bh + (n-1)A_s^+ + (n-1)A_s^-$$

$$y_b = \frac{\frac{b \times h^2}{2} + (n-1)A_s^+ \times db + (n-1)A_s^- \times (h - dt)}{A_g}$$

From $I_{bottom} = I_{NAg} + A_g y_b^2$

$$I_{NAg} = b \times \frac{h^3}{3} + (n-1)A_s^+ \times db^2 + (n-1)A_s^- \times (h-dt)^2 - A_g y_b^2$$

$$f_r = 0.64\sqrt{f_c'}$$

$$M_{cr}^+ = \frac{f_r * I_{NAg}}{y_b}$$

$$M_{cr}^- = \frac{f_r * I_{NAg}}{y_t}$$

Here the rotation can be calculated as below

$$f_r = \frac{M_{cr} y_t}{I_{NA}}$$

$$\epsilon_{cc} = f(\sigma_c) \; then \; \theta_{cr} = \frac{\epsilon_{cc}}{y_t}$$

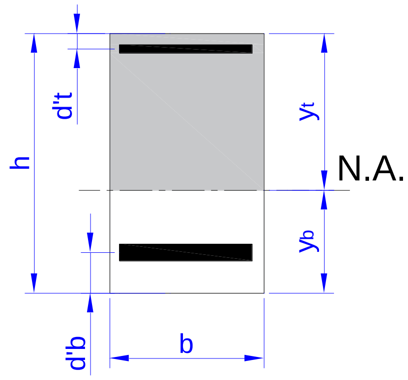

Equivalent Transformed Cracked Concrete Section

$A_g = by_t + (n)A_s^+ + (n-1)A_s^-$

From $I_{NA} = \frac{by_t^3}{3} + (n)A_s^+(h - db - y_t)^2 + (n-1)A_s^-(y_t - dt)$

From the first moment of area about NA

$\frac{by_t^2}{2} + (n-1)A_s^-(y_t - d_t) = (n)A_s^+(h - d_b - y_t)\ y_t^2 + \frac{2}{b}[(n-1)A_s^- - (n)A_s^+]y_t +$
$\frac{2}{b}[(n)A_s^+(h - db) - (n-1)A_s^- dt] = 0$

$$y_t = \left(-\frac{1}{b}[(n-1)A_s^- - (n)A_s^+] + \sqrt{\frac{1}{b^2}[(n-1)A_s^- - (n)A_s^+]^2 + \frac{2}{b}[(n)A_s^+(h - db) - (n-1)A_s^- dt]} \right)$$

$$y_t = \frac{-[(n-1)A_s^- - (n)A_s^+] \pm \sqrt{[(n-1)A_s^- - (n)A_s^+]^2 - 2b[(n)A_s^+(h-db) - (n-1)A_s^- dt]}}{b}$$

$$\sigma_{cc} = \frac{My_t}{I_{NA}} \rightarrow \epsilon_{cc} = \frac{\sigma_{cc}}{E} \rightarrow \theta = \frac{\epsilon_{cc}}{y_t}$$

$$\sigma_{st} = \frac{M(h - d_b - y_t)}{I_{NA}} \times n$$

$$\epsilon_{st} = \frac{\sigma_{st}}{E_s}$$

$$\theta = \frac{\epsilon_{st}}{(h - d_b - y_t)}$$

B. RESULTS OF PUSHOVER ANALYSIS

c) d)

Figure B. 1 to Figure B. 6 present the performance point and displacement for pushover cases

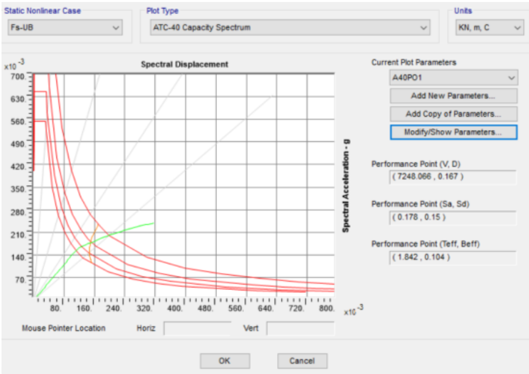

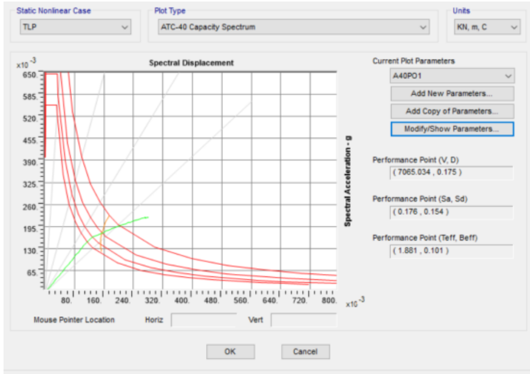

a) b)

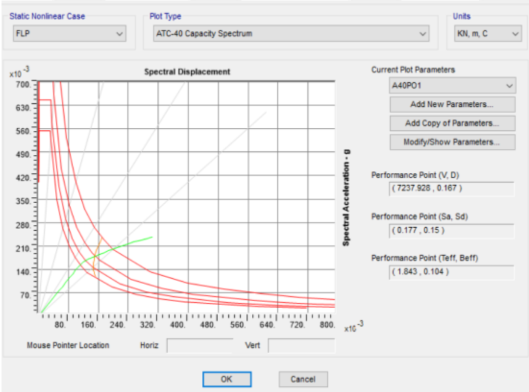

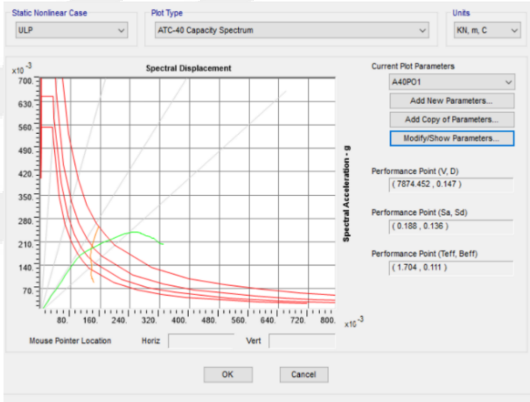

c) d)

Figure B. 1 Performance Point Based For a) Upper Bound Pushover Analysis In Y-Direction b) Triangular Load pattern c) Elastic first mode d) Uniform load pattern For M1-6S-R

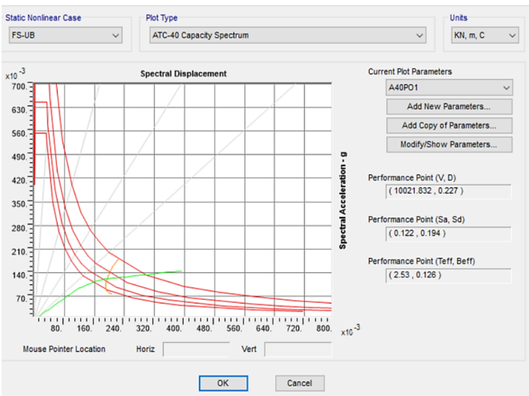

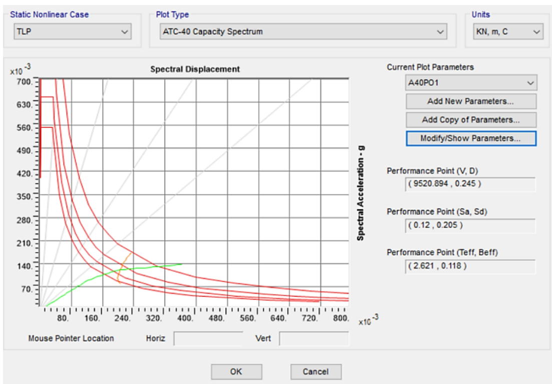

a) b)

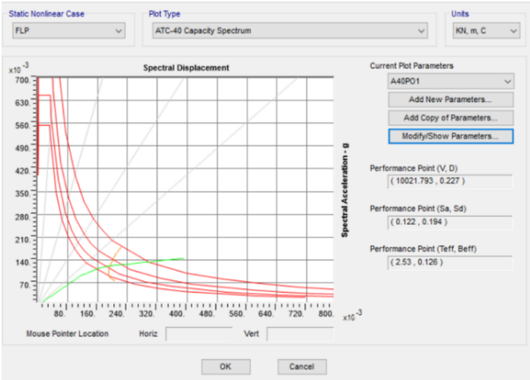

c)

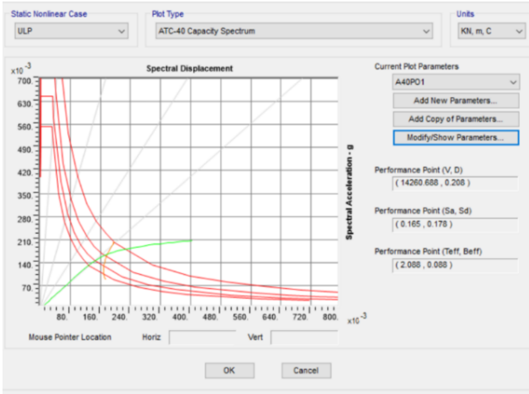

d)

Figure B. 2 Performance Point Based For a) Upper Bound Pushover Analysis In Y-Direction b) Triangular Load pattern c) Elastic first mode d) Uniform load pattern For M2-12S-R

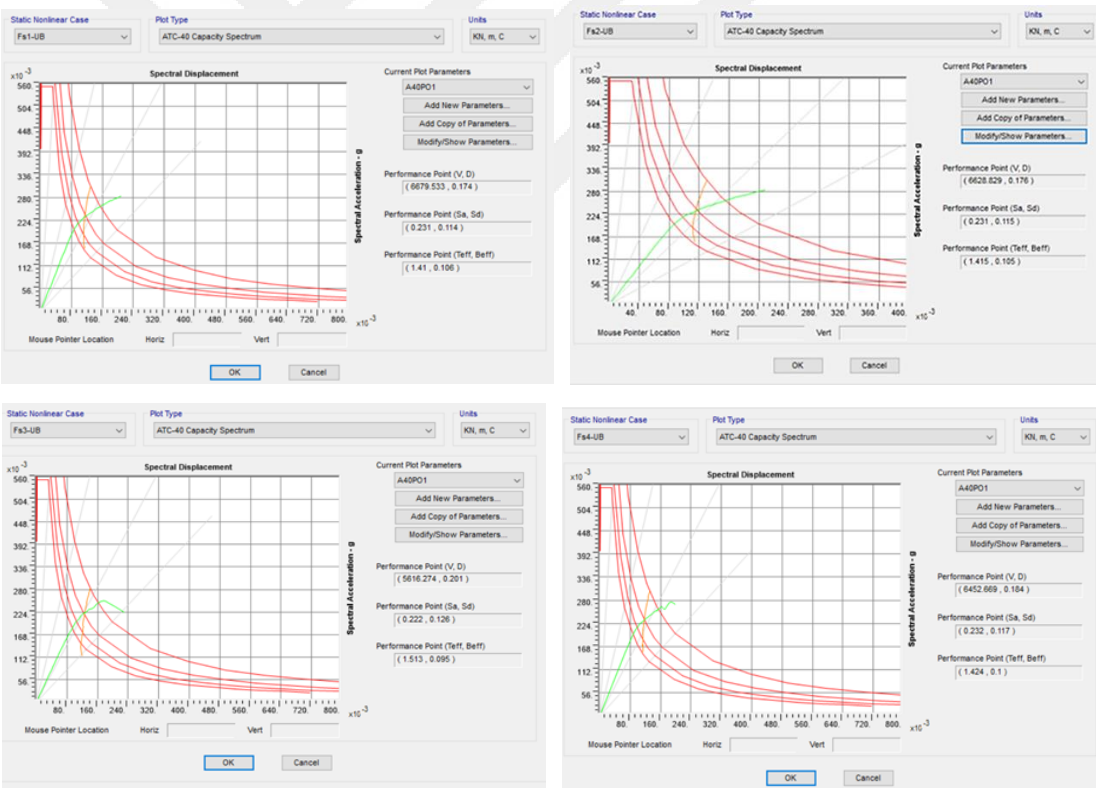

Figure B. 3 Performance Point based for upper bound Pushover Analysis in Y-Direction M3-6S-IR

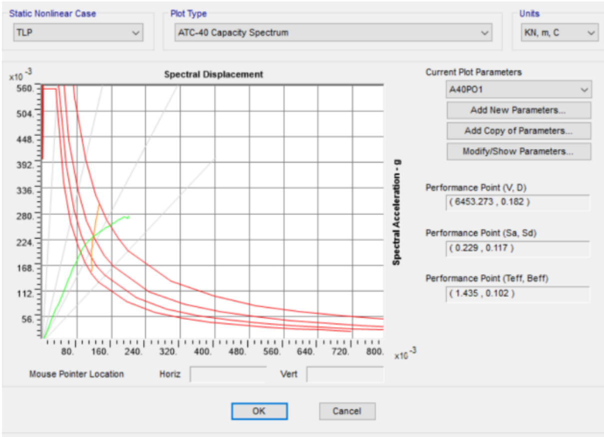

Figure B. 4 Performance Point Based for ASCE 7-22 [4] Triangular Load Pattern Pushover Analysis İn Y-Direction for M3-6S-IR

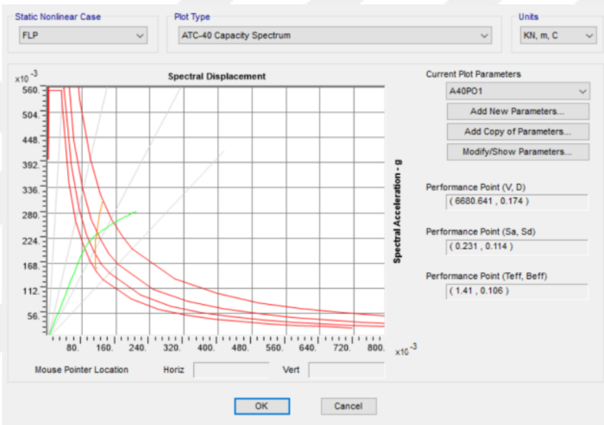

Figure B. 5 Performance Point Based on First Elastic Mode Pushover load In Y-Direction

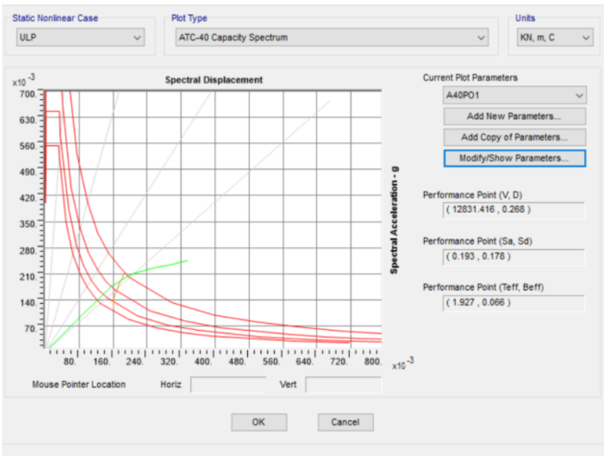

Figure B. 6 Performance Point Based on Uniform Pushover load In Y-Direction

C. PLASTIC HINGE FORMATIONS FOR ALL MODELS BASED ON PUSHOVER ANALYSIS

Figure C. 1 to Figure C. 10 presents the distribution of hinges at the point of collapse for 6 and 12 stories building with four bays, as derived via pushover analysis using four different load patterns. According to the findings shown in these figures, the distribution of the building's hinges and, therefore, its mechanism for collapsing are the same for both the triangular form and the first mode shape derived from the upper bound load pattern. Uniform load the production of plastic hinges at both ends of each beam and at the base of the columns supporting the first story.

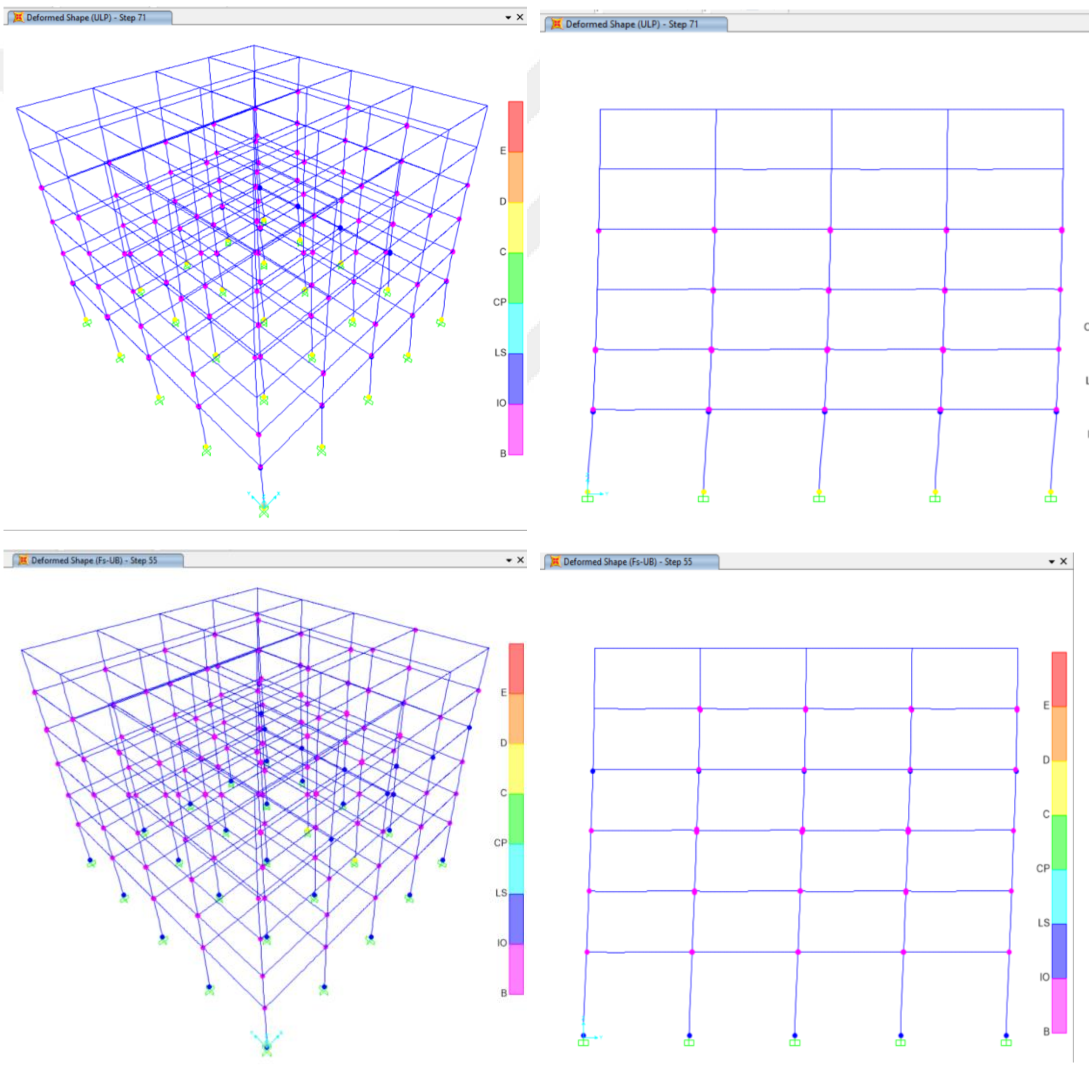

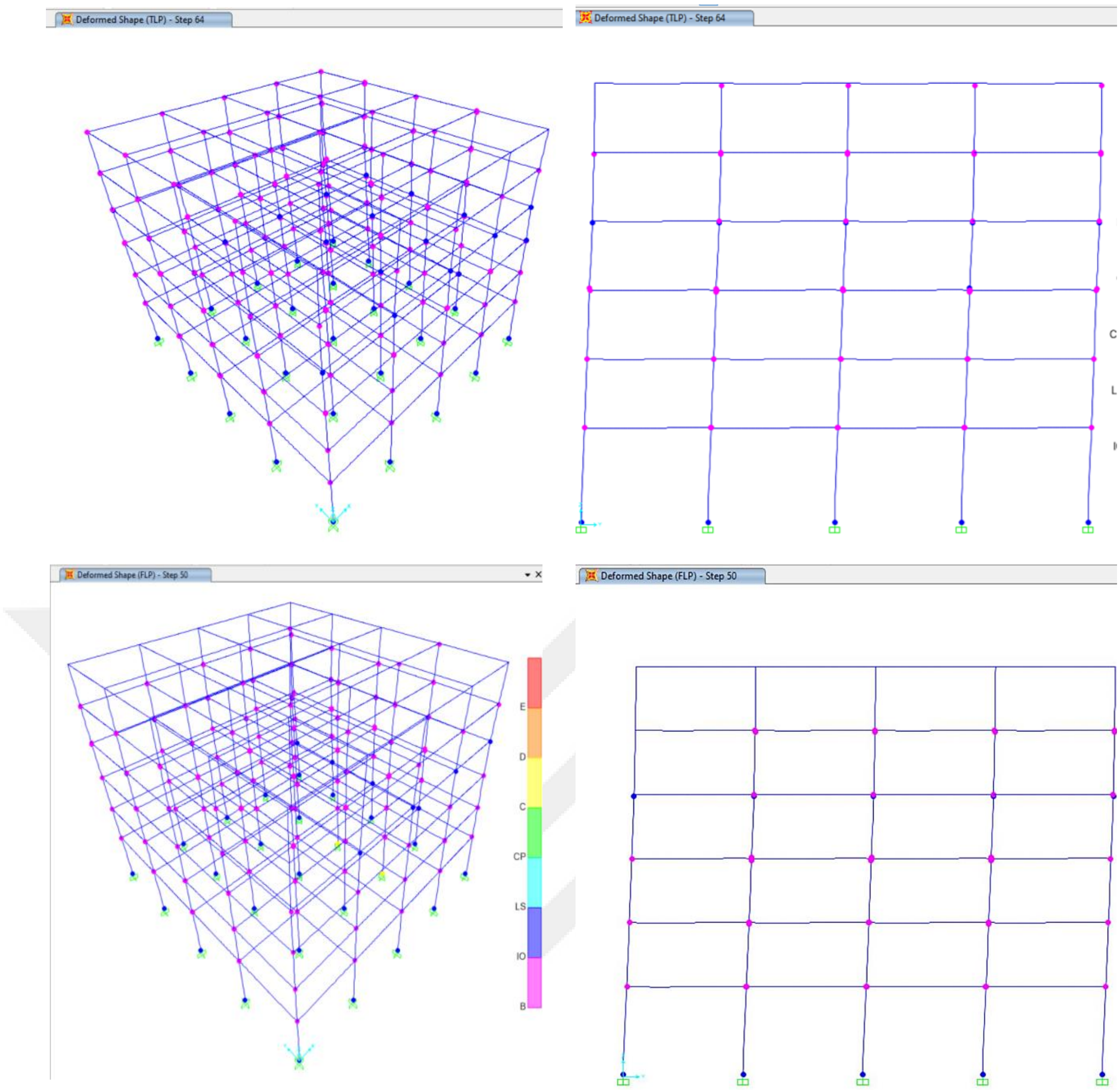

Figure C. 1 Plastic Hinge Distribution for M1-6S-R Model by Pushover Loads Pattern

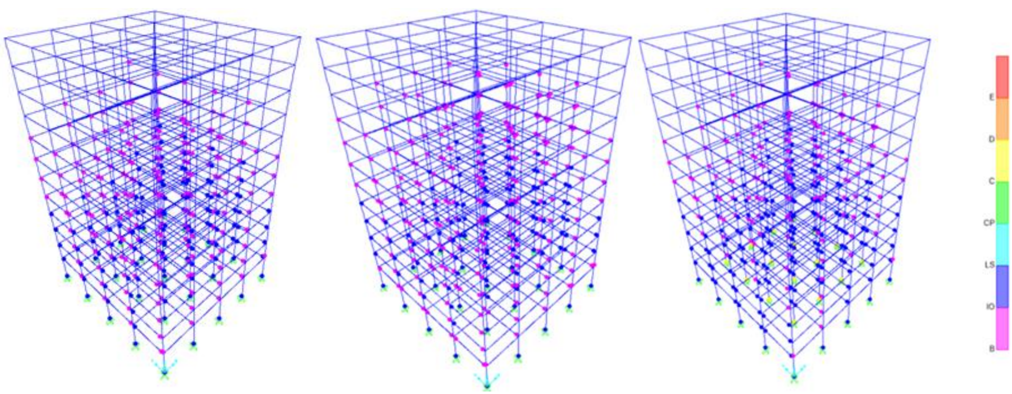

Figure C. 2 Plastic Hinge Distribution for M2-12S-R model by $F_S UB$,TLP, and FLP load pattern

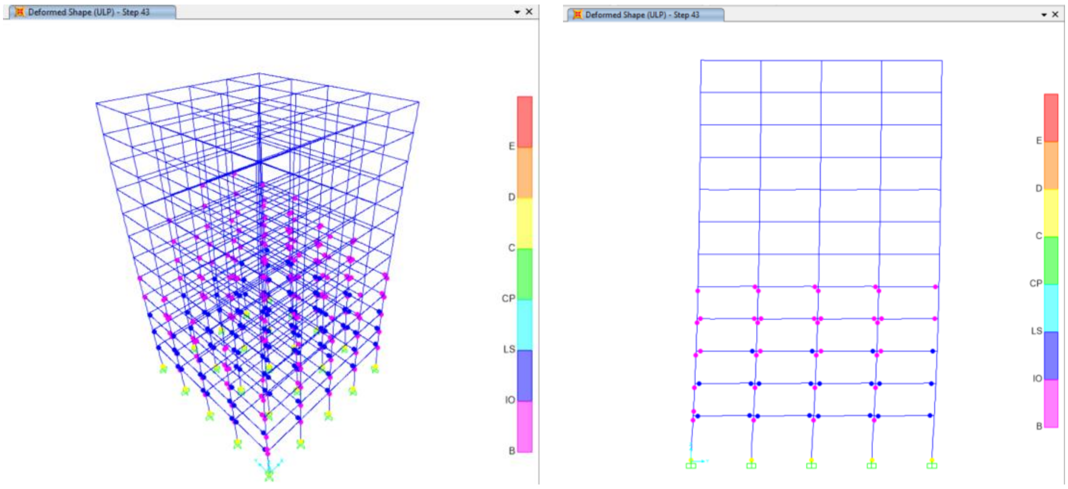

Figure C. 3 Plastic Hinge Distribution for M2-12S-R model by (ULP) load pattern

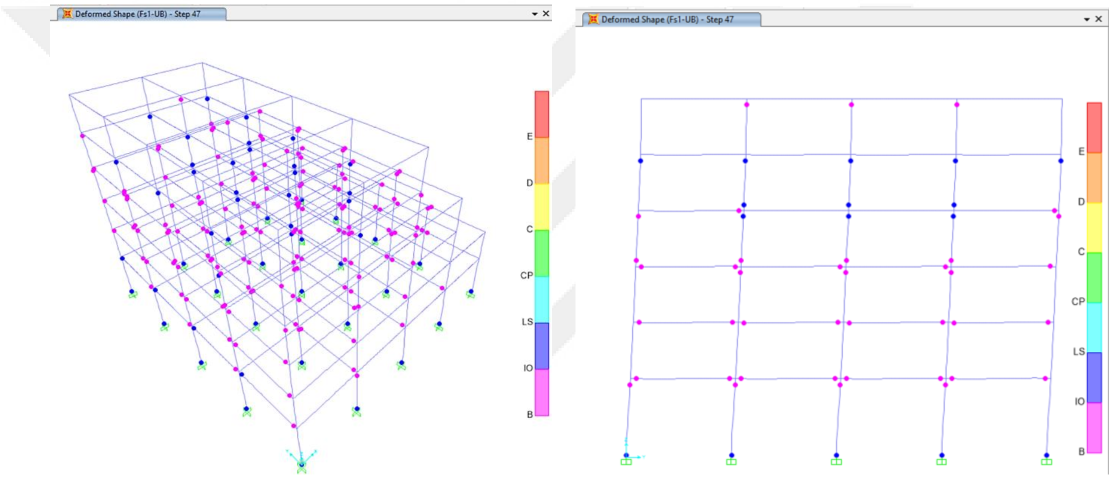

Figure C. 4 Plastic Hinge Distribution for Push Y Load Case for M3-6S-IR

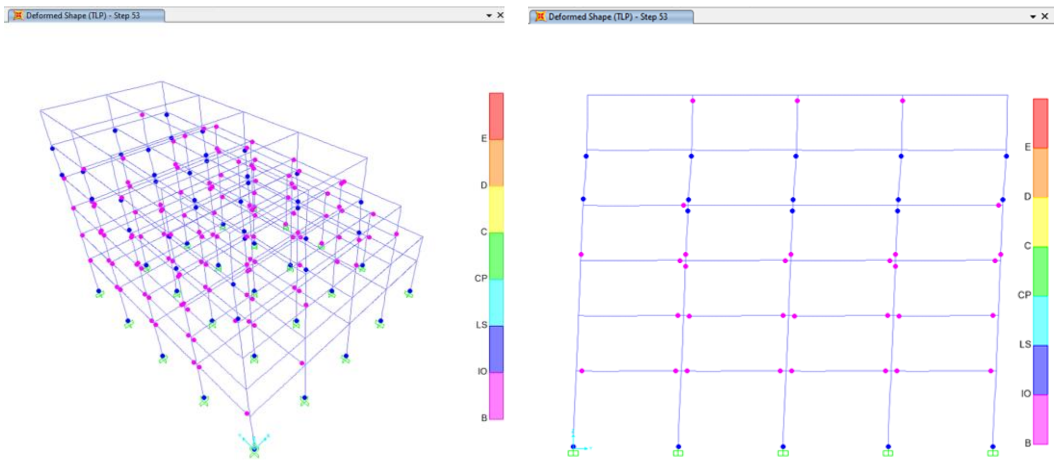

Figure C. 5 Plastic Hinge Distribution for M3-6S-R model by $\mathrm{F}_S UB$ load pattern

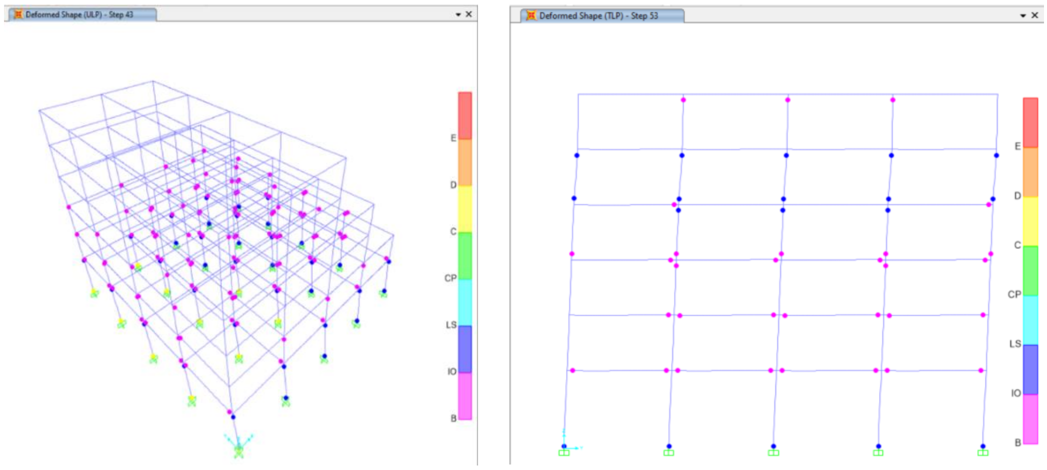

Figure C. 6 Distribution of Plastic Hinge in M3-6S-R model by $\mathrm{F}_S UB$ load pattern

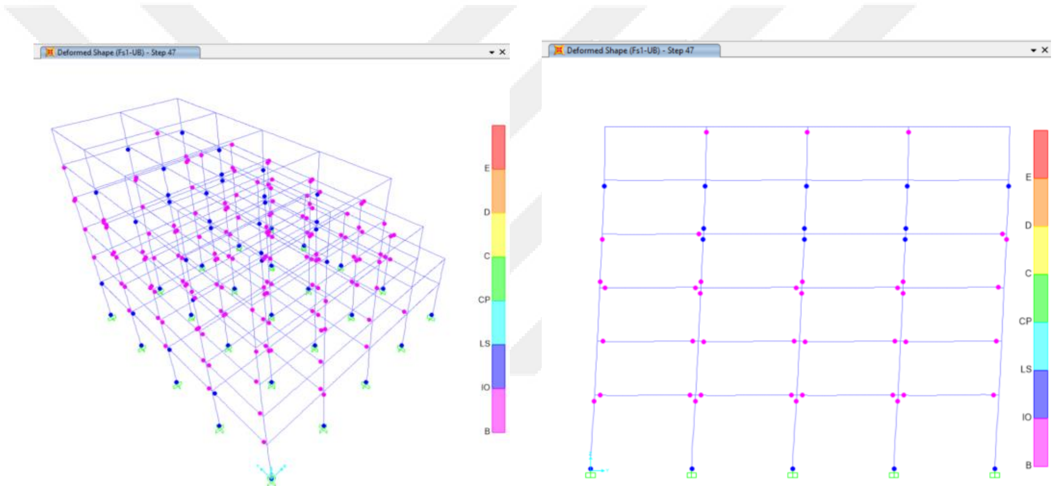

Figure C. 7 Plastic Hinge Distribution for M3-6S-IR2 model by $\mathrm{F}_{S1} UB$ load pattern

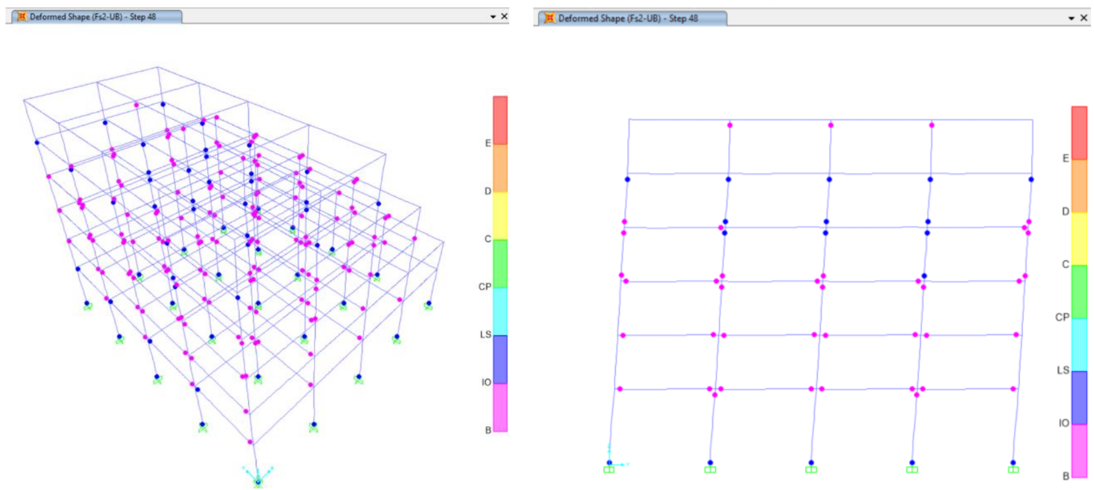

Figure C. 8 Plastic Hinge Distribution for M3-6S-IR2 model by $\mathrm{F}_{S2} UB$ load pattern

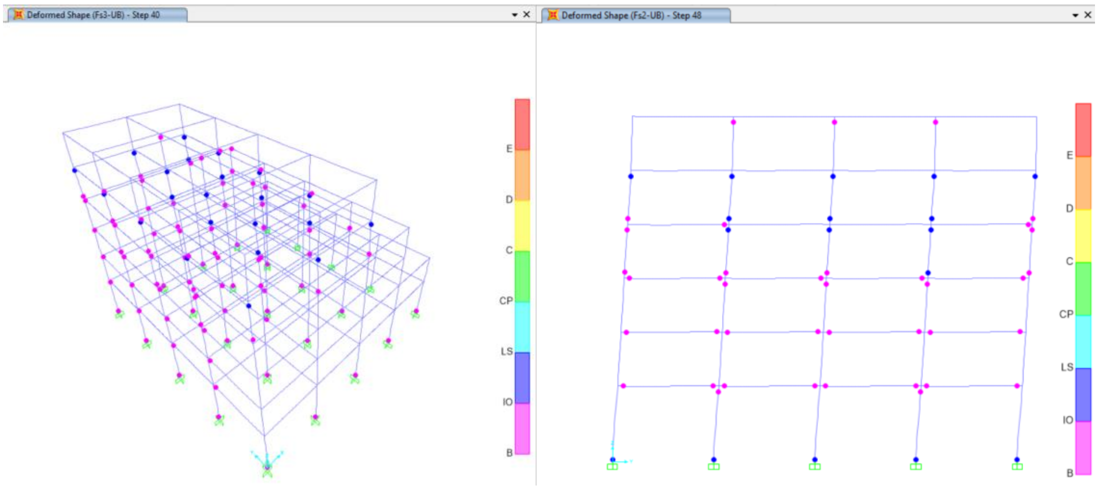

Figure C. 9 Distribution of Plastic Hinge in M3-6S-IR2 model by $F_{S3}UB$ load pattern

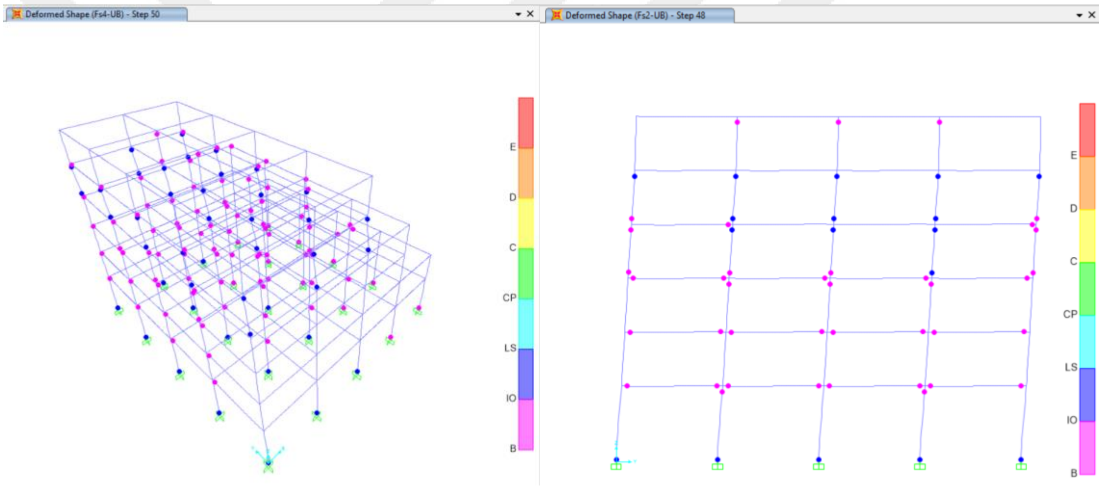

Figure C. 10 Distribution of Plastic Hinge in M3-6S-IR2 model by $F_{S4}UB$ load pattern

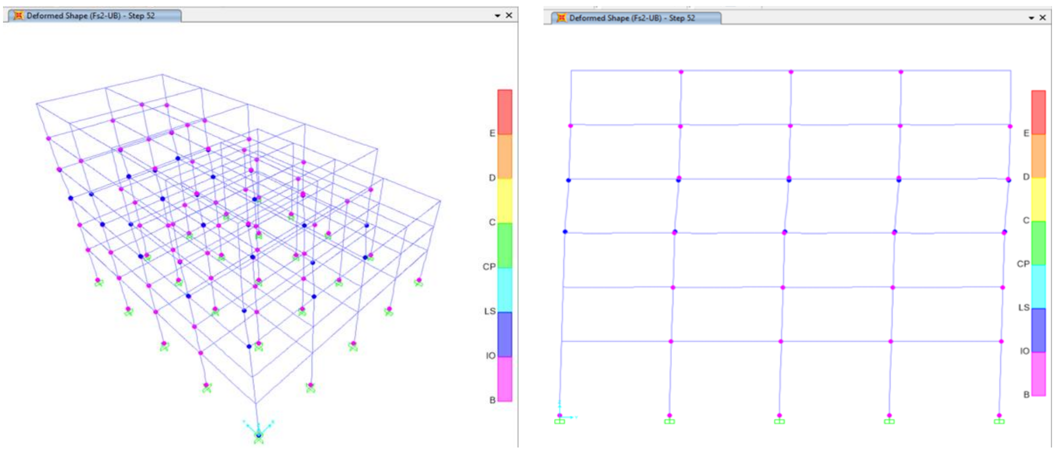

Figure C. 11 Distribution of Plastic Hinge in M3-6S-R model by $F_{S}UB$ load pattern

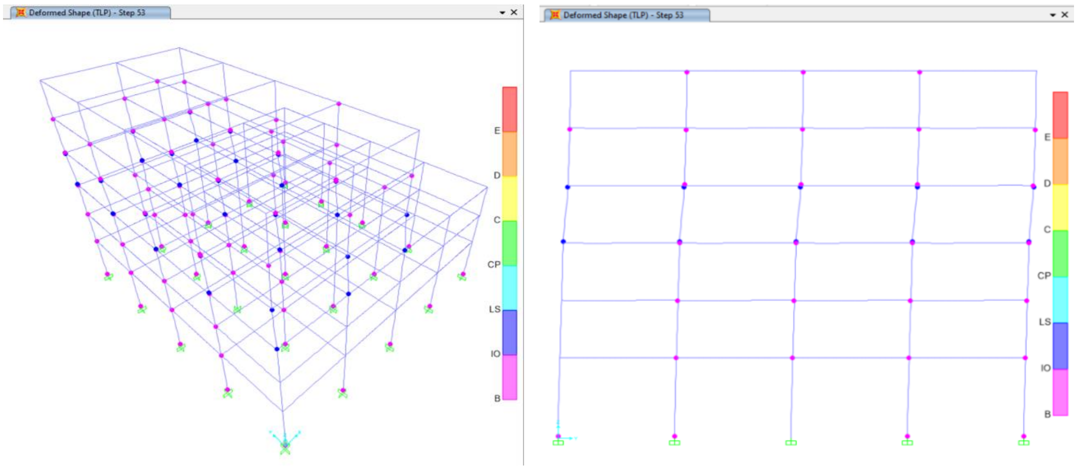

Figure C. 12 Distribution of Plastic Hinge in M3-6S-IR2 model by (TLP) load pattern

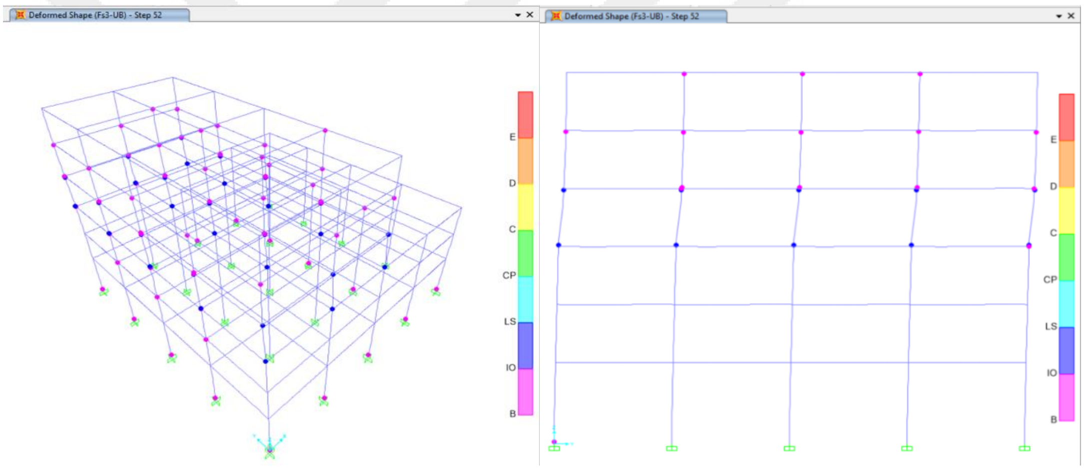

Figure C. 13 Distribution of Plastic Hinge in M3-6S-IR2 model by (TLP) load pattern

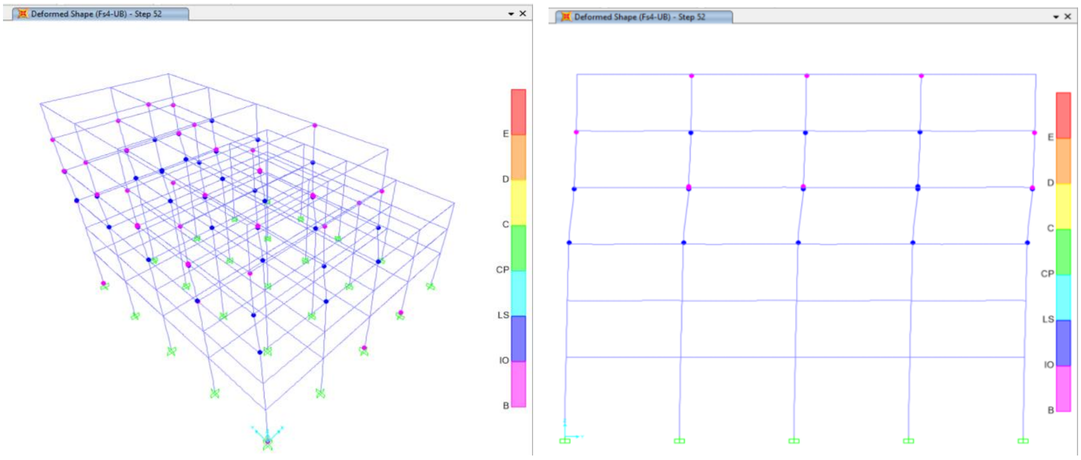

Figure C. 14 Distribution of Plastic Hinge in M3-6S-R model by $F_S UB$ load pattern

C.1 Performance Point

Pushover analysis is used to identify the performance point, which is the point at which the structure's capacity spectrum intersects with the seismic demand. In order to evaluate the performance of the structure, the state of the structure at the performance point must be considered. When the structure achieves its peak performance, the condition of the plastic hinges created at various points throughout the structure may be examined. As a consequence of this, it is essential to examine how the structure's hinges are performing in the real world in order to generate a table that provides the coordinates of each step of the pushover curve and summarizes the number of hinges that are in each condition (IO, LS, CP, or between D and E). Buildings with vertical irregularity have greater Performance point value than those with vertical irregularity. Several versions of hinges, including those with and without setback, are examined at the point of performance. are shown in Table C. 1 to Table C. 6. Nonlinear static (pushover) analysis results in the presentation of a capacity curve, which is often a plot of roof displacement vs base shear at a performance point as shown in Table C. 7

Table C. 1 Hinge Status at Performance Point from Pushover Capacity Curve along Y-direction for M1-6S-R.

Load Case	**Disp. (m)**	**F_b (KN)**	**A-B**	**B-IO**	**IO-LS**	**LS-CP**	**CP-C**	**C-D**	**D-E**	**>E**	**Total**
Fs-UB	0.3309	9850	473	238	57	0	0	12	0	0	780
FLP	0.3312	9778	485	231	56	0	0	8	0	0	780
ULP	0.3282	9089	538	188	15	0	0	39	0	0	780
TLP	0.3306	8974	479	235	66	0	0	0	0	0	780

Table C. 2 Hinge Status at Performance Point from Pushover Capacity Curve along Y-direction for M2-12S-R.

Load Case	Disp. (m)	F_b (KN)	A-B	B-IO	IO-LS	LS-CP	CP-C	C-D	D-E	>E	Total
FS-UB	0.454	12829	1197	165	182	0	0	16	0	0	1560
FLP	0.454	12828	1197	165	182	0	0	16	0	0	1560
ULP	0.452	19451	1256	177	102	0	0	25	0	0	1560
TLP	0.429	11686	1157	263	140	0	0	0	0	0	1560

Table C. 3 Hinge Status at Performance Point from Pushover Capacity Curve along Y-direction for M3-6S-IR.

Load Case	Disp. (m)	F_b (KN)	A-B	B-IO	IO-LS	LS-CP	CP-C	C-D	D-E	>E	Total
Fs1-UB	0.315	8588	407	153	52	0	0	0	0	0	612
Fs2-UB	0.315	8385	402	152	58	0	0	0	0	0	612
Fs3-UB	0.290	4601	498	84	0	0	0	30	0	0	612
Fs4-UB	0.290	6716	472	96	32	0	0	12	0	0	612
FLP	0.300	8452	420	145	47	0	0	0	0	0	612
ULP	0.291	9521	457	108	36	0	0	11	0	0	612
TLP	0.300	7649	427	127	58	0	0	0	0	0	612

Table C. 4 Hinge Status at Performance Point from Pushover Capacity Curve along Y-direction for M4-12S-IR

Load Case	Disp. (m)	F_b (KN)	A-B	B-IO	IO-LS	LS-CP	CP-C	C-D	D-E	>E	Total
Fs1-UB	0.484	13226	946	361	1	0	0	0	0	0	1308
Fs2-UB	0.479	13505	951	353	4	0	0	0	0	0	1308
Fs3-UB	0.443	9366	1086	192	30	0	0	0	0	0	1308
Fs4-UB	0.484	10723	1028	250	14	0	0	16	0	0	1308
FLP	0.485	13229	939	368	1	0	0	0	0	0	1308
ULP	0.482	17896	1032	242	33	0	0	1	0	0	1308
TLP	0.483	8874	800	156	20	0	0	0	0	0	1308

Table C. 5 Hinge Status at Performance Point from Pushover Capacity Curve along Y-direction for M5-6S-IR.

Load Case	Disp. (m)	F_b (KN)	A-B	B-IO	IO-LS	LS-CP	CP-C	C-D	D-E	>E	Total
Fs1-UB	0.215	7843	492	86	34	0	0	0	0	0	612
Fs2-UB	0.215	7183	495	87	30	0	0	0	0	0	612
Fs3-UB	0.215	5888	521	61	30	0	0	0	0	0	612
Fs4-UB	0.215	5115	537	39	36	0	0	0	0	0	612
FLP	0.215	7851	491	87	34	0	0	0	0	0	612
ULP	0.215	10001	470	115	27	0	0	0	0	0	612
TLP	0.22	6843	497	85	30	0	0	0	0	0	612

Table C. 6 Hinge Status at Performance Point from Pushover Capacity Curve along Y-direction for M6-12S-IR

Load Case	Disp. (m)	F_b (KN)	A-B	B-IO	IO-LS	LS-CP	CP-C	C-D	D-E	>E	Total
Fs1-UB	0.518	14933	1024	142	0	0	0	0	0	0	1280
Fs2-UB	0.508	12933	1114	166	0	0	0	0	0	0	1280
Fs3-UB	0.513	12933	1114	166	0	0	0	0	0	0	1280
Fs4-UB	0.529	13718	1060	219	1	0	0	0	0	0	1280
FLP	0.509	13131	1102	178	0	0	0	0	0	0	1280
ULP	0.501	18406	1055	204	21	0	0	0	0	0	1280
TLP	0.508	1466	8805	145	41	0	0	0	0	0	1280

Nonlinear static (pushover) analysis results in the presentation of a capacity curve, which is often a plot of roof displacement vs base shear at a performance point as shown in Table C. 7

Table C. 7 Base shear and displacement for different lateral load patterns

Model	**MUB**		**FLP**		**ULP**		**TLP**	
	V_b (kN)	Disp. (m)	V_b (kN)	Disp. (m)	V_b (kN)	Disp. (m)	V_b (kN)	Disp. (m)
M1-6S-R	7248	0.167	7238	0.167	7874	0.147	7065	0.175
M2-12S-R	10022	0.227	10022	0.227	14261	0.208	9521	0.245
	EUB		**FLP**		**ULP**		**TLP**	
M3-6S-IR	6685	0.174	6453	0.174	12631	0.266	6455	0.182
M4-12S-IR	10631	0.353	10436	0.337	12829	0.268	9315	0.369
M5-6S-IR	7547	0.181	7549	0.181	8664	0.152	6875	0.187
M6-12S-IR	9849	0.366	9848	0.366	12305	0.298	9848	0.166

C.2 Plastic hinge in Reinforced Concrete

When a concrete element, such as a beam or column, reaches its ultimate capacity or maximum load, it exhibits one of two behaviors: brittleness or ductility. Brittle failure occurs at the ultimate load, with sudden and unexpected collapse. This type of collapse can be avoided by changing the steel reinforcement to concrete ratio in the composition. Concrete codes recommend using a steel ratio that is at least 25% less than the balanced condition ratio. The flexural response for both behaviors is depicted in Figure C.1. If the member exhibits ductile behavior, it will continue to deflect under load without failing suddenly, even if many cracks have progressed before the final collapsed load.

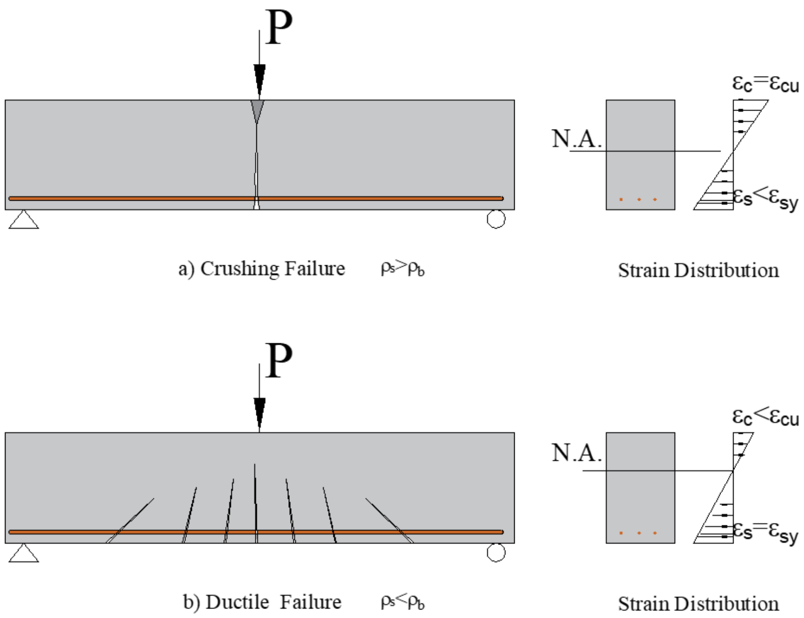

Figure C.1 Failure Mode of Reinforced Concrete Beams

Plastic hinges are used to test the ductility of concrete elements. A beam or column may continue to absorb energy after reaching its maximum capacity, rather than failing. Concrete's inelastic, or plastic, range of behavior includes the ability to deform beyond elastic deformation and generate moment redistribution. Steel reinforcement is commonly used to brace large inelastic curvatures caused by cracking in the tension zone of concrete.

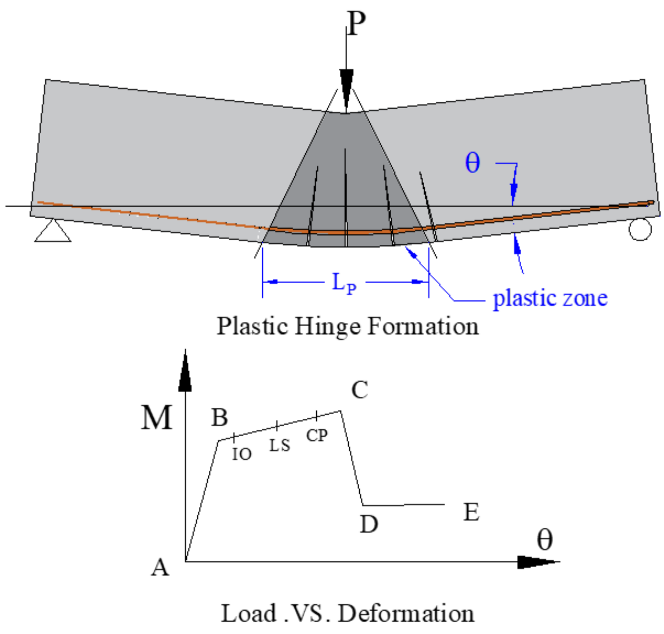

Figure C.2 Prior to Failure, Plastic Hinge Formation in Flexure Beams

The performance criteria are described in many codes of practice to impellent implement the level of building performance Table C. 8 depict these levels according to the ATC- 40 [12].

Table C. 8 Performance levels and criteria provided in ATC- 40 [12]

Performance Level	**Performance Criteria**
Immediate Occupancy (IO)	1. There shall not be any columns, beams or shear walls beyond IO level. 2. The ratio of beams in IO-LS region shall not exceed 10% in any storey. 3. There shall not be any beams beyond LS.
Life Safety (LS)	1. In any storey, the shear carried by columns or shear walls in LS-CP region shall not exceed 20% of storey shear. This ratio can be taken as 40% for roof storey. 2. In any storey, the shear carried by columns or shear walls yielded at both ends shall not exceed 30% of storey shear. 3. The ratio of beams in LS-CP region shall not exceed 20% in any storey.
Collapse Prevention (CP)	1. In any storey, the shear carried by columns or shear walls beyond CP region shall not exceed 20% of storey shear. This ratio can be taken as 40% for roof storey. 2. In any storey, the shear carried by columns or shear walls yielded at both ends shall not exceed 30% of storey shear. 3. The ratio of beams beyond CP region shall not exceed 20% in any storey.